UNIVERSITAT POLITÈCNICA DE CATALUNYA BARCELONATECH

Medium-transparent MAC protocols for converged optical wireless networks

by

Georgios Kalfas

UNIVERSITAT POLITÈCNICA
DE CATALUNYA
BARCELONATECH

Departament de Teoria
del Senyal i Comunicacions

Centre
Tecnològic
de Telecomunicacions
de Catalunya

Medium -Transparent MAC protocols for converged optical wireless networks

PhD Thesis Dissertation

by

Georgios Kalfas

Submitted to the Universitat Politècnica de Catalunya (UPC)
in partial fulfillment of the requirements for the degree of

DOCTOR OF PHILOSOPHY

Barcelona, May 2017

Supervised by Prof. Luis Alonso and Dr. Ch. Verikoukis
PhD program on Signal Theory and Communications

Page intentionally left blank

"Science is organized knowledge.
Wisdom is organized life."

Immanuel Kant

Page intentionally left blank

Στην μητέρα μου Φαίη,

στον πατέρα μου Γρηγόρη,

και στην αδερφή μου Σένια.

Page intentionally left blank

Abstract

In order to address the explosive demand for high-capacity and omnipresent wireless access, modern cell-based wireless networks are slowly adopting two major solution roadmaps. The first is the employment of small-cell formations in order to increase the overall spectral efficiency, whereas the second is the employment of higher frequency bands, such as the mm-wave 60GHz band, that offers vast amounts of bandwidth. Depending on the specific application, the above solutions inevitably require the installation and operational management of large amounts of Base Stations (BSs) or Access Points (APs), which ultimately diminishes the overall cost-effectiveness of the architecture. In order to reduce the system cost, Radio over Fiber (RoF) technology has been put forward as an ideal candidate solution, due to the fact that it provides functionally simple antenna units, often termed as Remote Antenna Units (RAUs) that are interconnected to a central managing entity, termed as the Central Office (CO), via an optical fiber. Although extensive research efforts have been dedicated to the development of the physical layer aspects regarding RoF technologies, such as CO/RAU physical layer design and radio signal transport techniques over fiber, very limited efforts have concentrated on upper layer and resource management issues. In this dissertation, we are concerned with access control and resource management of RoF-based mm-wave network architectures targeting the exploitation of the dual medium and its centralized control properties in order to perform optimal optical/wireless/time resource allocation.

We propose a Medium-Transparent MAC (MT-MAC) protocol that concurrently administers the optical and wireless resources of a 60GHz RoF based network, seamlessly connecting the CO to the wireless terminals through minimal RAU intervention. In this way, the MT-MAC protocol forms extended reach 60GHz WLAN networks offering connectivity amongst wireless devices that are attached to the same or different RAUs under both Line of Sight (LOS) and non LOS conditions. The notion of medium-transparency relies on two parallel contention periods, the first in the optical domain and the

second in the wireless frequency and time domains, with nested dataframe structures. The MT-MAC operation is based on a proposed RAU design that allows for wavelength selectivity functions, thus being compatible with completely passive optical distribution network implementations that are predominately used by telecom operators today. Two variants of the MT-MAC protocol are considered. The first offers dynamic wavelength allocation with fixed time windows, whereas the second targets fairness-sensitive applications by offering dynamic wavelength allocation with dynamic transmission opportunity window sizes, based on the number of active clients connected at each RAU. Both variants of the protocol are evaluated by both simulation and analytical means. For the latter part, this thesis introduces two analytical models for calculating saturation throughput and non-saturation packet delay for the converged MT-MAC protocol.

Finally, this thesis presents an extensive study regarding the network planning and formation of 60GHz Gigabit WLAN networks when the latter are deployed over existing Passive Optical Network (PON) infrastructures. Three possible architectures where studied: i) the RoF approach, ii) the Radio & Fiber approach and iii) the hybrid RoF-plus-R&F approach that combines the properties of both the architectures. During the elaboration of this thesis, one major key conclusion has been extracted: there is a fundamental requirement for implementing new converged optical/wireless MAC protocols, that have the complete overview of both available resources in order to effectively administer the hybrid Radio-over-Fiber networks.

Keywords

60 GHz wireless networks; 60GHz Local Access Network; Medium Access Control protocol; medium-transparent MAC; Passive Optical Network; Radio-over-Fiber networks

Resumen

A fin de atender la demanda explosiva de alta capacidad y acceso inalámbrico omnipresente, las redes inalámbricas basadas en celdas están poco a poco adoptando dos principales guías de solución. La primera es el empleo de formaciones de celdas pequeñas con el fin de aumentar la eficiencia espectral global, mientras que la segunda es el empleo de bandas de frecuencia superior, como la banda de 60GHz, la cual ofrece una gran cantidad de ancho de banda. Dependiendo de la aplicación en específico, las soluciones anteriores inevitablemente requieren de una instalación y una gestión operativa de grandes cantidades de Estaciones Base o Puntos de Acceso, que en última instancia disminuye la rentabilidad de la arquitectura. Para reducir el coste, la tecnología radioeléctrica por fibra (RoF) se presenta como una solución ideal debido al hecho de que proporciona unidades de antenas de simple funcionamiento, a menudo denominadas Unidades de Antenas Remotas (RAUs), las cuales están interconectadas a una entidad central de gestión, denominada Oficina Central (CO), a través de la fibra óptica. A pesar de que se han dedicado muchos esfuerzos de investigación al desarrollo de varios aspectos de la capas física con respecto a las tecnologías RoF, muy pocos esfuerzos se han concentrado en la capa superior y cuestiones de gestión de recursos. En esta tesis, nos enfocando en el control de acceso y gestión de recursos de arquitecturas RoF y comunicaciones milimétricas, con el fin de aprovechar y explotar el medio dual y las propiedades para realizar una óptima asignación de los recursos ópticos, inalámbricos y temporales.

Nosotros proponemos un protocolo Transparente al Medio MAC (MT-MAC) que simultáneamente administre los recursos ópticos e inalámbricos de una red RoF a 60GHz, conectando a la perfección el CO a los terminales inalámbricos a través de una mínima intervención RAU. El protocolo MT-MAC forma unas redes WLAN 60GHz de alcance extendido, ofreciendo así conectividad entre los dispositivos inalámbricos que están conectados al mismo o diferentes RAUs bajo con o sin Línea de Vista (condiciones LOS o NLOS) respectivamente. La noción de transparencia al medio se basa en dos

períodos de contención paralelos, el primero en el dominio óptico y el segundo en la frecuencia inalámbrica y dominio del tiempo, con estructuras de datos anidados. La operación MT-MAC se basa en proponer un diseño RAU que permita la selectividad de funciones de longitud de onda. Dos variantes del protocolo MT- MAC son considerados; el primer ofrece asignación de longitud de onda dinámica con ventanas de tiempo fijo, mientras que la segunda tiene como objetivo entornos de aplicaciones sensibles ofreciendo asignación de longitud de onda con tamaño de ventana de oportunidad de transmisión dinámico, basado en el número de clientes conectados en cada RAU. Ambas variantes del protocolo están evaluadas tanto por medios analíticos como de simulación. En la segunda parte, esta tesis introduce dos modelos analíticos para calcular el rendimiento de saturación y no saturación del retardo de paquetes para el protocolo MT-MAC convergente. Finalmente, esta tesis presenta un extenso estudio de la planificación de red y la formación de redes 60GHz Gigabit WLAN cuando esta se encuentra desplegada sobre las ya existente infraestructuras de Redes Ópticas Pasivas (PONs). Tres posibles arquitecturas han sido estudiadas: i) el enfoque RoF, ii) el enfoque Radio y Fibra, y iii) el enfoque híbrido, RoF más R&F el cual combina las propiedades de ambas arquitecturas anteriormente mencionadas.

Durante la elaboración de esta tesis, se ha extraído una importante conclusión: hay un requerimiento fundamental para implementar nuevos protocolos ópticos/inalámbricos convergentes, que tengan una completa visión de ambos recursos disponibles para poder administrar efectivamente las redes de tecnología RoF.

Palabras clave

60 GHz redes inalámbricas; 60GHz Red de Acceso Local; Protocolo de control de Acceso al Medio; MAC transparente del medio; Red Óptica Pasiva; Radio por redes de fibra

Acknowledgements

It is exceptionally difficult for me to summarize my thoughts now that I stand at the end of the longest and certainly most interesting journey of my life! Simply put, a few words in ink and paper are not adequate to fully express my gratitude towards the long list of people that stood by me all those years and made this thesis a reality. Nonetheless, I will give it my best try and hope to achieve an accurate approximation of a proper thank you.

I would like to sincerely thank my thesis supervisors, Dr. Christos Verikoukis and Dr. Luis Alonso, who have so generously offered me their guidance, assistance, continuous support and motivation all those years. It has been an honor to learn from you and I hope that the future holds further collaboration opportunities. My gratitude also goes towards Dr. Nikos Pleros: thank you for your teachings, problem solving, late night efforts, opportunities, mentoring, your immense patience-*to be completely accurate I should have written this twice!*-, and most importantly your friendship!

I would also like to thank all the people I have collaborated with during this time in our joint research efforts: Dr. Amalia Miliou, Dr. John Vardakas, Dr. Dimitris Tsiokos, Dr. Konstantinos Tsagkaris, Mr. Pavlos Maniotis and Ms. Stella Markou. It has been a great pleasure and honor working with you.

A special thanks goes to my friends from the "Phos-Net: the first generation" series with whom we have shared the same anxieties, frustrations, deadlines and damn good fun times: Dr. Sotirios Papaioannou, Dr. Theoni Alexoudi, Dr. Dimitris Fitsios, Dr. Christos Vagionas, Mr. Pavlos Maniotis-again!- and Ms. Stella Markou-again!-. We have stayed together all those years, trying to survive between the hammer and the anvil for longer than we would like to remember, but sincerely one could not have hoped for better travel companions! I hope all the best for you in your future endeavors.

To the original “caclab crew”, Dr. K. Vyrsokinos, Dr. S. Petridou, Dr. S. Basagiannis and Dr. F. Loukos, I would like to extend a special thank you for all those nights of wine and good fellowship that made university life special besides the hardships. Fotis I owe special gratitude to you for making my military service a time to remember with joy and not dread.

Dr. Angelos Antonopoulos, although typically I should have added you in the previous list, you deserve a special mention not only for proof-reading this thesis but also for carrying the bureaucratic load for me all those years and making my life easier. I can only hope that the future holds many opportunities for me to buy enough rounds at the *Magraner Boig* to make amends. In the same context, I would also like to thank Angeliki Nt. and Akis M. for the lovely time I had in Barcelona and for making me feel like home from day 1.

My love and thoughts go to my university gang, aka “*pareaki*”, that became the very definition of what I call friendship in my life (alphabetically): Athina A., Christos Ch., Dimitris P., Dimitris R., Eleni R., Eleni S., George M., Haris, K., Hercules S., Konstantina T., Maria A., Maria P., Marianthi K., Ourania K. and Theofanis Ec. It has been an honor and a blessing to share my life with you (17 years and going strong!). Thank you for always standing by me and for being my friends in the good and most importantly in the bad days.

Above all, I want to dedicate this thesis to my mother Faye, my father Gregory and my sister Senia. Have it not been for your countless sacrifices, continuous unending support and your good example I would have never make it here. Consider this work as your own.

Georgios Kalfas

Barcelona, Spain

May 2017

List of Publications

===Journals===

[J1] **G. Kalfas**, J. Vardakas, L. Alonso, C. Verikoukis and N. Pleros, "Non-saturation delay analysis of Medium Transparent MAC protocol for 60GHz Fiber-Wireless networks", *submitted in* IEEE Journal of Lightwave Technology.

[J2] **G. Kalfas**, N. Pleros, L. Alonso and C. Verikoukis, "Network planning for 802.11ad and MT-MAC 60 GHz fiber-wireless gigabit wireless local area networks over passive optical networks" in IEEE/OSA Journal of Optical Communications and Networking, vol. 8, no. 4, pp. 206-220, April 2016.

[J3] **G. Kalfas**, P. Maniotis, S. Markou, D. Tsiokos, N. Pleros, L. Alonso, and C. Verikoukis, "Client-Weighted Medium-Transparent MAC Protocol for User-Centric Fairness in 60 GHz Radio-Over-Fiber WLANs", IEEE/OSA Journal of Optical Communications and Networking, vol.6, no.1, pp.33,44, Jan. 2014.

[J4] **G. Kalfas**, N. Pleros, K. Tsagkaris, L. Alonso, C. Verikoukis, "Saturation Throughput Performance Analysis of a Medium-Transparent MAC protocol for 60GHz Radio-over-Fiber Networks", IEEE Journal of Lightwave Technology, vol.29, no.24, pp.3777 – 3785, December 2011.

===International Conferences===

[C1] **G. Kalfas**, J. Vardakas, N. Pleros, L. Alonso, C. Verikoukis, "Delay analysis of converged Medium Transparent fixed service Optical-Wireless networks", IEEE Globecom, December 2016, Washington D.C., USA.

[C2] **G. Kalfas**, L. Alonso, Ch. Verikoukis, N. Pleros, "Medium Transparent MAC protocols for Fiber-Wireless mm-wave multi-Gbps WLANs", International Wireless Symposium 2014, March 2014, Xi'An, China.

[C3] **G. Kalfas**, D. Tsiokos, N. Pleros, C. Verikoukis, M. Maier, "Towards medium transparent MAC protocols for cloud-RAN mm-wave communications over next-generation optical wireless networks", 15th IEEE ICTON, June 2013, Cartagena, Spain.

[C4] **G. Kalfas**, S. Markou, D. Tsiokos, Ch. Verikoukis, N. Pleros, "Very High Throughput 60GHz wireless enterprise networks over GPON infrastructure", IEEE ICC, Optical-Wireless Workshop, June 2013, Budapest, Hungary.

[C5] P. Maniotis, **G. Kalfas**, L. Alonso, Ch. Verikoukis, N. Pleros, "Throughput and Delay Fairness through an agile Medium-Transparent MAC protocol for 60GHz Fiber-Wireless LAN networks", IEEE WCNC 2012, Hybrid Optical-Wireless Access Networks Workshop, April 2012, Paris, France.

[C6] **G. Kalfas**, N. Pleros, K. Tsagkaris, L. Alonso, C. Verikoukis, "Performance Analysis of a Medium-Transparent MAC protocol for 60GHz Radio-over-Fiber Networks", IEEE Globecom, December 2011, Houston, Texas.

[C7] **G. Kalfas**, N. Pleros, K. Tsagkaris, C. Verikoukis, "60GHz Radio-over-Fiber networks: Optical-Wireless Convergence through Medium-Transparent MAC protocols", Euro-NF International Workshop on Traffic and Congestion Control for the Future Internet, April 2011, Volos, Greece.

Contents

Page intentionally left blank

List of Tables

Page intentionally left blank

List of Figures

Page intentionally left blank

List of Acronyms

ABL	Average Burst Length
ADAP	802.11ad Access Point
ADC	Analog Digital Converter
AP	Access Point
BS	Base Station
CDF	Cumulative Distribution Function
Cloud-RAN	Cloud Radio Access Network
CO	Central Office
CPRI	Common Public Radio Interface
CSMA	Carrier Sense Multiple Access
CTS	Clear to Send
CWA	Client-Weighted Allocation scheme
CW-MT-MAC	Client-Weighted MT-MAC
DATA_TX	Data Transmission Period
D-RoF	Digitized RoF
DAC	Digital Analog Converter
DCF	Distributed Coordination Function
DF	Data Frame
DL	Download
DOCSIS	Data Over Cable Service Interface Specification
DSB	Dual SideBand Modulation
DSP	Digital Signal Processing
DWA	Dynamic Wavelength Allocation
E/O	Electrical/Optical Conversion
EPON	Ethernet PON
FDM	Frequency Division Multiplexing
FiWi	Fiber Wireless
FSAN	Full Service Access Network

FTTH	Fiber to the Home
GEM	GPON Encapsulation Method
GPON	Gigabit PON
HD	High Definition
HDMI	High-Definition Multimedia Interface
HNT	Hidden Node Terminal
IC	Integrated Circuit
IF	Intermediate Frequency
IP	Internet Protocol
ISM	Industry-Science-Medical (RF band)
LAN	Local Area Network
LOS	Line of Sight
LR-PON	Long Reach PON
LTE	Long Term Evolution
MAC	Medium Access Control
MTDF	MT-MAC Data Frames
MT-MAC	Medium Transparent MAC
MZM	Mach-Zehnder Modulator
NAV	Network Allocation Vector
NGN	Next Generation Network
NG-PON2	Next Generation PON v.2
OADM	Optical Add-Drop Multiplexer
OBF	Optical Bandpass Filter
OBSAI	Open Base Station Architecture Initiative
ODN	Optical Distribution Network
O/E	Optical/Electrical Conversion
OFDM	Orthogonal Frequency-Division Multiplexing
OLT	Optical Line Terminal
ONU	Optical Network Unit
PDV	Packet Delay Variance
PMF	Probability Mass Function
PON	Passive Optical Network
QoS	Quality of Service
R&F	Radio-and-Fiber
RAU	Remote Antenna Unit

RF	Radio Frequency
RoF	Radio over Fiber
RRA	Round-Robin Allocation scheme
RRF	Resource Request Frame
RTS	Request to Send
SF	Superframe
SMF	Single Mode Fiber
SOA	Semiconductor Optical Amplifier
SSB	Single Side Band
SSP	Steady State Probability
STA	802.11 Station
TDM	Time Division Multiplexing
TWDM-PON	Time Wavelength Division Multiplexing PON
TX_OP	Transmission Opportunity window
UB	Upstream Bandwidth
UL	Upload
USB	Universal Serial Bus
VHT	Very High Throughput
VoIP	Voice over IP
WDM	Wavelength Division Multiplexing
WiFi	802.11 Standard (Wireless Fidelity)
WiFi-N	802.11n Standard
WiMAX	Worldwide Interoperability for Microwave Access
WLAN	Wireless Local Area Network
WMN	Wireless Metropolitan Networks
WPAN	Wireless Personal Area Network
WR	Number of Wavelengths to number of RAUs ratio
UMTS	Universal Mobile Telecommunications System
$\boldsymbol{UC_q}$	Utilization Counter for RAU q
MWP	Microwave Photonics

Page intentionally left blank

Chapter 1 Introduction

1.1 Consolidation of wired and wireless infrastructure

In recent years we have witnessed the profound mobile data service proliferation and the ever-growing need for fast omnipresent wireless access caused by a major shift of consumer trends. The service demands of modern users have evolved around the "everything in the cloud" notion, which envisions an unhindered desktop-like experience while the consumers are on the move. Besides their staggering sales figures [1], smart mobile devices are increasingly becoming the main Internet access means for the majority of the users [2], and as such they are used for a plethora of demanding applications like video streaming and videoconference that require better network performance and guaranteed resources (Fig. 1-1) [3]. This paradigm shift constitutes the dawn of a new age in the telecommunications industry that has placed an unprecedented strain on the existing infrastructure, quickly highlighting its weaknesses regarding the offered capacity, the coverage area and the quality of the provided services.

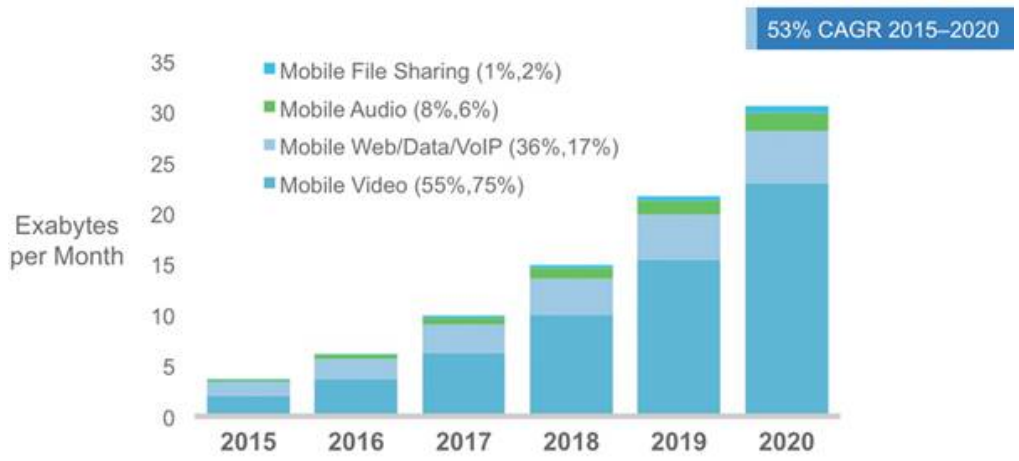

Fig. 1-1 Evolution of mobile Internet traffic per application type (Figures in parentheses refer to 2015 and 2020 traffic share.) Source: Cisco VNI Mobile, 2016

In order to respond to the mobile revolution, the industry has put forward two approaches. The first is the employment of small-cells, i.e., short range Base Stations

(BSs) that are densely deployed and can accommodate more users by enhancing the spectral efficiency and frequency reuse factors of the network. Hyper-dense deployment of small-cells is currently at the spotlight of research effort, since it is considered as a key enabling technique towards realizing the next generation ubiquitous, ultrahigh bandwidth communication system, known as 5G [4]-[8]. The second approach is the employment of the millimeter wave (mm-wave) frequency bands that offer immense bandwidth in both licensed and unlicensed spectra, given however at the cost of high propagation losses. The above solutions inevitably lead to complicated and costly deployments since demanding functions such as signal processing, handover and frequency allocation algorithms have to be carried out at the numerous antenna sites, effectively multiplying the amount of active equipment that has to be deployed. To this end, Radio-over-Fiber (RoF) technology has drawn significant attention as a highly effective paradigm for consolidating all required network intelligence in a central unit and thus alleviating the complexity, functionality and cost requirements away from the antenna equipment.

A typical RoF network is comprised of two parts: i) the Central Office (CO), where all routing, Medium Access Control (MAC) and resource management functions are performed, and ii) a large number of functionally simple and compact Remote Antenna Units (RAUs) that broadcast the wireless signal. The CO is connected to the RAUs through an optical fiber link, which can be in either bus, ring or tree topology. The deployment of an array of inexpensive RAUs results in vast and dense coverage wireless networks that optimally combine the mobility and ubiquity advantages of a wireless link with the high speed and long-distance service delivery credentials of fiber-based infrastructure [9],[10]. In summary, the most important characteristics of the RoF technology are [11]:

- All intelligent system control functions, such as MAC and modulation/demodulation schemes, are performed by the CO, thus simplifying the design of the RAU. The primary functions of the RAUs are optical/wireless conversion, Radio Frequency (RF) amplification, and wireless/optical conversion.

- RoF's centralized configuration allows sensitive equipment to be located in safer environments and enables the cost of expensive components to be shared

among several RAUs. Moreover, a centralized location makes upgrading procedures easier and therefore future proofs RoF installations.

- Due to the very simple RAU structure, the hardware reliability is higher and the system maintenance becomes simpler.

- In principle, optical fiber in RoF is transparent to radio interface format such as modulation, radio frequency, bitrate and protocol functions. Thus, multiple services can be concurrently supported on a single fiber.

- Fiber has very low loss properties and is immune to Electro-Magnetic Interference (EMI), therefore making possible the transmission of RoF signals over long distances.

- The vast capacity of the optical fiber enables the parallel co-habitation of RoF technologies with already deployed optical networks such as the Ethernet Passive Optical Networks (EPONs)[12] or Gigabit Passive Optical Networks (GPONs)[13] that are used nowadays to provide wireline broadband access to domestic and corporate users, therefore promoting the quick and non-disruptive adoption by the operators.

Outside the scope of small-cells and RoF applications, mm-wave radio has been studied extensively for a plethora of short range bandwidth-demanding applications[14]-[17]. The industry's conviction towards the adoption of the mm-wave spectrum can also be witnessed by the significant number of emerging or recently issued 60 GHz standards such as the 802.11ad[21], the 802.15.3c[22], the WirelessHD[23] and the 802.11ay[24] protocols. The high propagation losses, exhibited by mm-wave radio, inherently reduce the cell size, rendering mm-wave the ideal supporting technology to accommodate the notion of small-cell formation. To this end, the consolidation of RoF technologies with mm-wave bands has received considerable attention [25]-[32], since a converged mm-wave/RoF system offers a great potential to support Very High Throughput (VHT) wireless applications in very dense environments and in a cost-effective manner. In such a system, the RF signals to and from the RAUs can either be mm-wave modulated optical signals (RF-over-fiber)[29],[31], or lower Intermediate Frequency (IF) subcarriers (IF-over-fiber) [27],[28]. Although transmitting mm-wave signals directly over

fiber carries the advantage of a simplified RAU design, it is susceptible to chromatic dispersion that can limit the transmission distance [33]. In contrast, IF signals' transmission is much less susceptible to chromatic dispersion effects, at the cost however of incorporating additional electronic hardware such as a mm-wave local oscillator (LO) for frequency up-and down-conversion operations.

The combined mm-wave RoF research activities fueled by rapid developments in both photonic and mm-wave technologies suggest that RoF technologies will play a crucial role in the years to come. However, the physical layer technological progress has not been followed by respective advances towards enriching the functional properties of RoF applications with the traditional benefits of single medium networks, such as end to end resource management and dynamic allocation schemes. As a result, it is required to reconsider conventional resource management schemes in the context of RoF networks.

1.2 Motivation and contribution

As mentioned previously, in networks comprising a large number of small cells, two major challenges stand out: i) the system must be very cost-effective in order to enable the coverage of large areas and ii) resource allocation should be fast and efficient in both wired and wireless domains.

Regarding the first issue, the most promising candidate technology is a RoF based network since the latter enables the employment of functionally simple and cost-effective antenna units in contrast to active Access Point (AP)/BS equipment utilized in conventional wireless systems. However, the second issue remains a challenge and is difficult to realize as all conventional access schemes have been specifically designed for the medium that are destined to be deployed and are therefore incapable of administering dual-media resources, as is the case of RoF networks. To this day, two major schools of thought exist regarding resource allocation and access control in the Fiber/Wireless converged networks. The first approach, termed as *Radio & Fiber(R&F)*, employs two distinct optical and wireless APs, each one running a distinct MAC protocol and administering the respective portion of the network, with all intra-communication between the two networks taking place at the routers' interfaces. This approach demands the installation of active communication equipment at all antenna sites, capable of run-

ning the respective MAC, routing, buffering and flow control functionalities at the media interface. Considering the short range and high propagation losses of the mm-wave radio, a large number of antenna elements will be required to provide coverage in typical environments, therefore constituting this approach as prohibitively expensive and ultimately unsuitable for application in converged small-cell/mm-wave networks. The second approach is the direct implementation of currently existing wireless MAC protocols at the CO station. Considering that all wireless MAC protocols have been designed for exclusive use over the wireless medium, they are completely unaware of the optical physical layer that lies between the RAU and the CO, and therefore demand the continuous existence of active optical links between the latter entities, in order to achieve valid operation. In this way, the static wavelength assignment leads to major resource and energy waste, since every RAU cell must maintain a persistently active connection to the CO, even when not in use.

The aforementioned characteristics stress the need for revisiting various aspects of communications, such as resource allocation, scheduling, channel access and performance modelling when addressing converged optical and wireless architectures. The work presented in this dissertation goes beyond the two previously mentioned approaches and proposes an entire new class of functionally converged RoF network architectures and protocols aimed at providing optimal and concurrent optical/wireless resource allocation by exploiting the intertwined architecture and centralized control capabilities of the RoF schemes. In particular, this dissertation concerns the formation, administration and evaluation of RoF-based WLAN networks operating at mm-wave bands in indoor environments. The case of mm-wave communication in indoor spaces presents a particular challenge since mm-wave signals are extremely attenuated by walls and other relatively large obstacles due to the fact that their electromagnetic properties resemble more closely that of a particle and less that of a wave. As opposed to outdoor environments, where the lack of large obstacles promotes oxygen absorption as the dominant range-limiting factor [15],[17], in indoor cases the signal is confined by walls and therefore the cell size is diminished to the dimensions of a typical room. In turn the very small cell sizes demand the deployment of an even larger number of antennas in order to cover a broad service area, therefore increasing the network dimensionality, resource allocation management and energy consumption overheads.

The work presented here aims at responding at all of the aforementioned challenges and proposes a fully converged centralized architecture and a dual access control scheme that unifies the currently distinct fiber and wireless technologies. Having a centralized access control scheme enables the optimal utilization of the available resources in a dynamic way, by assigning capacity slices only to currently active users whereas disengaging them from unused cells. The simultaneous management of optical/wireless resources that stretch all the way to the end-user enables the creation of link models based on a vast number of combinations and in turn allows the direction of the full network's capacity to specific micro-cells while also clustering complementary services in other areas, thus ensuring uninterrupted connectivity and enhanced user perceived quality of service. In this way, the functional consolidation of the fiber and wireless control plane will be fully capable to optimally exploit the unique properties of the dual media. By enabling the optical/wireless convergence in the network intelligence side while addressing the common resources in a holistic approach, our work attempts to synergize the strengths of both optical and wireless media in order to overcome the shortcomings of currently employed optical/wireless access control schemes.

1.3 Structure of this thesis

There are effectively three network aspects that have to be considered when designing a converged RoF multi-Gbps network: i) the hybrid architecture, ii) the control and network intelligence and iii) the physical device that will be able to support both. This thesis presents novel access control protocols that are capable of dynamically allocating capacity and resources both in the optical and wireless domains, accompanied by full schematics of a RAU unit, specifically designed to carry out the protocols' functionalities. The proposed medium transparent access control protocols are measured for performance in various bus and tree topologies under a plethora of network conditions, such as load, fiber lengths, number of users etc., while synergy with established Passive Optical Networks (PON) architectures is also investigated. This thesis goes beyond the currently established functional split between the RoF and R&F architectures and tests both against a proposed hybrid scheme consisting of converged RoF-plus-R&F networks, highlighting in each case the conditions where each architecture prevails. Finally, this thesis presents the first of their kind analytical models for mathematical derivation of saturation throughput and non-saturation end-to-end packet delay for converged RoF networks operating under medium transparent resource allocation schemes.

The remaining part of the thesis consists of 6 chapters, whereas the contents and the contributions of each chapter are described in detail as follows:

- **Chapter 2**: The second chapter introduces the basic background regarding the main concepts employed in this thesis. Firstly, we briefly overview the basic types of RoF systems and explain the advantages that they offer. Secondly we present the existing RoF architectures and establish the difference of RoF versus R&F schemes. Finally, we introduce the state of the art regarding RoF mobility schemes and RoF-based MAC protocols that exist in the literature.

- **Chapter 3**: The third chapter presents an agile and Medium-Transparent Medium Access Control (MT-MAC) protocol for seamless and dynamic capacity allocation over both optical and wireless transmission media in 60GHz broadband Radio-Over-Fiber (RoF) networks. Medium transparency is achieved by means of parallelism between two simultaneously running contention periods and through nesting of wireless user-specific data frames within RAU-specific optical Superframes. The proposed MAC protocol is demonstrated to operate successfully both in RoF-over-bus as well as in RoF-over-PON architectures requiring only minor variations for getting adapted to the network topology. Its performance for both network topologies is evaluated through simulations for different number of end-users, different loads and network node densities and for bit-rates up to 3Gb/s, both for a Poisson and for a burst-mode traffic model. All examined cases confirm the MT-MAC's ability to successfully provide highly efficient 60 GHz Wireless LAN functionality, offering connectivity also between wireless devices without Line-Of-Sight (LOS), while providing a suitable framework for wireless serving high-bandwidth latency-sensitive applications.

  The proposals discussed in this chapter have been published in two conference proceedings, cited next:

  – **G. Kalfas**, L. Alonso, Ch. Verikoukis, N. Pleros, "Medium Transparent MAC protocols for Fiber-Wireless mm-wave multi-Gbps WLANs", International Wireless Symposium 2014, Xi'An, China, April 2014, Xi'An, China.

– **G. Kalfas**, N. Pleros, K. Tsagkaris, C. Verikoukis, "60GHz Radio-over-Fiber networks: Optical-Wireless Convergence through Medium-Transparent MAC protocols", Euro-NF International Workshop on Traffic and Congestion Control for the Future Internet, 31 March – 1 April 2011, Volos, Greece.

- **Chapter 4**: This chapter presents the Client-Weighted Medium-Transparent MAC (CW-MT-MAC) protocol that exhibits enhanced fairness service delivery properties in comparison to normal MT-MAC. This approach relies on incorporating a Client Weighted Algorithm (CWA) in the optical capacity allocation mechanism employed in the MT-MAC scheme, so as to distribute the available wavelengths to the different antenna units according to the total number of active users served by each individual antenna. The protocol's throughput and delay fairness characteristics are evaluated and validated through extended simulation-based performance analysis for non-saturated network conditions and for different end-user distributions, traffic loads and available optical wavelengths. The results confirm that complete throughput and delay equalization can be achieved even for highly varying user population patterns when certain wavelength availability conditions are satisfied.

  The proposals discussed in this chapter have been published in one journal and one conference proceedings, cited next:

  – **G. Kalfas**, P. Maniotis, S. Markou, D. Tsiokos, N. Pleros, L. Alonso, and C. Verikoukis, "Client-Weighted Medium-Transparent MAC Protocol for User-Centric Fairness in 60 GHz Radio-Over-Fiber WLANs", IEEE/OSA Journal of Optical Communications and Networking, vol.6, no.1, pp.33,44, January 2014.

  – P. Maniotis, **G. Kalfas**, L. Alonso, Ch. Verikoukis, N. Pleros, "Throughput and Delay Fairness through an agile Medium-Transparent MAC protocol for 60GHz Fiber-Wireless LAN networks", IEEE WCNC 2012, Hybrid Optical-Wireless Access Networks Workshop, 1st April 2012, Paris, France.

- **Chapter 5**: The first part of this chapter demonstrates an analytical model for calculating the saturation throughput performance of the MT-MAC and CW-MT-MAC protocols. The proposed models incorporate effectively the Medium-Transparent MAC mechanism, assuming a finite number of terminals and ideal channel conditions, while taking into account contention both at the optical and wireless layer. This model enables extensive saturation throughput performance analysis for the MT-MAC protocol and has been applied to 60 GHz RoF network scenarios considering variable numbers of available optical wavelengths, wireless nodes and serving antenna elements and for two different data rate values, namely 155 Mbps and 1 Gbps. The displayed comparison between the model-based throughput results and respective simulation-based outcomes reveals that the analytical model is extremely accurate in predicting the system throughput. The second part of this chapter presents an analytical model for computing the end to end packet delay of a converged Optical/Wireless 60GHz Radio-over-Fiber (RoF) network operating under the Medium-Transparent MAC (MT-MAC) protocol. For the calculation of the cycle times this model takes into account contention at both layers, thus enabling an extensive delay performance analysis of various performance aspects of hybrid RoF networks, such as various optical capacity availability scenarios, varying load conditions, optical network ranges, transmission window and data packet sizes. The theoretical results are found to be in excellent agreement with the respective simulation-based findings.

  The proposals discussed in this chapter have been published in two conference proceedings, cited next:

  – **G. Kalfas**, J. Vardakas, L. Alonso, C. Verikoukis and N. Pleros, "Non-saturation delay analysis of Medium Transparent MAC protocol for 60GHz Fiber-Wireless networks", *submitted in* IEEE Journal of Lightwave Technology.

  – **G. Kalfas**, N. Pleros, K. Tsagkaris, L. Alonso, C. Verikoukis, "Saturation Throughput Performance Analysis of a Medium-Transparent MAC

protocol for 60GHz Radio-over-Fiber Networks", IEEE Journal of Lightwave Technology, vol.29, no.24, pp.3777 – 3785, December 2011.

- **G. Kalfas**, N. Pleros, K. Tsagkaris, L. Alonso, C. Verikoukis, "Performance Analysis of a Medium-Transparent MAC protocol for 60GHz Radio-over-Fiber Networks", IEEE Globecom, 5-9 December 2011, Houston, Texas.

- **G. Kalfas**, N. Pleros, K. Tsagkaris, L. Alonso, C. Verikoukis, "Saturation Throughput Performance Analysis of a Medium-Transparent MAC protocol for 60GHz Radio-over-Fiber Networks", IEEE Journal of Lightwave Technology, vol.29, no.24, pp.3777 – 3785, Dec.15, 2011.

- **Chapter 6**: Chapter 6 presents our study concerning the network planning of 60GHz Gigabit WLAN networks over existing PON infrastructures. Two configurations for Gbit WLAN network formations are investigated: i) the R&F approach that considers several 802.11ad access points connected to conventional GPON ONUs, termed as the GPON-plus-802.11ad approach, and ii) the RoF paradigm that employs several RAUs operating under the MT-MAC protocol, termed as the MT-MAC-over-PON approach. Simulation-based throughput and delay results are presented for both network scenarios, revealing the dependence of the 60GHz enterprise network performance on several network planning parameters such as the load, the traffic shape, the number of optical wavelengths in the backhaul as well as the optical backhaul fiber length. The derived results suggest that: i) the GPON-plus-802.11ad approach is highly-efficient in intra-cell communication but at the cost of massive active AP equipment making it highly impractical for network deployments beyond typical room sizes and ii) the MT-MAC-over-PON approach is inherently capable of relaying inter-cell traffic and form extended reach gigabit WLAN networks making it an excellent match for modern cloud applications but demanding high optical capacity for serving Long-Reach PONs (LR-PONs). Based on the above findings this chapter also presents our study of a hybrid multi-tier architecture termed as GPON-plus-MT-MAC approach that fuses the abilities of both the RoF and R&F architectures in order to optimally combine their properties and set a framework for next-generation 60Ghz Fiber-Wireless networks.

The proposals discussed in this chapter have been published in two conference proceedings, cited next:

- **G. Kalfas**, N. Pleros, L. Alonso and C. Verikoukis, "Network planning for 802.11ad and MT-MAC 60 GHz fiber-wireless gigabit wireless local area networks over passive optical networks" in IEEE/OSA Journal of Optical Communications and Networking, vol. 8, no. 4, pp. 206-220, April 2016.

- **G. Kalfas**, D. Tsiokos, N. Pleros, C. Verikoukis, M. Maier, "Towards medium transparent MAC protocols for cloud-RAN mm-wave communications over next-generation optical wireless networks", 15th IEEE ICTON, June 2013, Cartagena, Spain.

- **G. Kalfas**, S. Markou, D. Tsiokos, Ch. Verikoukis, N. Pleros "Very High Throughput 60GHz wireless enterprise networks over GPON infrastructure", IEEE ICC, Optical-Wireless Workshop, June 2013, Budapest, Hungary.

- **Chapter 7**: This chapter concludes the dissertation by providing a summary of our major contributions, together with some potential lines for future investigation.

Page intentionally left blank

Chapter 2 Background

By merging the immense optical fiber capacity with the mobility and pervasiveness of the wireless networks, the Fiber-Wireless (FiWi) architectures construct a versatile and powerful paradigm that can support demanding modern applications as well as create a new market for future services. As it has been defined in the respective literature, Fiber-Wireless (FiWi) is an overarching term, denoting both the families of RoF and R&F networks[34][35]. In order to fully cover the necessary background material for this thesis, this chapter serves a twofold purpose. Initially it provides a brief introduction into the FiWi paradigm and reviews the key characteristics of both RoF and R&F technologies while highlighting challenges that arise when implementing mm-wave communications in R&F environments. Secondly, it presents a detailed review of the state of the art in RoF physical layer architectures, protocols and systems, on which the main contributions of this thesis are based on.

2.1 RoF and R&F architectures for mm-wave communications

The FiWi (Fiber-Wireless) network paradigm defines two approaches for the integration of optical and wireless networks; Radio-over-Fiber (RoF) and Radio-and-Fiber (R&F).

RoF technologies refer to the technique where Radio Frequency (RF) signals are transmitted and propagated through an optical fiber in order to provide wireless communication services[18]-[20]. In a RoF system, communication is achieved by modulating RF signals that originate from wireless networks onto an optical carrier signal. Although the technique of modulating RF signals onto optical carriers has been done in various applications, for example cable television, the term RoF is used in the literature strictly when referring to telecommunication systems. Fig. 2-1 presents a simple example of a RoF architecture, where a signal from a central station, referred as Central Office (CO) is being propagated through an optical fiber to remote antennas that are termed Remote Antenna Units (RAUs), where it is demodulated and in turn broadcasted

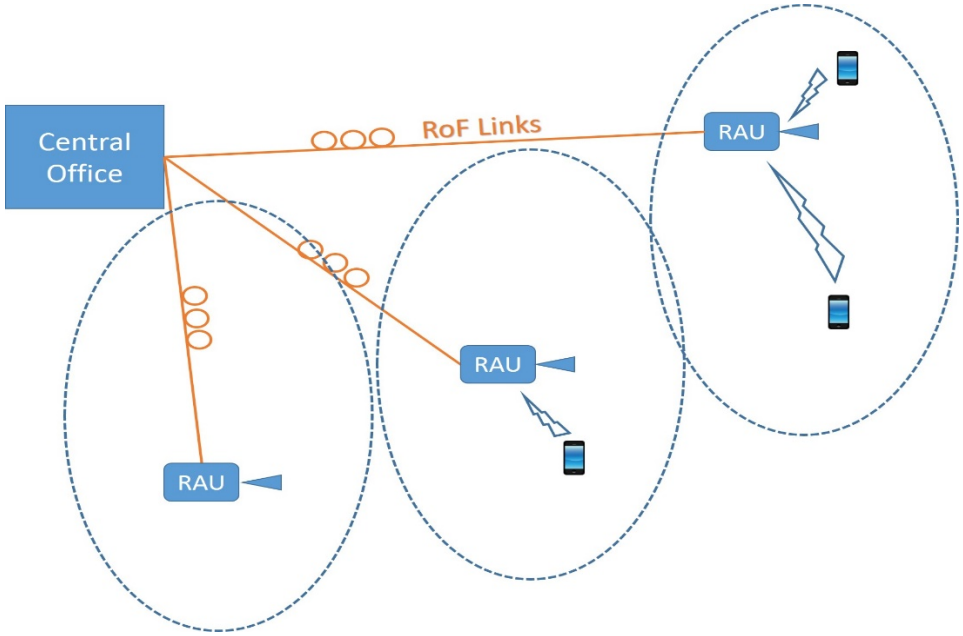

Fig. 2-1 Simple RoF access scheme with point-to-point fiber links

towards the wireless terminals through the wireless channel. The reverse procedure takes place in the uplink direction, meaning that the RF signals broadcasted by wireless terminals are modulated onto the optical carrier by the RAU and are in turn transmitted back to the CO. From this basic schematic it becomes apparent that RoF architectures are a cost-effective manner to create micro/picocellular radio architectures, since the traditional costly active Base Stations (BSs) are being replaced by a single central intelligent terminal and many low-cost RAUs. The replacement of the BS with a CO requires minimum modification in the hardware level, since the RF signals will be transmitted in an "as is" manner to the RAUs after they pass all signal processing, coding and modulation stages. This also enables the construction of very simple and low-cost RAU modules that minimize the overall capital costs while enabling the coverage of large areas, since the former do not need to perform baseband signal-processing and their small size makes their installation possible even in space-limited areas.

On the other hand of the FiWi family stand the Radio-&-Fiber (R&F) architectures that have emerged as an alternative means to provide high-speed and omnipresent access networks [34],[35]. R&F schemes consolidate existing optical and wireless infrastructures by attaching wireless APs to the Optical Network Units(ONUs), whereas access to the two distinct media is controlled separately by employing two different MAC protocols with protocol translation taking place at their interface. To this end, R&F

architectures are essentially two distinct networks, one being optical and the other wireless, that operate independently but only serve traffic generated from and for wireless clients. Fig. 2-2 displays a R&F network where a PON network is interfaced with wireless APs through the ONUs. Optical/Wireless integration is a topic of major research interest and many approaches have been presented in the literature with the most predominant being EPON/GPON integration with WiMAX/LTE/DOCSIS[36]-[39] or 802.11[40] and mesh networks[41],[42]. In that context, R&F approaches present the potential to provide high data transmission rates with minimal time delay since packets destined for intra-WLAN recipients remain in the WLAN territory whereas only inter-WLAN traffic traverses the fiber-based network. However, R&F still requires the use of fully functioning intelligent APs at every ONU branch, therefore considerably increasing the costs for WLAN mm-wave deployment.

2.1.1 FiWi networks in mm-wave applications

The nature of mm-wave communications sets a particular challenge when considering the formation of converged mm-wave/optical networks. As discussed earlier, under the RoF paradigm the role of the wireless AP is assumed by the Central Office (CO), which is attached through a fiber to a number of RAUs that in turn provide 60 GHz broadband connectivity to mobile users. The RAU modules perform the optical-to-RF and RF-to-optical conversions, bringing in contact the wireless clients and the CO without employing any further intelligent operations, thus serving as "passive" gateways. Therefore, compared to R&F, RoF schemes enable the replacement of two active equipment elements, the ONU terminal and the wireless AP, with one functionally simple RAU module. Together with the fact that mm-wave signals have high propagation losses and are extremely attenuated by walls, raises a strong argument against R&F mm-wave implementations, since the latter would require numerous arrays of active optical terminals and wireless APs in order to cover an area equivalent to the one covered by traditional 2.4-5GHz WLANs. Therefore, the implementation of mm-wave access RoF networks enables the formation of extended reach 60GHz WLANs, coming forward as a solution that avoids the added costs of the active AP equipment deployment.

In consideration of the above, R&F architectures do not come without advantages. The presence of active ONU and AP equipment in R&F systems means that intra-cell traffic (traffic that originates and terminates in the same AP) does not propagate towards the

optical network and thus avoids the fiber's extra propagation delays that are compulsory in RoF architectures. This feature also alleviates all wireless MAC restrictions from the optical portion of the network that can inhibit several aspects of the design, such as the maximum fiber length. However, the range of mm-wave signals suggests that the physical presence of the partaking nodes must be within a very confined area (<10m as specified in 802.11ad) in order to make use of the above operation, therefore severely limiting the range of applications where the adoption of mm-wave R&F architectures derives a clear benefit.

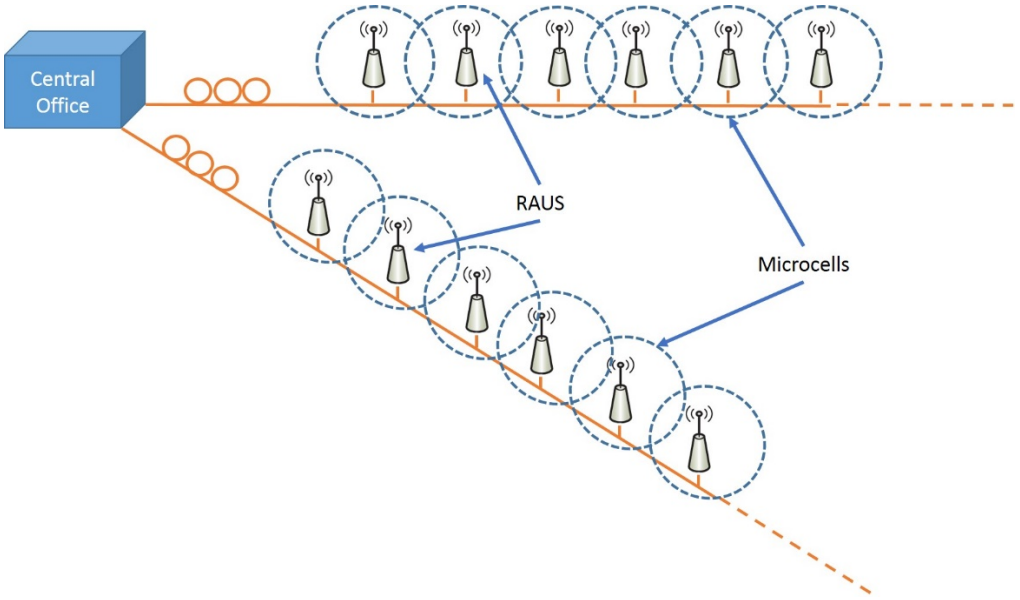

Fig. 2-2 Fi-Wi access scheme with a fiber bus network

2.2 Basics of RoF systems

RoF communications are essentially analog in nature, despite the fact that the wireless links that are propagated through the fiber carry digital data. To this end we define the analog optical links used in RoF as links where the laser is always on or links where the optical modulation depth is small enough that small signal analysis is possible. In contrast, digital optical links are the links where the modulation depth can approach 100% or the laser is turned off and on depending on the data sequence. The main principle behind RoF systems is to use the optical fiber's ample bandwidth to provide broadband wireless access by reducing the distance that the wireless channel has to travel until it reaches the wireless terminals.

Moreover, the optical fibers offer a tremendous bandwidth which allows the transmission of multi-GHz wide radio signals to far away destinations with little propagation

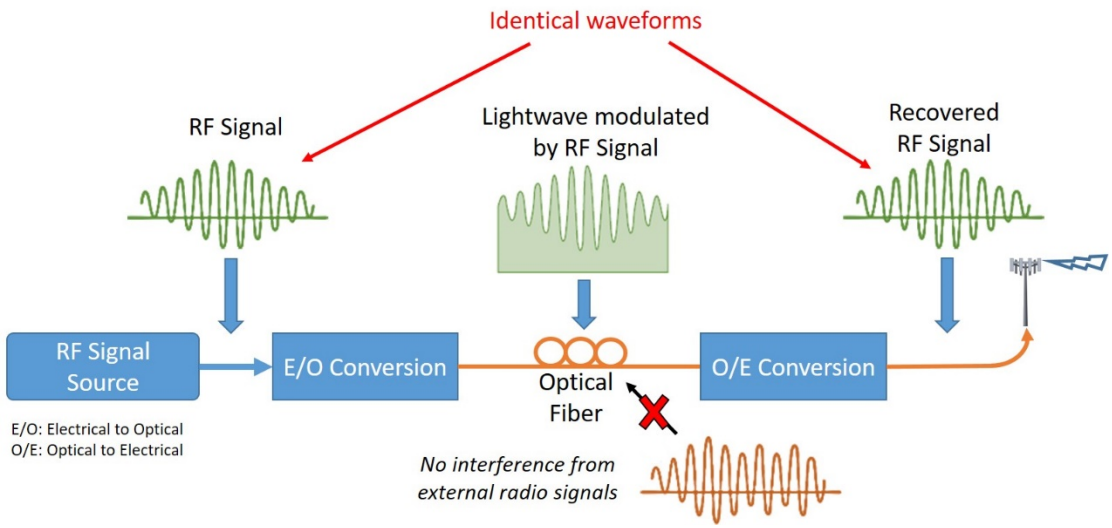

Fig. 2-3 Basic concept of a RoF system

distortion thanks to their very low attenuation properties (up to 0.2dB/km). In contrast to electrical transmission in traditional wires, propagation loss in the optical fiber is a function of the optical wavelength and is not depended on the frequency of the radio signal being transported. Therefore, the fiber's bandwidth abundance and frequency-independent low-loss properties allow for multiple RF signals to be multiplexed and transmitted via a single optical fiber or a single wavelength as it is displayed in Fig. 2-2. Because of the above, it becomes evident that RoF architectures can support multi-provider operation through infrastructure sharing not only between mobile operators that can transmit different RF signals but also amongst wireline and mobile providers that can use distinct optical wavelengths.

Fig. 2-3 shows the basic physical structure of a RoF system. As can be noted, the RoF system consists of an optical fiber link that is used for transmission and components for electrical-to-optical (E/O) and optical-to-electrical (O/E) conversions. RoF schemes have in general two major features in common:

- **Conservation of the waveform**: the waveform of the radio signal is essentially passed unchanged through the fiber-optic transmission under ideal or close to ideal conditions.
- **Electromagnetic interference resistance**: RoF signals traveling through the fiber are not affected by frequency interference from radio communication signals.

Since the RoF system is generally treated as an analogue transmission system, the overall signal-to-noise ratio and the overall dynamic range should be properly specified in order to maximize the potential of the two RoF features listed above. Digitized RoF (D-RoF) technology is an alternative candidate for transmitting radio signals over fiber, especially in cases where distortion and poor sensitivity deteriorate the analogue transmission under conditions of high noise and nonlinearity. D-RoF's efficiency strongly depends on the performance of the Digital Signal Processing (DSP) function, which is in turn influenced by the performance of analogue-to-digital and digital-to-analogue converters (ADCs/DACs). However, the introduction of DSP functions inserts also quantization noise due to digitization, which itself causes distortion in the radio waveform. Furthermore, each time domain sample is digitized to many quantized bits for binary transmission in D-RoF, therefore bandwidth efficiency of D-RoF can be much lower than that of analogue RoF. Finally, D-RoF increases overall deployment costs since it requires added DSP hardware at the RAU side. Digital interfaces for mobile base stations, such as the Common Public Radio Interface (CPRI) and Open Base Station Architecture Initiative (OBSAI), make use of the concept of D-RoF technology.

2.3 Radio-over-Fiber Physical Layer Architectures

There are several system architectures based on the RoF concept. For the typical RoF systems, where a single CO is connected to several RAUs using a single fiber-optic link, two types of signal transmissions are considered: subcarrier signal transmission and baseband signal transmission. Note here that the RoF architectures shown in this section are the most predominant examples and that alternative approaches are conceivable.

2.3.1 Analogue RoF system

a) Subcarrier signal transmission

Fig. 2-4 depicts the most fundamental architectures for transmitting subcarrier signals, such as the RF-band subcarrier, the Intermediate-Frequency band (IF-band) subcarrier and reference frequency subcarrier signals. In Fig. 2-4, all equipment located on the left

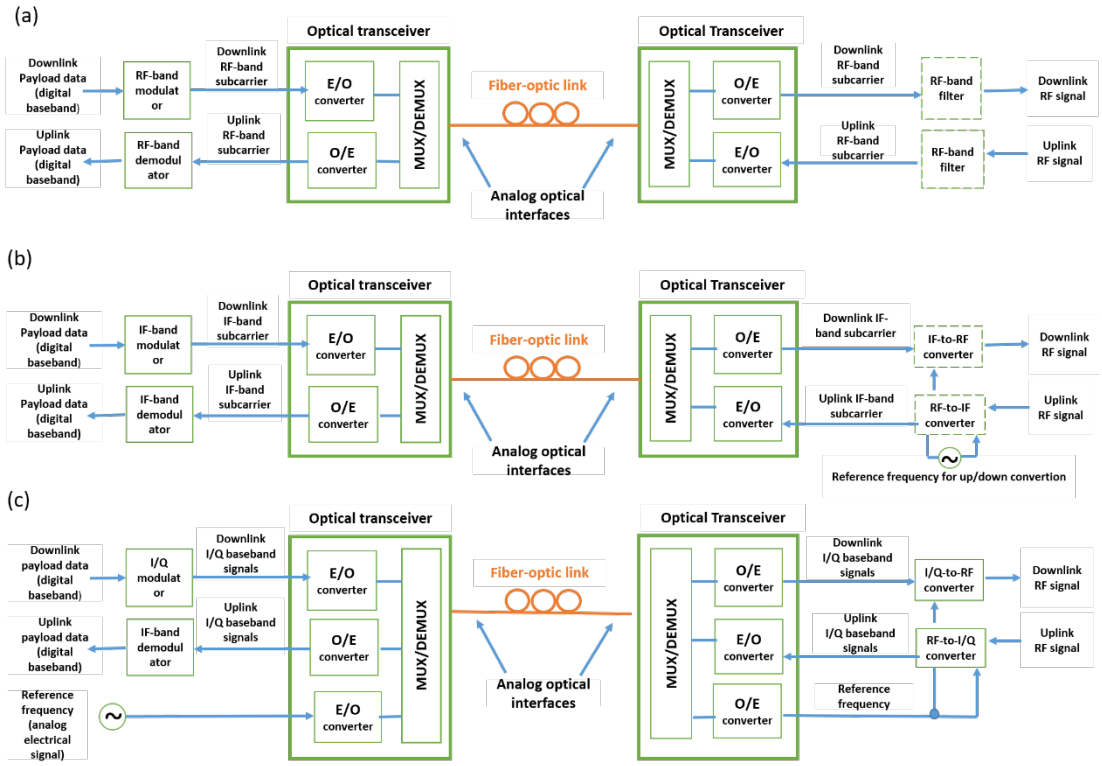

Fig. 2-4 Configuration examples for transmitting subcarrier signal(s): (a) RF-band; (b) only IF-band signal; and (c) IF-band signal and reference frequency

side of the fiber link is considered to be located in the CO, whereas equipment on the right side is considered to be located at the RAU.

In an RF-band RoF transmission scheme, such as the one shown in Fig. 2-4(a), the architecture comprises an RF-band modulator, an RF-band demodulator, two optical transceivers, the fiber link, and two RF-band filters. The latter are optional and can be used in order to comply to specific national radio regulations. In the downlink direction, payload data are being modulated onto the RF-band carrier using the RF-band modulator located at the CO. In turn, the generated subcarrier signal modulates the optical carrier using an E/O converter in the optical transceiver. The generated optical signal travels over the fiber-optic link. At the RAU site, the received RoF signal is optically detected (by means of a photodiode) and is converted to electrical form by the O/E converter. At this point, the electrical signal carries the same data as the RF-band subcarrier signal at the CO side and is transmitted over the air, optionally passing through an RF-band filter beforehand. In the uplink direction, an uplink RF signal that was received by the antenna modulates an optical carrier using another E/O converter in the optical transceiver. The generated analogue RoF signal is in turn transmitted over the optical fiber. At the CO, the received RoF signal is optically detected and modulated

upon an electrical carrier in the optical transceiver. Finally, the electrical signal is demodulated using the RF-band demodulator to recover the uplink payload data.

In an IF-band RoF architecture, like the one shown in Fig. 2-4(b), the system comprises an IF-band modulator, an IF-band demodulator, two optical transceivers, a fiber-optic link, an IF-to-RF up-converter, an RF-to-IF down-converter, and a reference frequency generator. Since the intermediate frequency is generally a lot lower that the RF, this scheme offers a much higher bandwidth efficiency compared to the RF-band RoF scheme. In the downlink direction, payload data are being modulated onto the IF-band carrier using the IF-band modulator located at the CO. In turn, the generated subcarrier signal modulates the optical carrier using an E/O converter in the optical transceiver. The generated optical signal travels over the fiber-optic link. At the RAU site, the received RoF signal is optically detected (by means of a photodiode) and is converted to electrical form by the O/E converter. At this point, the electrical signal, which carries the same data as the IF-band subcarrier signal at the CO side, is frequency up-converted by the IF-to-RF up-converter in a reference frequency in order to produce the desired downlink RF signal. In the uplink direction, the received uplink RF signal is down-converted by the RF-to-IF down-converter to an IF-band subcarrier signal. In turn, the generated IF-band subcarrier signal modulates the optical carrier using the second optical transceiver. The analogue RoF signal travels through the fiber-optic link. At the CO side, the received signal is optically detected at the optical transceiver and converted to electrical form. The electrical signal is demodulated using the IF-band demodulator and the uplink payload data is recovered. In an IF-band RoF and reference frequency transmission scheme, such as the one displayed in Fig. 2-4(c), the system configuration is the same as the one described in the IF-band RoF transmission scheme shown in Fig. 2-4(b), with the exception that the reference frequency is provided by the CO and is delivered to the RAU site.

Because the main parts of the radio transceiver, like the modulators/demodulators, are being placed in the CO, the actual hardware of the RAU becomes simpler and therefore cheaper. In the architectures where the radio frequency does not change between the CO and the RAU, the mobile operators can readily adopt the RoF technologies, since there is no requirement for change in the antenna sites' configurations. Also, since the main part of the radio transceivers is located at one central location, it becomes very easy to maintain, repair and upgrade the CO and therefore the level of service.

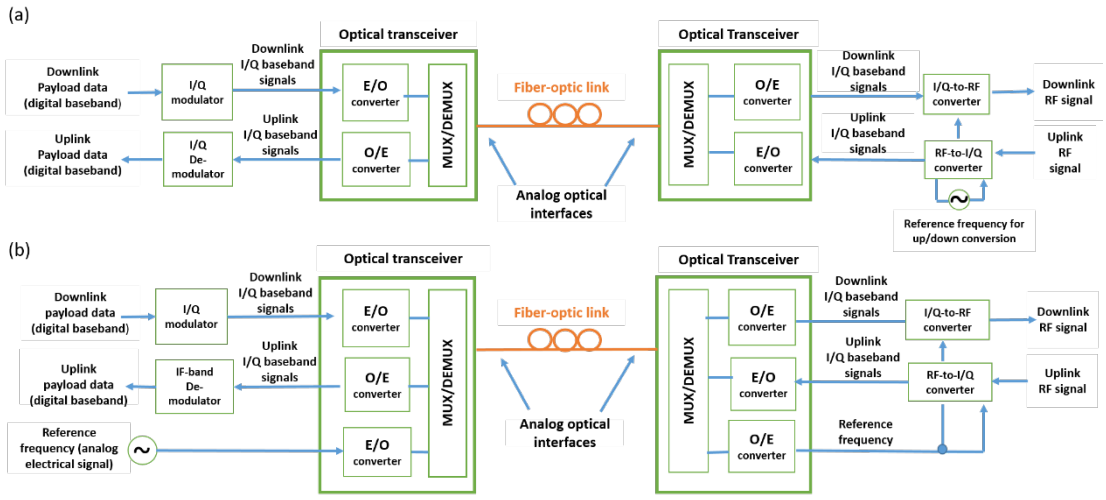

Fig. 2-5 Configuration examples for transmitting equivalent low-pass signal(s): a) only I/Q baseband signals; and b) I/Q baseband signals and reference frequency

b) Equivalent baseband signal transmission

Fig. 2-5 illustrates generic architectures for transmission of orthogonal equivalent low-pass (equivalent baseband) signals, such as (non-binary) in-phase and quadrature-phase (I/Q) baseband signals. In all illustrations, the equipment that resides on the left side of the figure is considered to be located in the local office, whereas the equipment that is located on the right side is considered to be on the remote antenna.

Fig. 2-5(a) depicts an I/Q baseband signals transmission scheme that consists of an I/Q modulator, an I/Q demodulator, a pair of optical transceivers, a fiber-optic link, an I/Q-to-RF up-converter, an RF-to-I/Q down-converter, and a reference frequency generator. In the downlink direction the I/Q modulator generates the I/Q baseband signals from the downlink payload data that is received at the CO. The generated I/Q baseband signal modulates the optical carrier through the E/O converter of the optical transceiver. In turn, the produced downlink multi-level or analogue baseband signal, is transmitted over the fiber-optic link. At the RAU end, the received downlink optical signal is optically detected by means of the O/E converter in the optical transceiver. The generated electrical signal, is then frequency up-converted with the I/Q-to-RF up-converter and a reference frequency to the desired downlink RF signal. In the uplink direction, the received I/Q baseband signal modulates an optical carrier using the E/O converter in the optical transceiver. The generated multi-level or analogue baseband signal is then propagated towards the CO over the fiber-optic link. The CO receives the optical signal through a photodiode and in turn converts is to electrical through the use of the O/E

converter in the optical transceiver. The electrical signal is demodulated at the I/Q demodulator and the uplink payload data is recovered.

Regarding the I/Q baseband signals and reference frequency transmission scheme depicted Fig. 2-5(b), the system formation is the same as that of the I/Q baseband RoF signal transmission scheme depicted in Fig. 2-5(a), except that the reference frequency is provided by the CO and is delivered to the RAU site.

2.3.2 Digital RoF system

a) Digital radio signal(s) transmission

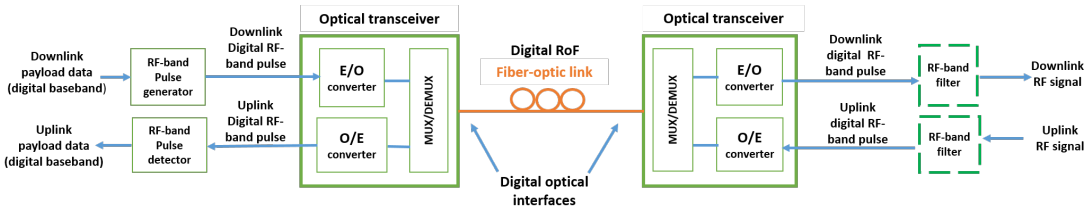

Fig. 2-6 Configuration examples for transmitting digital signal(s): RF-band pulse

Fig. 2-6 depicts a digital RoF architecture for transmitting digital radio signals, such as RF-band pulses. In Fig. 2-6 the equipment that resides on the left side of the figure is considered to be located in the CO, whereas the equipment that is located on the right side is considered to be on the remote antenna.

A digital RoF system consists of an RF-band pulse generator, a RF-band pulse detector, two optical transceivers, the fiber-optic link, and two RF-band filters. The latter are optional and can be used in order to comply to specific national radio regulations. In the downlink direction, the RF-band pulse generator located at the CO generates an RF-band pulse containing downlink payload data. The pulse modulates an optical carrier by means of an E/O converter located in the optical transceiver side. The newly formed downlink digital RoF signal is in turn transmitted over the optical fiber. Note here that although the optical link is treated as being digital, the nature of the signal transmission could be closer to analogue form. This is due to the fact that the produced/received signal's intensity may carry an analogue form, like a monocycle pulse, doublet pulse etc. At the RAU end, the received downlink optical signal is optically detected by means of the O/E converter in the optical transceiver. The derived electrical signal has the same form as the modulating RF-band pulse. In the uplink direction, an uplink RF-band pulse, modulates an optical wavelength using an E/O converter in the optical

transceiver. The generated uplink digital RoF signal is then propagated towards the CO over the fiber-optic link. The CO receives the optical signal through a photodiode and in turn converts is to electrical through the use of the O/E converter in the optical transceiver. The electrical signal, which is exactly the same as the uplink RF-band pulse, is demodulated by means of a RF-band pulse detector and the uplink payload data is recovered.

b) Digitized radio signal(s) transmission

Fig. 2-7 presents a general schematic for transmitting digitized radio signals, such as digitized RF-band subcarrier, digitized IF-band subcarrier, and digitized I/Q baseband signals. In Fig. 2-7, the equipment that resides on the left side of the figure is considered to be located in the CO, whereas the equipment that is located on the right side is considered to be on the remote antenna.

Fig. 2-7(a) displays an RF-band RoF transmission scheme comprising a digital RF-band modulator, a digital RF-band demodulator, a pair of optical transceivers, a fiber-optic link, a D/A Converter, an A/D Converter, and two RF-band filters. The latter are optional and can be used in order to comply to specific national radio regulations. Regarding the downlink direction, a digitized RF-band subcarrier is digitally generated containing data by employment of a digital RF-band modulator located at the CO. The digitized RF-band subcarrier signal modulates an optical carrier by means of an E/O converter located in the optical transceiver side. The newly formed downlink RF-band D-RoF signal is in turn transmitted via the optical fiber towards the RAU. At the RAU side, the received signal is converted to electrical form by means of an O/E converter in the optical transceiver. The generated electrical signal that, in this stage is equivalent to the digitized RF-band subcarrier signal produced in the CO, is converted to analogue form in order to recover the desired downlink RF signal. In the uplink direction, a received uplink RF signal is converted from analogue form to digital by means of the D/A converter. In turn this signal modulates an optical carrier using the other E/O converter in the optical transceiver. The generated signal is propagated over the fiber-optic link. At the CO side, the received D-RoF signal is optically detected by means of an

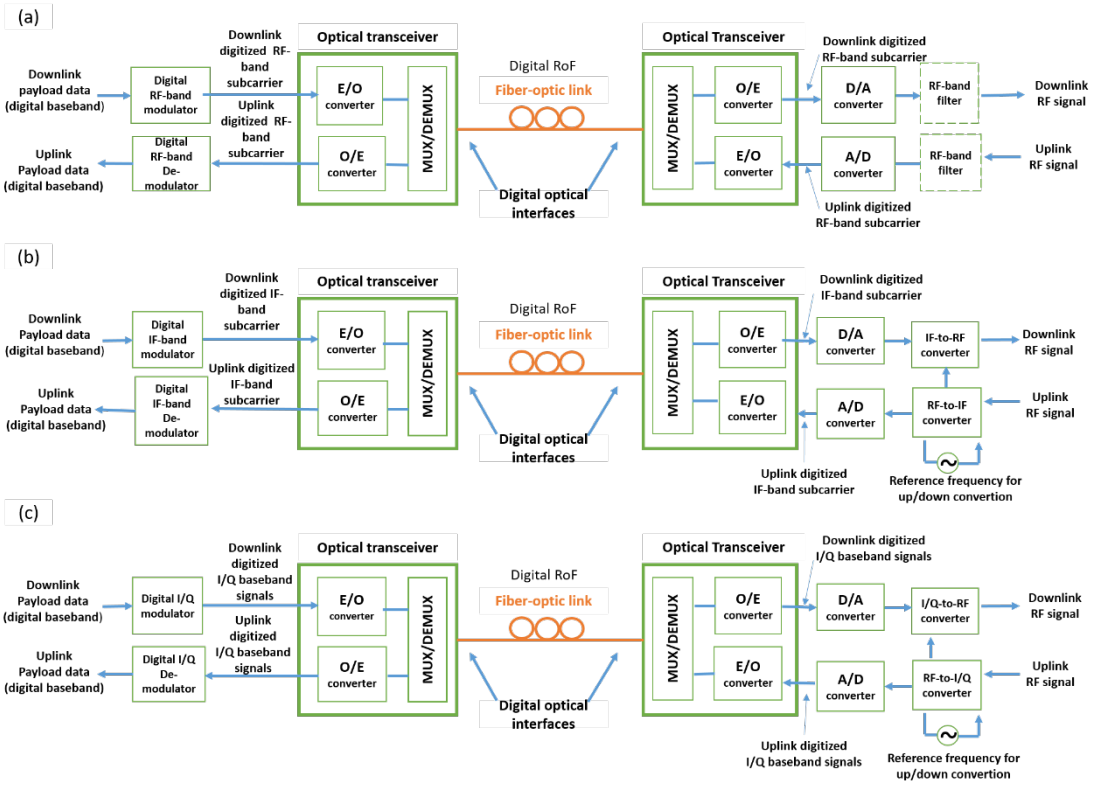

Fig. 2-7 Configuration examples for transmitting digitized signal(s): a) digitized RF-band signal(s); b) digitized IF-band signal(s) and c) digitized I/Q baseband signal(s)

O/E converter in the optical transceiver. The detected electrical signal, which is equivalent to the digitized RF-band subcarrier signal, is digitally demodulated with the digital RF-band demodulator to extract the data payload.

Fig. 2-7(b) displays the equivalent digitized RoF systems with the use of IF bands. The only difference to the previous scenario is that the modulators are designed to modulate to and from the IF band and that at the receiver a reference frequency generator is employed to provide the mean for the up-conversion. The choice of the reference frequency should be made such that it complies to the frequency stability specifications regarding the downlink RF signal.

Fig. 2-7(c) displays a digitized I/Q baseband signals RoF transmission scheme. In such a system a digital I/Q modulator/demodulator is used instead of the RF and IF modulators described in the cases above. In both directions, the digital I/Q modulators generate digitized I/Q baseband signals from the downlink and uplink payloads received at the CO and RAU ends. In turn the generated downlink digitized I/Q baseband signals modulate an optical carrier using an E/O converter and are transmitted to the other end.

Again as with the previous cases the digitized radio signal(s) (D-RoF) transmissions require DACs and ADCs at the RAU end to be converted to analogue form.

2.3.3 RoF for Millimeter Wave RF transmission

The modern communication patterns of home and enterprise mobile users, such as E-health/Telemedicine[43], High-Definition (HD) real-time multimedia streaming and remote wireless display applications[23] require the exchange of unprecedented amounts of data, resulting in the placement of excessive load strain on the existing wireless infrastructure. This has forced governments, mobile operators and hardware manufacturers to gradually expand their activities from GSM/WiFi-centric networks, that currently employ frequencies up to 5 GHz, to higher portions of the wireless spectrum such as the millimeter-wave band, where several GHz of bandwidth is available. However, mm-wave signals suffer from high free-space propagation losses. According to Friis' equation, free-space power loss of a wireless signal is proportional to the square of its carrier frequency f_c:

$$path\ loss = \left(\frac{4\pi d f_c}{c}\right)^{\gamma}$$

where c is the speed of light, γ is the path-loss exponent ($\gamma = 2$ in free-space), and d is the distance between the base station and the mobile user. However, γ can vary from 1.5 to 6 depending on the environmental conditions. According to Friis' formula in free space, the loss at 60 GHz will be 5184 times, or 37 dB higher than the loss at 1 GHz. If the path-loss exponent is higher, for example 4, this loss would be 25 million times higher or 74 dB. In addition, the millimeter-wave bands have some other peculiar characteristics such as very high losses through obstacles and are greatly affected by water molecules in the air. 60 GHz signals in particular have an added property that is known as oxygen attenuation, meaning that 60 GHz signals react with the oxygen molecules in the air and as a consequence loose a part of their energy. This loss is considered to be around 12–16 dB/km, which is relatively high and is therefore the main reason that 60 GHz links fail to cover excessively large distances. To this end RoF technologies are a perfect match to be used in conjunction with 60 GHz signals since they can alleviate the distance barrier and can feed 60 GHz access points located several km away from the CO. Moreover, innovative and efficient microwave photonic techniques that allow the generation and processing of mm-wave signals natively in the RoF domain

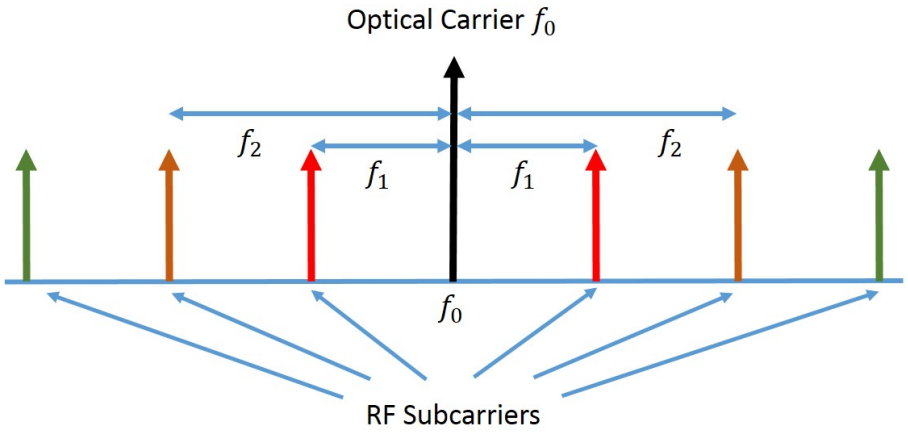

Fig. 2-8 Subcarrier-multiplexed ROF signal

have recently been presented[44], bringing an added incentive towards implementing practical converged RoF/mm-wave networks.

Recent advances in Microwave Photonics (MWP) have made possible the generation, transmission and processing of microwave signals and offer various advantages compared to other electrical approaches, such as high bandwidth, low losses, freedom from electromagnetic interference, fast tunability and reconfigurability [45]. These techniques have opened up many new possibilities since it is now possible to generate very stable and clean microwave signals by optical heterodyning or by frequency multiplying/dividing techniques. When these radio signals travel through fiber, they can be amplified through erbium-doped fibers or through Semiconductor Optical Amplifiers (SOAs). In Wavelength Division Multiplexed (WDM) networks, the use of various filters, such as Bragg gratings, have been demonstrated to demultiplex wavelengths along with RF subcarriers[46]. RF signals can be very easily up or down-converted using optical nonlinearities, which in turn enables the transmission of the signals in low frequencies over the fibers and only upconvert them at the RAU module. Singe-Side Band (SSB) modulation, a refinement of amplitude modulation which uses transmitter power and bandwidth more efficiently, can be generated at the millimeter-wave scale using MWP techniques. Fig. 2-8 shows the spectrum of a double sided subcarrier-modulated (DSB) signal. We can note that each subcarrier is separated from the main carrier signal by its radio frequency f_1, f_2, respectively. Fig. 2-9 displays how DSB signals can be optically demultiplexed using ultra-narrow bandpass filters.

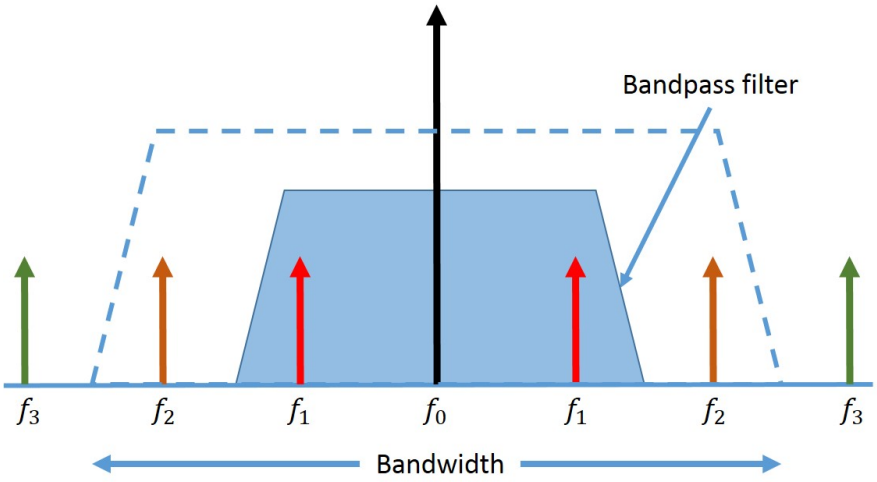

Fig. 2-9 Ultra-narrow microwave photonic filters can be used to demultiplex subcarrier-multiplexed RF signals

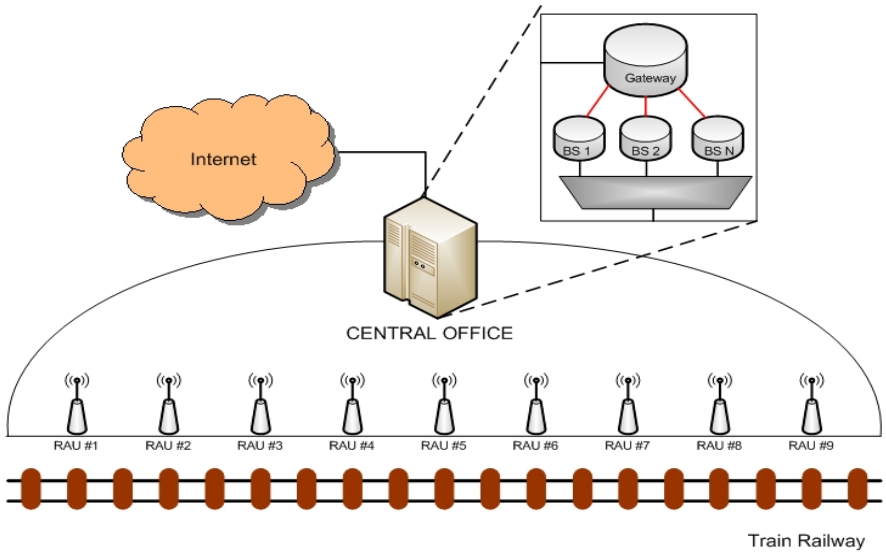

Fig. 2-10 Moving cell-based RoF network architecture for train passengers

2.4 Mobility in RoF networks

2.4.1 Moving Cell

High velocity moving terminals, like the case of train passengers, suffer from frequent handovers when hopping from one BS to another in the common cellular networks. Frequent handovers may cause numerous data losses and intolerable degradation of the end-user experience, resulting in a significantly decreased network throughput. A modern approach towards the solution of this problem is the employment of a RoF network installed along the rail tracks in combination with the higher level moving cell concept[47]. Fig. 2-10 illustrates the moving cell-based RoF network architecture

for a rail example. An optical WDM ring connects the RAUs with the CO who acts as a central hub and performs all the necessary processing. Each RAU uses an Optical Add-Drop Multiplexer (OADM) fixed tuned to a separate optical wavelength. At the CO, a WDM laser generates the set of the available and currently desired optical wavelengths, which are passively switched and introduced into an array of RF modulators, one for each RAU. The now modulated wavelengths are multiplexed onto the optical fiber which follows a ring formation and are received by the corresponding RAUs on their respective assigned wavelength. The RAU modules retrieve the RF signal and transmit it into the air which is consequently received by the antennas of a passing train. Following the upstream direction, the RAUs receive all RF signals from the air and modulate them into a CO transmitted optical wavelength which travels back to the CO for processing. By processing the received RF signals, the CO is able to keep track of the current train positioning by identifying the RAU closest to the moving clients. Consequently, it assigns downstream RF signals to the corresponding RAU such that the train and moving cells move along in a synchronous fashion.

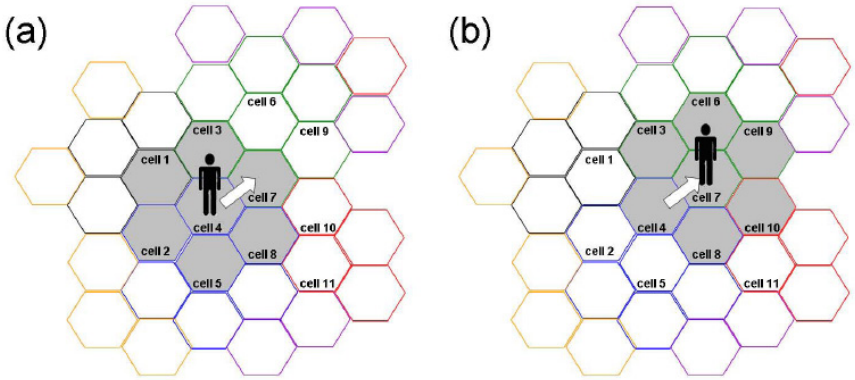

Fig. 2-11 Moving cell-based RoF network architecture for train passengers

2.4.2 Moving Extended Cell

The Moving Extended Cell[48] is essentially an upgraded version of the Moving Cell. This scheme guarantees zero packet loss and speedy handovers by providing connectivity in any possible direction. A hybrid Frequency-Division Multiplexing FDM/WDM network architecture was used in order to support the deliverance of multiple RF channels in the 60 GHz spectral band travelling over the same wavelength. As it is depicted in Fig. 2-11, the extended cell is essentially a cell comprising the current user's cell and the surrounding cells, ensuring continued connectivity in any possible random direction. The extended cell scheme adaptively adapts and relocates the center

of the extended cell when the user moves into a new cell. It was shown experimentally that the proposed concept can provide zero packet loss and call dropping probability in high-rate wireless services for a great range of mobile speeds of up to 40 m/s independent of fiber link distances.

It must be noted here that concepts revolving around the spatial extension of RoF cells in order to cope with mobility problems, by unifying existing picocells face new challenges since the introduction of high speed trains, capable of achieving speeds up to 80 m/s, is becoming a reality throughout the globe, and therefore stricter mobility configurations should be tested.

2.4.3 The Chessboard protocol

The Chessboard protocol[49] is a MAC protocol designed to provide handover functionalities in a RoF based WLAN operating at 60 GHz. This protocol is based on the employment of Frequency Switching (FS) codes. Adjacent cells employ orthogonal FS codes to avoid possible co-channel interference. This mechanism allows a mobile host (MH) to stay tuned to its frequency during handover.

The simple structure of the BS and 60-GHz wave characteristics leads to a centralized network architecture with many picocells, where most of the BS functions of conventional WLANs are shifted to the CS. By subdividing the total system bandwidth, 2M (frequency) channels are obtained, where M channels $(f_1, f_2, \dots, f_M)$ are used for down-link transmission and the other M channels $(f_{M+1}, f_{M+2}, \dots, f_{2M})$ for up-link transmission. In addition, the time axis is also subdivided into time slots of equal length and M time slots are grouped into a frame. The reason for having the same number of time slots and frequency bands is to formulate a square array that resembles a chess board, which consequently will be used as the basis of the FS codes. The MS is assigned a pair of channels $(f_i, f_{M+i})\ i = 1, 2, \dots M$ and a pair of time slots $(t_k\ mod\ M, t_{k+1}\ mod\ M)\ k = 1, 2, \dots$ for down- and up-link communication, respectively. Only after having received a permit from the down-link channel f_i during the time slot $t_k\ mod\ M$, the MS may transmit up-link packets over the up-link channel f_{M+i} during the next time slot $t_{k+1}\ mod\ M$. Every BS supports all channels, but each of them

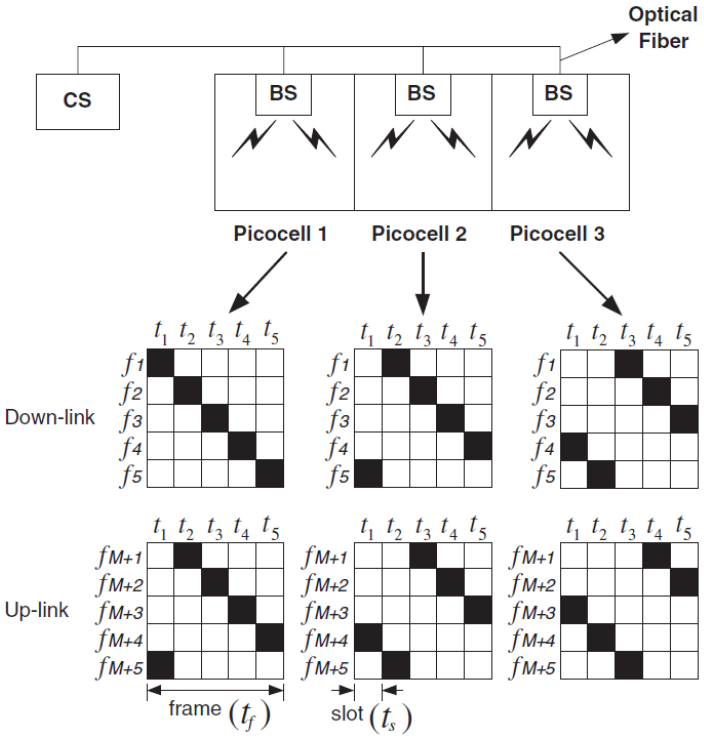

Fig. 2-12 Example of Chessboard protocol operation. The FS patterns here correspond to 5 channels. Each room(picocells) has its own BS and BSs are connected to the control station (CS) using optical fiber. Adjacent picocells have different FS patterns to avoid interference[49].

is used in the proper time slot. Fig. 2-12 shows an example FS patterns for down- and up-link, respectively, when M is five. During every frame time, each of the M time slots and M channels is utilized once and only once. Adjacent picocells must not use identical FS patterns to avoid possible co-channel interference.

2.5 Multiservice Access Networks

One of the major advantages of the RoF architectures is that they can be deployed alongside other services by exploiting the immense bandwidth of the optical fiber thus setting themselves as the future of multiservice access networks. In order to achieve that however, it is important to integrate RoF systems with existing optical access networks. [50] presents a novel approach for simultaneous modulation and transmission of both RoF RF and Fiber-To-The-Home (FTTH) baseband signals using a single external integrated modulator, as shown in Fig. 2-13. This external integrated modulator is comprised of three distinct Mach-Zehnder Modulators (MZMs) 1, 2, and 3. RF and FTTH baseband signals independently modulate the optical carrier generated by a common laser diode by using either one of the first two MZMs respectively. Subsequently, the optical wireless RF and wireline baseband signals are combined at the third MZM. After propagation of the aggregated signal over an SMF downlink, an optical filter (e.g.,

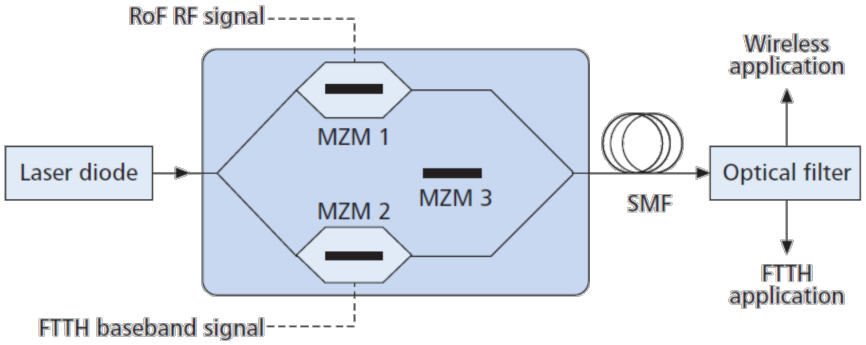

Fig. 2-13 Simultaneous modulation and transmission of FTTH baseband signal and RoF RF signal using an external integrated modulator consisting of three Mach- Zehnder Modulators [35]

fiber grating) is used to split the two signals and route them to the wireless and FTTH module respectively. It has been experimentally demonstrated that a 1.25 Gb/s baseband signal and a 20 GHz 622 Mb/s RF signal can be simultaneously modulated and transmitted over 50 km standard SMF with acceptable performance penalties.

In [51] the transmission of a wireless IF over a WDM PON architecture was experimentally investigated. The proposed network configuration was designed to provide service for third-generation cellular and WiMAX subscribers, as well as wired optical subscribers. In [51] a single wavelength for the downstream direction and multiple wavelengths for the upstream direction were considered. The displayed results prove that a WDM PON with 8 orthogonal FDM (OFDM) channels is able to support 32 ONUs with a 3 dB power penalty.

2.6 MAC Protocols in RoF systems

Under this section we provide a summarization of the published work considering MAC protocols established on top of RoF infrastructures.

2.6.1 Performance Impairments of existing protocols over RoF

Below we present various published studies that have been carried out in terms of adapting existing wireless protocols to underlying RoF infrastructures and the problems that arise due to the medium's duality. [52]-[54] offer extensive analytical and experimental implementations of IEEE 802.11 over RoF, specifically focusing on the impact of the introduced fiber delay which is nonexistent in traditional WLAN links. As it has been shown, data throughput decreases as fiber length increases although the performance degradation is being kept below 15% in most cases. What is noteworthy though is that when fiber length exceeds a certain point, a total network failure was observed.

This is due to the time constraint nature of 802.11, which dictates the use of certain Inter Frame Spacing (IFS) limits on which the protocol's synchronization depends. 802.11 works in two modes. In the first one, which we refer to as "Basic Access Method" or "Two Way Handshake", the receiving station acknowledges a successful reception by transmitting an ACK packet after a certain short interframe time interval called SIFS. The transmitting station waits for the ACK packet for a time duration specified as the ACK_Timeout parameter, at the end of which if no ACK has been received the transmission is considered lost and the station prepares for retransmission. When the fiber delay associated with each optical link exceeds the ACK_Timeout value, the network's performance degrades rapidly. In the second mode of operation, where the RTS/CTS mechanism is employed, each station tries to "capture the floor" by transmitting a Ready To Send (RTS) or Clear To Send (CTS) message, depending on the whether it is the source or destination station. After the transmission of the RTS frame the source station starts a countdown timer (CTS_Timeout), which leaves enough time for the reception of the CTS frame. If the expected response is not received within the CTS_Timeout window, the source station assumes that the frame is lost and hence prepares itself for retransmitting the RTS frame. The problematic behavior here multiplies due to the fact that other stations in the vicinity hearing either an RTS or a CTS or both, defer their transmission by adjusting their Network Allocation Vector (NAV), a timer, to the duration field value of the RTS/CTS frame, which essentially leads quicker to a complete network failure. The maximum supported fiber lengths where found to be 13.2 km for the Basic Access scheme and 8.1 km when the RTS/CTS mechanism was employed. Fig. 2-14 depicts the experimental results derived from [53].

The above studies depict clearly the pros and cons regarding the adaption of existing protocols onto RoF architectures. Although it is proven that under certain conditions 802.11 is able to be straightly utilized, we argue that the "as is" basis fails to fully comprehend and exploit the possibilities of RoF technologies, since the optical based infrastructure is strictly considered as a passive medium destined only to propagate wireless signals. This creates an inflexible network where restrictions apply not only on the maximum fiber length, but also on the maximum number of the serviced RAUs, since each one requires a dedicated optical wavelength. The latter increases RoF deployment costs since more CO units will be required for coverage of large area, due to the finite number of supported optical wavelengths by the optical fibers, whereas with

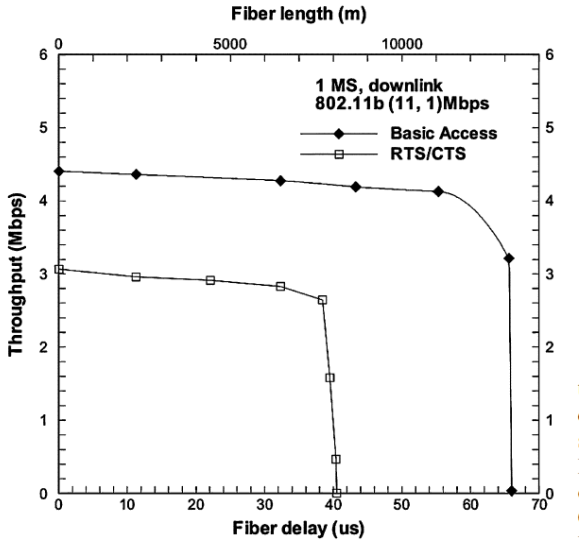

Fig. 2-14 Experimental result of an 11 Mbps TCP Basic and TCP RTS 802.11 system. Note, the ACK Timeout is greater than the CTS Timeout [53].

the use of a flexible and dynamically allocated optical medium it is possible to service significantly larger areas by the same residential gateway. In addition, the above fail to provide a provisional discussion over the adoption of the high bandwidth, future proof, mm-wave bands that would clearly tip the scale over cost issues.

2.6.2 MAC protocols for Wireless Sensor Networks over RoF

Wireless Sensor Networks (WSNs) are networks whose main purpose is to autonomously interconnect small functionally simple and usually battery operated Sensor Nodes (SNs) and cooperatively pass information to one or more BSs, that in turn propagate the traffic to extra-WSN destinations. Their main target is to monitor physical or environmental conditions, such as temperature, sound, pressure etc., and they are currently used in a variety of versatile applications such as area monitoring, health care monitoring, pollution monitoring, forest fire detection, battlefield reconnaissance and emergency rescue operations. The convergence of WSNs networks with RoF architectures has received notable attention, since RoF links can provide for low delay and increased reliability when compared to traditional WSN connectivity [55]. In addition, RoF-enabled WSN networks can significantly decrease the cost of WSN deployment in areas with underutilized fibers since it alleviates the need to install several new BSs. Several protocols have been proposed for use in RoF-based WSNs.

The SPP-MAC protocol[56][57] combines polling and prioritization queueing allowing the designation of different amount of slots to each sensor node, depending on

the importance this node plays in the network's function. For energy saving purposes which is a crucial factor in WSNs, the SSP-MAC turns transceivers on only when the SNs need to transmit frames. When an SN has outstanding data to transmit it activates its transceivers and waits the reception of a polling frame from the BS. When such a frame is received, the node transmits its stored date. In turn the BS checks if the SN has requested an acknowledgment and, if so, it sends back an ACK frame to the SN before transmitting a polling frame to the next node on the polling list. In order to avoid overhearing, the SPP-MAC also facilitates header scanning operations, where an SN will examine the destination address of a MAC frame as soon as the latter arrives at the SN, and if found to be destined to another node the SN transceiver is automatically turned off, thus avoiding reception of the whole frame.

The HMARS protocol[58][59] uses a combination of Time Division Multiple Access (TDMA) and Carrier Sense Medium Access (CSMA) mechanisms. The first approach is used to ensure a collision-free optical channel while the second is used in the wireless domain to avoid a collision. In HMARS it is considered that the SNs that are within the coverage area of a single RAU form a cluster. All clusters transmit data to the same CO. In the optical medium that employs TDMA operation, time is divided into frames and each frame is divided further into slots. HMARS assigns a static and unique slot to each cluster during which this cluster has the exclusive right to transmit. A direct consequence of that is that transmissions originating from SNs belonging to different clusters do not collide. In the wireless domain where CSMA is employed, a SN having outstanding packet transmissions senses the wireless channel, and in case it finds it busy, it postpones its transmission for a later time. In case the channel is found idle then it waits a random time interval and transmits the frame. In this way HMARS avoids RTS/CTS exchange and instead utilizes random back off timers in order to reduce overhead and collisions.

The authors in [56] have recently introduced the D-HMARS protocol, which stands for Dynamic-HMARS and differs from HMARS by incorporating a dynamic contention period. The D-HMARS protocol defines an extra type of frame, termed as the beacon frame, which is employed by the BS in order to transmit the scheduling configurations of the Superframe. The latter defines the transmission intervals and the number of data packets used in all data transmissions. Each transmission round is comprised of two phases: the setup and the execution phase. During the setup phase, the BS and the

SNs synchronize their clocks, the Superframe is devised and transmitted via the beacon frames. In the execution phase, all data packets are transmitted by both the BS and the SNs using the dynamic and non-persistent CSMA/CA mechanism.

All of the aforementioned protocols are designed to be used specifically in RoF enabled WSNs and as such lack some necessary qualities for being deployed in general purpose mm-wave communications. First of all, WSN communications are extremely low-bandwidth. Most WSNs assume a transmission rate of around 250kb/s [56]-[61] which means that several hundred SNs can transmit simultaneously without overburdening the fiber capacity. In mm-wave connections however, each node is assumed to operate at the Gbps range therefore necessitating an optical arbitration scheme that schedules and prioritizes transmission windows in order to cope with incoming traffic. Secondly SNs employ a frequency of sub-1GHz[56]-[61] and therefore can employ mechanisms such as CSMA which is unsuitable in the mm-wave band due to directional transmission. In addition, all the above protocols assume that the SNs are un-movable and always connected to the same RAU, a principle that does not apply to general purpose terminals which can go in and out of range of the RAUs as the users constantly move. Finally, the large transmission range offered by the sub-1GHz bands means that only few RAUs are necessary in order to provide WSNs with large areas of coverage and therefore the small number of RAUs is assumed to always have an active connection. In the mm-wave environment however, the large number of RAUs necessitates a multi-wavelength source and wavelength assignment/de-assignment, as constant connectivity with a huge number of limited range RAUs that are not continuously used would be extremely bandwidth demanding and inefficient.

2.6.3 Mm-wave based adaptations of existing protocols over RoF

RoF advantages become increasingly important as the unprecedented escalation in wireless bandwidth demand drives the need for employment of wireless frequencies capable of delivering enhanced data rates but with the downside of exhibiting range crippling propagation losses. A noteworthy example is the license exempt 60GHz band which has by now been adopted by the industry as the prevailing candidate region for broadband wireless data transfer and has already been enforced in a significant number of emerging standards. Since the high loss nature of the mm-wave radio constitutes a significant constraint in terms of effective range coverage, 60GHz functionalities are

still inevitably bound to PAN applications. [62] offers a study of both the IEEE 802.11 and ETSI HiperLAN/2 protocols adapted on a mm-wave backhaul RoF architecture. The presented results show that when radio operates in the mm-wave band 802.11 performance degrades significantly due to synchronization problems, issued by the mm-wave medium, which consequently deems the protocol's performance as unsatisfactory and unacceptable. Specifically, the main reason for this behavior is the peculiarity of the mm-wave radio which exhibits extreme propagation losses. An immediate consequence of this configuration is that mobile stations in one radio cell are completely hidden to mobile stations in other cells. Hence it is logical to consider that the radio cells are independent to each other. As a result, several wireless terminals in different cells can decide that the medium is idle and start sending their packets at the same time. Collision will thus occur at the CO when these signals are collected. In accordance to the previous, [62] also displays the argument that a centralized protocol like the HiperLAN/2 is more suitable for RoF applications since it suffers less from hidden terminal phenomena, although is actually not immune to them. In HiperLAN/2 all mobile stations have to use the so called Random Access (RA) phase to transmit Resource Request (RR) messages to the CO. As a result, HiperLAN/2 networks employing RoF also suffer from the hidden-terminal problem, since the high propagation loss nature of the radio prohibits the formation of fully connected networks. However, once a wireless terminal has successfully reserved the resource, it enters the contention-free phase in which resource is explicitly reserved for that Mobile Station (MS). As a result, the hidden-terminal problem does not affect the contention-free phases in HiperLAN/2 MAC frames. Moreover, since the number of active connections in a radio cell/room in the indoor environment is normally small, in an H/2 network the probability of two or more packets transmitted at the same time is much less than the probability of collision caused by packets transmission in an 802.11 network.

2.7 Practical demonstrations of RoF technology

The first major applications that set RoF research in motion started in the early 1990s with a goal to provide fast and uninterrupted wireless access to subway stations. Until recently, the installation of RoF systems had mostly been considered as suitable for special areas like tunnels, underground stations and mines, where the traditional BSs could not provide service. Later on, RoF systems were proposed as cost effective solutions for other types of scenarios such as very crowded areas like airport, malls, city

centers etc. [63]. The first real and large scale testbed for ROF-based FiWi solutions took place in the Sydney Olympics of 2000. The organizing committee selected RoF as the technology of choice in order to set up a microcellular network for all venues and stadiums with more than 500 indoor and outdoor microcells. The available optical bandwidth was used by three distinct mobile providers, each one operating at a dedicated licensed radio frequency. The concurrent transmission of all three spectral bands was realized by employment of the subcarrier multiplexing technique. Each RAU module provided coverage for a 0.8×1.8 km^2 area, with the network capacity being dynamically reallocated through the day as the crowds moved from venue to venue. This successful demonstration of the potency of RoF technology has been the major incentive for adopting RoF systems in mainstream wireless networks with even more large-scale projects taking place after 2000.

Other notable projects that have been recognized as milestones in the development of novel RoF architectures are China's Telecom 3G project named FUTURE[64], Korean Telecom's 3G broadband project WiBro[65], and the EU Framework 7 project codenamed FUTON[66]. In lab-based testbeds researchers have demonstrated various RoF FiWi systems capable of transmitting at rates above 3 Gbit/s[67]. In [68] the authors present a full duplex 10-Gbit/s, 60 GHz RoF Orthogonal Frequency-Division Multiplexing (OFDM) system transmitting over a 50-km single-mode fiber (SMF) optical network and in turn feeding the wireless signal in a mm-wave antenna capable of establishing wireless links at 4m. [69] exhibits a 48-Gbit/s FiWi systems operating over a 400-km fiber link using coherent RoF.

2.8 Conclusions

The introduction of the mm-wave carrier nowadays seems both required and problematic in nature. The 60GHz band is inherently more suitable for PAN applications, but RoF seems to be the prevailing candidate solution for breaking the range barrier and deployment of Gbps rate future proof networks in vast areas. On the other hand, currently established WLAN protocols that can operate (under conditions) over RoF, are incapable of handling the mm-wave radio idiosyncrasies, due to hidden terminal problems, lack of central entity and the employment of Random Access schemes that are totally unfit for the 60GHz radio. On top of that as it has been mentioned before, all proposed and studied architectures neglect the powerful capabilities of the underlying

optical infrastructure which is solemnly used as a passive medium. To this end we argue that a complete change of mind should occur that would eventually lead to the design of a new generation of RoF oriented protocols that will be able to unify the now distinct operative portfolio of the dual medium and unleash the new architecture's full potential.

Chapter 3 The Medium Transparent MAC protocol (MT-MAC)

In this chapter we present our proposed Medium-Transparent MAC (MT-MAC) protocol that is capable of dynamically allocating capacity and resources both in the optical and wireless domains, effectively enabling 60GHz RoF WLAN functionality. Medium Transparency stems from the fact that capacity and resource allocation is negotiated directly between the wireless users and the CO and is performed within two contention periods running in parallel: the first contention process decides on the optical capacity per RAU distribution, whereas the second contention period is responsible for traffic arbitration between wireless clients located in the same RAU cell. Dynamic wavelength allocation (DWA) is achieved by means of a Broadcast-and-Select architecture where all wavelengths are broadcasted into the network and a wavelength-tunable RAU unit selects its specifically assigned data wavelength. Remote uplink (UL) and downlink (DL) channel generation is employed and an optical control signal carried at a separate control wavelength is responsible for collecting traffic requests of RAUs and for assigning wavelengths and optical SuperFrames (SF) to each RAU. Each optical SF incorporates a set of time-division multiplexed wireless contention slots that rely on a simple POLL-ACK handshaking procedure, completing in this way the assignment of traffic to every individual end-user. The performance of the proposed MAC protocol is evaluated through simulations for two different network types: a bus topology being suitable for indoor RoF deployment in office environments and a PON topology currently comprising the mainstream architecture for broadband home connections. In both network scenarios, high-throughput and low-delay values are obtained in non-saturated network load conditions even for Gb/s burst-mode traffic. To this end, the MT-MAC scheme allows for high-rate 60GHz WLAN-over-RoF connections with small number of available optical resources and even between 60GHz wireless devices with non-Line-Of-Sight (LOS) conditions, yielding extended reach 60GHz WLAN areas capable of supporting bandwidth- and latency-sensitive applications like HD video streaming.

3.1 The Medium-Transparent MAC protocol concept

The 60GHz RoF network infrastructure enforces some special requirements and characteristics to WLAN MAC protocol design, especially when Dynamic Wavelength Allocation (DWA) mechanisms are also employed in the fiber-based network part. First of all, the network's economic viability necessitates the use of cost-effective RAUs that can perform optical-to-RF and RF-to-optical signal conversion without requiring 60GHz-to-baseband and baseband-to-60GHz down- and up-conversion hardware, respectively[70]-[78]. This implies that no useful processing functionality can be offered at the RAU, so that all MAC protocol processes have to be carried out at the CO with frames travelling over a hybrid optical-wireless end-to-end-link, resulting also to significantly increased propagation delays with respect to conventional WLAN MAC schemes [52]-[54].

Moreover, the LOS requirement for 60GHz communications renders connectivity susceptible to the Hidden Node Terminal (HNT) problem. Even if LOS is established between the RAU and each individual wireless terminal, the wireless nodes might not satisfy the LOS requirement between each other. For example, a 60GHz RAU can be placed at the ceiling of a room so that node-to-RAU LOS is ensured, whilst all wireless nodes are located at the office's height, so that possible obstacles at the same height impede LOS between them. This scenario makes the use of Carrier Sense Multiple Access (CSMA)-based protocol designs ineffective, necessitating the intervention of the RAU unit for definitely ensuring the wireless medium availability[79].

The employment of optical DWA mechanisms for optical capacity and resource sharing purposes introduces an additional important MAC protocol design factor. Optical DWA suggests that the optical channel will be not always present at a RAU, resulting in an end-to-end-channel link between the wireless users and the CO that is not continuously available. This situation is unique for conventional wireless LANs, where contention can be resolved at every AP and the wireless medium is always present at least in non-energy saving normal operating conditions. To this end, DWA allows only for short time availability for carrying out any wireless capacity arbitration, whilst rendering bandwidth utilization a vital factor for the communication effectiveness.

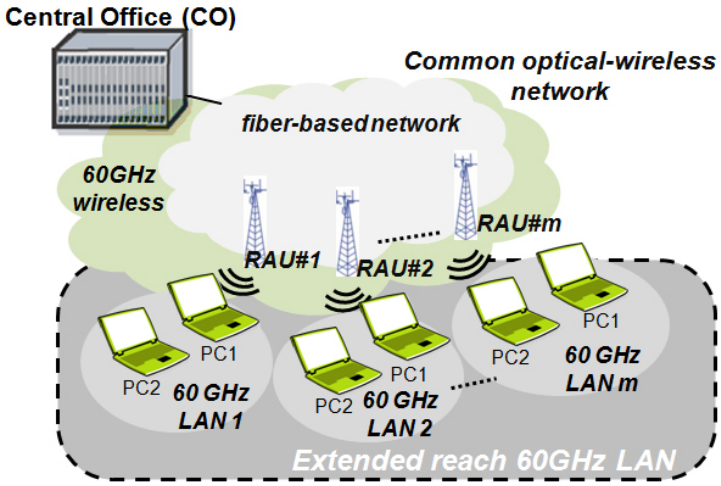

Fig. 3-1 The concept of RoF-enabled 60GHz LAN functionality within each individual RAU cell and among all RAUs served by a single Central Office.

3.1.1 Physical layer architectural aspects

Fig. 3-1 depicts a generic layout of a 60GHz Radio-over-Fiber network showing that a single CO serves a number of wireless clients distributed among different RAUs. Traffic exchange between the CO and the clients is performed over both the optical and wireless media with the data packets being in the optical domain for the fiber-based CO to RAU network part and in the 60GHz wireless domain for the RAU to end-user link. The RAU modules are responsible for the optical-to-wireless signal conversion functionalities without employing any advanced signal processing schemes, leaving the entire network intelligence located at the CO. This indicates that LAN capabilities can be offered both to the end-users served by the same RAU as well as between all clients distributed among the different RAUs, utilizing 60GHz wireless capacity sharing or both optical and wireless capacity sharing techniques, respectively. As such, capacity is negotiated directly between the wireless users and the CO without any decisive intervention of the RAU units, yielding an extended reach WLAN network between all users served by the same CO, even when no LOS between the users is present.

All UL and DL channels are generated at the CO and are broadcasted into the network. These are considered to form w wavelength pairs, namely $\{\lambda_1, \lambda_1'\}, \{\lambda_2, \lambda_2'\}, \dots, \{\lambda_w, \lambda_w'\}$, following the spectral arrangement shown in Fig. 3-2(a). Each wavelength pair λ_k carries single-side-band (SSB) DL traffic at a 60GHz subcarrier from the CO to the RAU, while λ_k' carries UL traffic (also SSB) back to the CO. An additional wavelength pair $\{\lambda_c, \lambda_c'\}$ is used for bandwidth control operations: λ_c

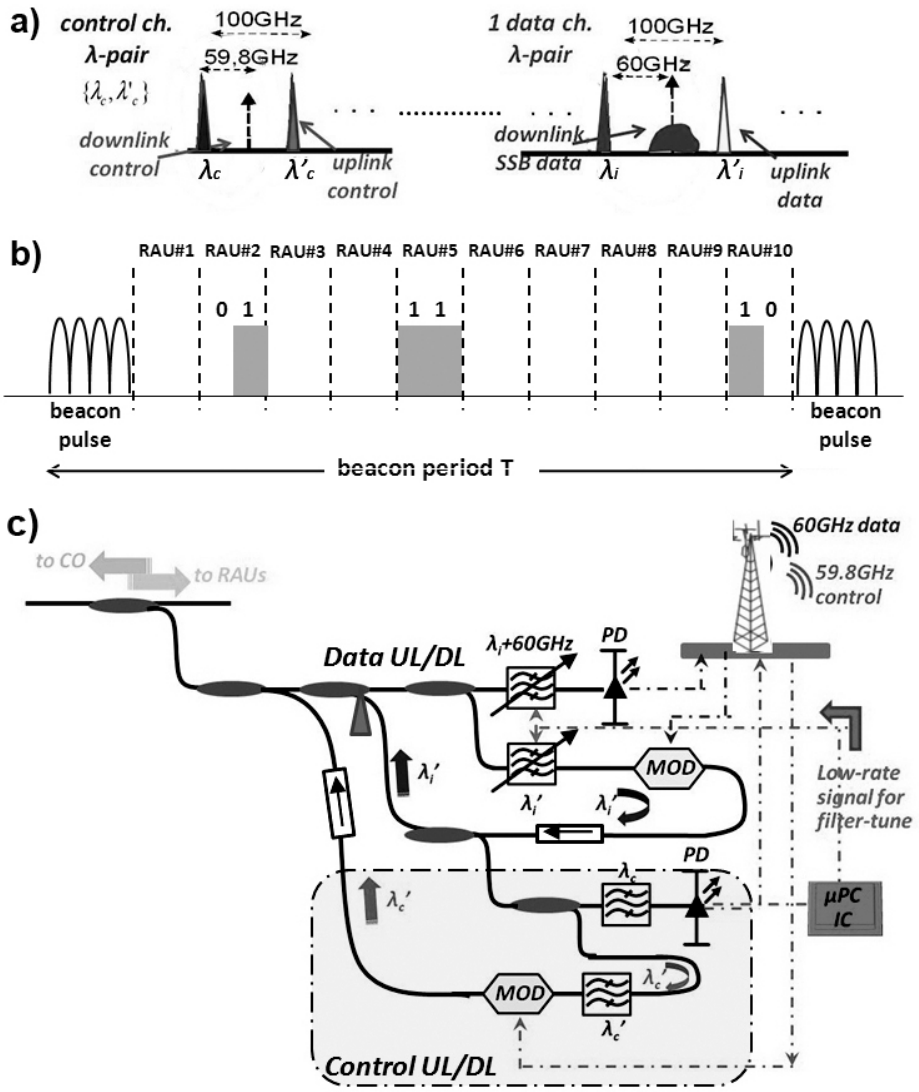

Fig. 3-2: (a) The data/control signal spectral arrangement, (b) an example of the DL control channel content within a beacon period for the case of a network with 10 RAUs and 3 available wavelengths, and (c) the RAU design.

serves both for signaling purposes carrying a sub-carrier modulated beacon pulse, as well as for wavelength assignment purposes informing each RAU about its allocated wavelength λ_k through a proper control code pulse sequence. At the same time, λ_c' carries the wireless nodes' response pulses and updates the CO about each RAU's traffic request.

The control code pulse sequence dictating the wavelength assignments to the RAU units comprises $\log_2 w + 1$ bits, with each binary sequence designating one of the w different data DL/UL wavelength pairs. The code sequence that contains only "0"s is not considered as a valid control code. To this end, the downlink control signal structure within each beacon period T_{beacon} is as follows: One optical beacon pulse followed by

a number of time slots equal to the number of RAUs in the network, with each time slot employing a baseband control code. The optical beacon pulse is modulated at a RF subcarrier different than 60GHz, i.e. 59.8GHz, and its role is to periodically trigger the wireless nodes after being opto-electronically converted, providing at the same time a synchronization signal for all RAUs. The time slots following the beacon pulse contain the control codes for each RAU unit, with the *i*-th time slot corresponding to the *i*-th RAU module. When no data wavelength pair is assigned to a RAU, the corresponding time slot of the control signal for this RAU will be empty. Fig. 3-2(b) illustrates the control signal structure between two successive beacon pulses in an example of a network with 10 RAUs and 3 available wavelengths. According to this signal structure, RAU#2 will be assigned the DL data wavelength pair #1, RAU#5 will be assigned the DL data wavelength pair #3, RAU#10 will be assigned the DL data wavelength pair #2, and all remaining RAUs will have no assigned channels. The pulse shape of both the beacon and the control code pulses can be Non-Return-to-Zero (NRZ) with their pulse duration being fully determined by the beacon period, the total number of available RAUs and the control code sequence length $\log_2 w + 1$ bits. It should be noted that the relatively small number of bits required at the control channel could in principle also allow for Time-Division Multiplexing (TDM) techniques between the control and data channels at the same 60GHz band, relaxing the need for the additional 59.8GHz frequency band.

Dynamic capacity allocation is performed by utilizing wavelength-selective RAU units and a Broadcast-and-Select architecture: all wavelengths are generated at the CO and launched into the entire network, whereas each RAU unit tunes to its respective data wavelength pair that has been dictated by the control channel information. Fig. 3-2 (c) shows the architecture of a RAU unit so as to enable wavelength-tunability and subsequently dynamic optical capacity allocation. An optical coupler arrangement allows the entire CO traffic including all the data DL/UL as well as the control wavelengths to enter each RAU. The low-rate control channel information at λ_c is then filtered in an Optical Bandpass Filter (OBF) and converted to an electronic form by means of a photodiode. The subcarrier modulated beacon pulse is subsequently transmitted into the air via a microwave antenna at a small frequency band slightly detuned with respect to the 60GHz wireless data signal, in our case considered to be a 59.8GHz RF

carrier. The baseband control code sequence becomes decoded in a low-rate Integrated Circuit (IC) microcontroller. The decoded λ_c content informs the RAU about its assigned data wavelength pair and the RAU-specific wavelengths λ_k and λ'_k are selected by two respective optical tunable filters [80] controlled by the IC circuit. To this end, only this DL/UL data wavelength pair enters the RAU unit. At the same time, λ'_c is filtered in a separate OBF, becomes modulated with the wireless nodes' response pulses and is fed back into the network for informing the CO about the RAU's traffic requests. It should be noted that the data wavelength selection could be also performed by means of a programmable or electronically controllable Wavelength Selective switch, replacing the optical coupler and tunable optical filtering stages of the RAU and allowing for more compact and lower insertion loss RAU configurations.

Data at λ_k is then launched into a second photodiode prior entering the microwave antenna that feeds the 60GHz wireless signal into the air. Channel at λ'_k travels back to the CO after being modulated by RAU's UL traffic. All wireless nodes are considered to be equipped with two transceivers; one utilized for the main data exchange at 60GHz (Data Channel), and one operating at a narrow bandwidth channel utilized exclusively for control signaling (Control Channel). However, both transceiver units can share the same 60GHz antenna and broadband RF amplification modules taking advantage of their broadband operational bandwidth, discriminating data and control information by means of simple microwave bandpass filtering elements.

3.1.2 The Medium Access Control protocol

Medium transparency of the MAC protocol relies on enabling capacity negotiation between the wireless nodes and the CO directly without the intervention of the RAU module. This can be achieved by considering contention broken down in two discrete periods, referred to as the 1st and the 2nd Contention Period. The 1st Contention Period is responsible for allocating the optical capacity to a group of wireless nodes clustered within the same RAU cell, whereas the 2nd Contention Period undertakes the finer distribution of the already per user-cluster assigned optical capacity to each individual wireless node being present in this RAU cell.

During the 1st Contention Period the CO emits a short optical beacon pulse in the Control Channel that is in turn broadcasted into the air through every RAU. When the

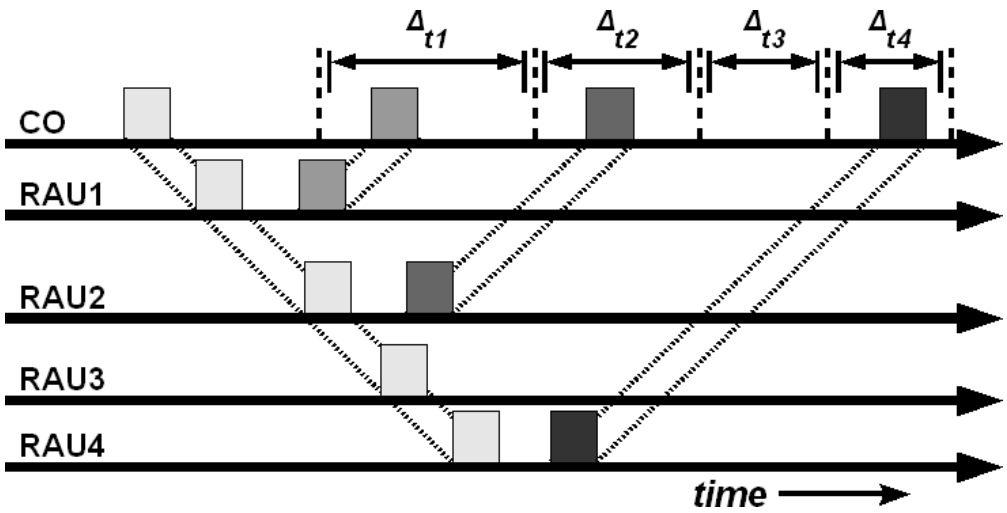

Fig. 3-3: Traffic requests collection procedure during the 1st Contention Period in the case of active clients located within RAUs 1, 2 and 4.

node or nodes present within the range of the RAU detect the pulse, they respond immediately by emitting a short pulse of the same duration in order to notify of its presence and its desire to transmit data. Nodes that detect the pulse but have no outstanding packets waiting for transmission remain silent in this phase. These pulses are received by the respective RAU and modulate its allocated timeslots in the λ_c' channel, which subsequently propagates towards the CO. This procedure is illustrated for an example of four different RAUs served by the CO in Fig. 3-3 , revealing also the need for having clearly time-discriminated RAU response pulses in order to avoid overlapping between their replies. This can be easily achieved by considering the presence of differential fiber delays between the RAUs due to their location at different distances from the CO. To this end, when ΔL_i is the differential fiber path between the two closer located RAUs with respect to their distance from the CO, the available response time window for ensuring time-isolated replies has to be $\Delta t_i = 2\Delta L_i {}^{r}/_{c}$, with r denoting the fiber refractive index and c the speed of light in vacuum. The maximum response pulse width has to be below the minimum of these Δt_i time intervals, which is easily fulfilled for realistic pulse duration values taking into account that even 1m of differential fiber path between two RAUs allows for a time interval of 10nsec.

The synchronized reception of the control channel response pulses informs the CO about the RAUs having active clients and requesting capacity. After reception of the λ_c', the CO assigns a data transmission wavelength pair $\{\lambda_k, \lambda_k'\}$ to each RAU by transmitting a short optical bit sequence that uniquely identifies the wavelength where the

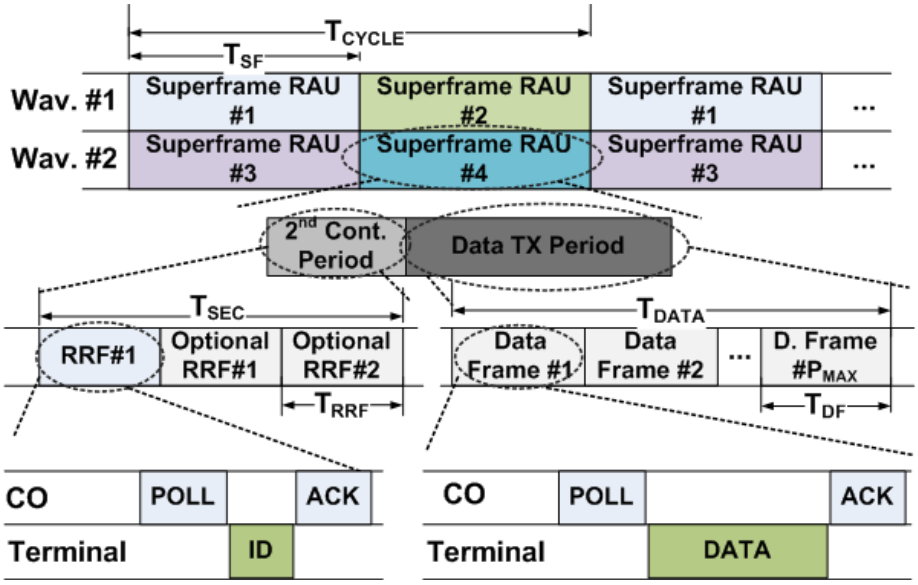

Fig. 3-4 Example of the 2nd Contention Period of an MT-MAC network with 2 wavelengths and 4 RAUs

RAU's tunable filter should tune into, ergo ending the 1st Contention Period. In high load conditions, where the number of RAUs containing active clients exceeds the number of available wavelength pairs, the CO assigns the wavelengths in a Round-Robin fashion fairly distributing the available bandwidth amongst all RAUs.

The 2nd Contention Period takes place entirely in the Data Channel. All traffic is contained within Superframes (SF), with each SF comprising of either Resource Requesting Frames (RRF) or Data Frames (DF), as shown in Fig. 3-4 , both being of equal duration. The sum of RRFs and DFs is always constant and equal to P. The role of RRFs is the identification of the active nodes residing within the RAU cell so as to increase bandwidth utilization by allowing only active nodes' participation in the subsequent DFs, which in turn carry out the actual data exchange procedure on the basis of a polling-based scheme. RRFs are further divided into m slots, with each slot comprising of POLL, ID and ACK packets, whereas DFs contain DATA packets instead of ID packets. At the beginning of each RRF, all the active clients randomly choose an integer value y in the interval $[0, m)$, where y corresponds to the number of POLL packets that have to be received by the terminal before responding with an ID packet. During a slot, the CO transmits a general POLL packet with no receiving node specified in its body. Upon correct ID packet reception, the CO responds with an ACK packet, notifying the corresponding node that it has been correctly identified. This node will not participate in a subsequent RRF (if any) within the current SF. Should, however, two nodes choose the same y value at the beginning of the RRF, they will both transmit

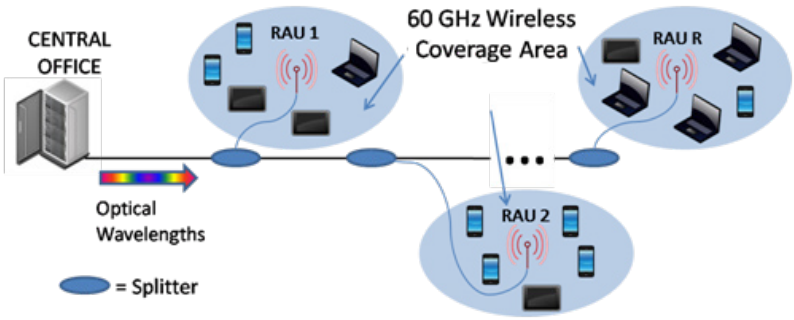

Fig. 3-5 Representation of an MT-MAC Radio-over-Fiber bus architecture.

an ID packet during the same slot. The collision will render both ID packets unreadable and the CO will not respond with an ACK forcing the nodes to participate in the next RRF, after choosing a new y value. The CO continues transmitting RRFs until zero collisions occur and all nodes are successfully identified, ending in this way the 2nd Contention Period. Having full knowledge of the nodes that are active within a RAU, the CO initiates the transmission of a series of DFs. If P_{RRF} RRFs were needed for the 2nd Contention Period to be resolved, then $(P - P_{RRF})$ DFs will be broadcasted until the end of the SF is reached, polling the wireless nodes in a Round-Robin fashion. A node is considered to be no longer active and is removed from the polling sequence if it remains silent for a number of data frames. If all nodes within a RAU are inactive or if the SF has exceeded its maximum allowed duration while other RAUs await for wavelength assignment, the CO de-assigns the wavelength pair from that RAU. As long as none of the above applies, the CO extends the SFs' duration by continuing DF transmission. In parallel to the data exchange, the CO periodically reruns the 1st Contention Process in the control channel so as to update the list of RAUs requesting traffic. If no known active clients exist within a newly wavelength allocated RAU, the 2nd Contention Process is repeated.

3.2 60GHz LAN in RoF-over-Bus Network Topology

This section presents the performance evaluation analysis of the MT-MAC protocol when applied to a 60GHz RoF network configured in a bus topology. The bus topology is consisted of the CO office that is connected through a single optical fiber to the RAUs, as shown in Fig. 3-5. This architecture is compatible with network deployment in office environments, where a common CO is considered to serve multiple floors and rooms over a single fiber bus providing a discrete RAU connectivity point to every

room. The distribution of RAUs along the common fiber bus facilitates the synchronization of the control channel optical response pulses received by the CO, since the differential fiber paths and subsequently the differential time intervals Δt_i apply in a serial way to the extending RAU modules.

TABLE 3-1: SIMULATION PARAMETERS WITH POISSON TRAFFIC MODEL

MEDIUM-TRANSPARENT MAC		802.11 DCF	
Fiber Prop. Delay	1μs= 200m	**Fiber Prop. Delay**	1μs= 200m
Slots in *RRF*	10	**Slot_Time**	20 μs
Air Prop. Delay	0.16μs	**Air Prop. Delay**	1 μs
Data Bitrate	155Mbps	**Data rate**	11 Mbps
Frames in *SF*	10	**SIFS (Short Inter-frame Space)**	10 μs
ACK Size (bytes)	8	**DIFS = (2.σ+SIFS)**	50 μs
DATA Size (bytes)	1288	**RTS**	20 bytes
ID Size (bytes)	64	**CTS or ACK**	14 bytes
POLL Size (bytes)	64	**min Content. Window**	32
		max Content. Window	1024
		ACK_Timeout or CTS_Timeout	(314 + 2δ) μs

Fig. 3-6 presents simulation results carried out in a bus topology containing the CO and 10 RAU units with a total bus length of 950m, considering a typical 60GHz RAU coverage of 50m radius and a distance between the CO and the closest RAU equal to 500m. The simulation program was developed in Java and the parameters used are summarized in Table 3-1.

Fig. 3-6(a) and Fig. 3-6(b) depict throughput and delay results obtained for load values ranging from 10% up to 100% of the maximum theoretical network capacity, and for three different #Wavelength Pairs/#Rau Units ratios (WR), namely 30%, 50% and 80%. Throughput was measured as the packets that were correctly delivered per time slot, with a time slot being equal to the time required for a data packet to be transmitted. Delay was measured as the average time interval between a packet's arrival at the buffer and its delivery to the end user. The proposed MAC protocol succeeds in utilizing almost all of the available bandwidth, since throughput increases almost linearly with the offered load as long as load resides within the WR ratio. When load exceeds the WR value, throughput arrives at its natural saturation point reaching an almost

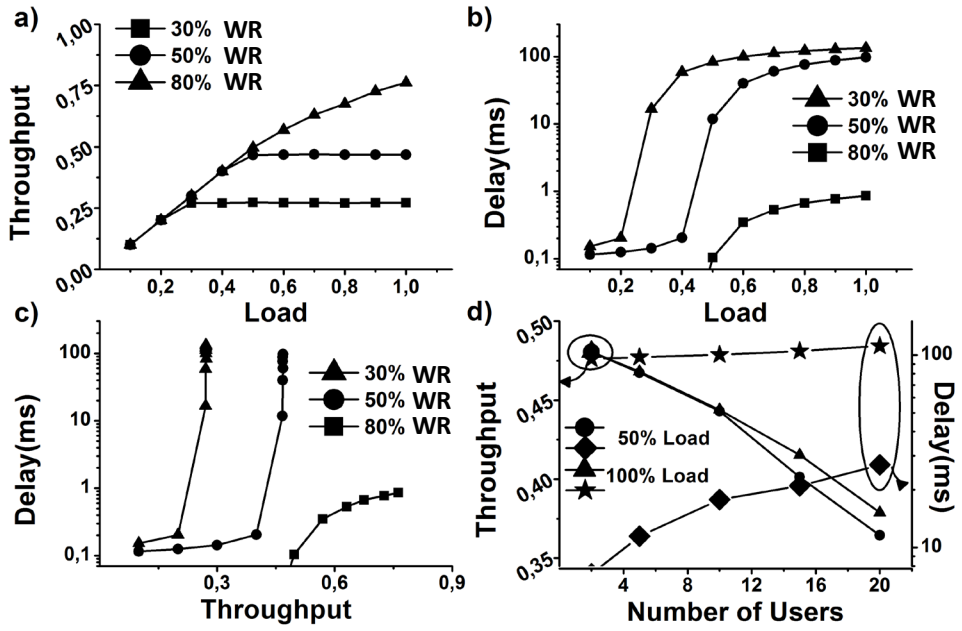

Fig. 3-6 Performance results for RoF bus network topology with 10 RAUs (a) Throughput vs. Load for 30%, 50% and 80% WR, (b) End to end packet delay vs. Load for 30%, 50% and 80% WR, (c) End to end packet delay vs. Throughput for 30%, 50% and 80% WR, (d) Throughput and Packet Delay vs. Number of RAUs in the network.

constant value. At the same time, delay values remain in the μsec range when load is below the WR value and increase rapidly when load approaches WR. After the offered load has exceeded the WR value, delay follows a slowly increasing course, however always being below 100msec. Fig. 3-6(c) illustrates the respective delay versus throughput graph for these 3 different WR ratios. It can be seen that for 80% WR the average delay increases logarithmically with the network throughput, meaning that delay increases more slowly to infinity than throughput thus confirming that the network operates efficiently and remains constantly in stable state. On the other hand, regarding the 30% and 50% WR, delay increases exponentially as throughput approaches saturation, denoting that the number of wavelengths does not suffice to serve incoming traffic and the network enters an unstable condition where small throughput increments result in disproportionately large delay penalties. The protocol's scalability performance for growing number of wireless nodes per RAU is addressed in Fig. 3-6(d), which depicts throughput and delay results as the number of per RAU users increases and for two different network load conditions (50% and 100%) with a constant WR ratio of 50%. It should be noticed that only 10% throughput reduction is obtained when the number of

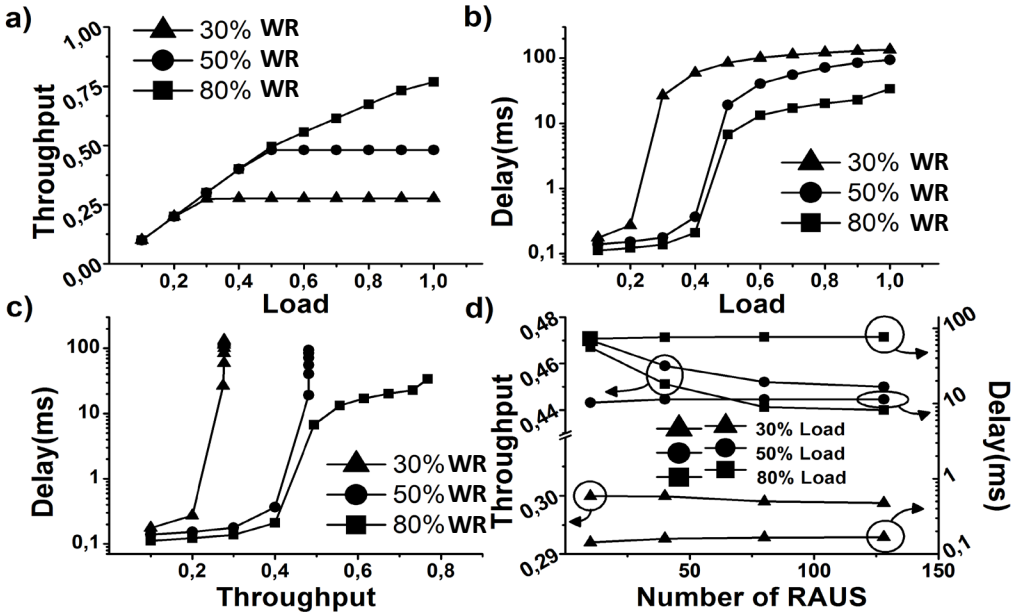

Fig. 3-7 Performance results for RoF bus network topology with 128 RAUs (a) Throughput vs. Load for 30%, 50% and 80% WR, (b) End to end packet delay vs. Load for 30%, 50% and 80% WR, (c) End to end packet delay vs. Throughput for 30%, 50% and 80% WR, (d) Throughput and Packet Delay vs. Number of RAUs in the network.

users increases by a factor of 1000% from 2 to 20, mainly due to the enhanced wireless arbitration processes.

The scalability analysis of the proposed protocol is completed by addressing its performance also for increased number of interconnected RAUs. Fig. 3-7(a)-(d) show respective throughput and delay results obtained for enhanced network dimensions, where traffic from a large number of RAUs and wireless clients has to be regulated. Fig. 3-7(a) and Fig. 3-7(b) display throughput and end-to-end packet delay vs load, respectively, for a network comprising of 128 RAUs with a total bus length of 6.5km and for three different WR ratios, namely 30%, 50% and 80%. Both throughput and delay follow a similar behavior as in the case of the network employing only 10 RAUs, confirming a smooth scaling of the protocol's performance with only minor throughput and delay degradation. Fig. 3-7(c) illustrates the respective delay vs. throughput curves which again follow the same curvature as the respective Fig. 3-6(c) indicating that for 80% WR the network remains in stable condition, whereas for 30% an 50% WR the network becomes unstable as throughput enters its saturation regime. Fig. 3-7(d) provides a more detailed insight into the protocol's performance as RAUs are gradually added in the network, again for three different load conditions (30%, 50% and 80%)

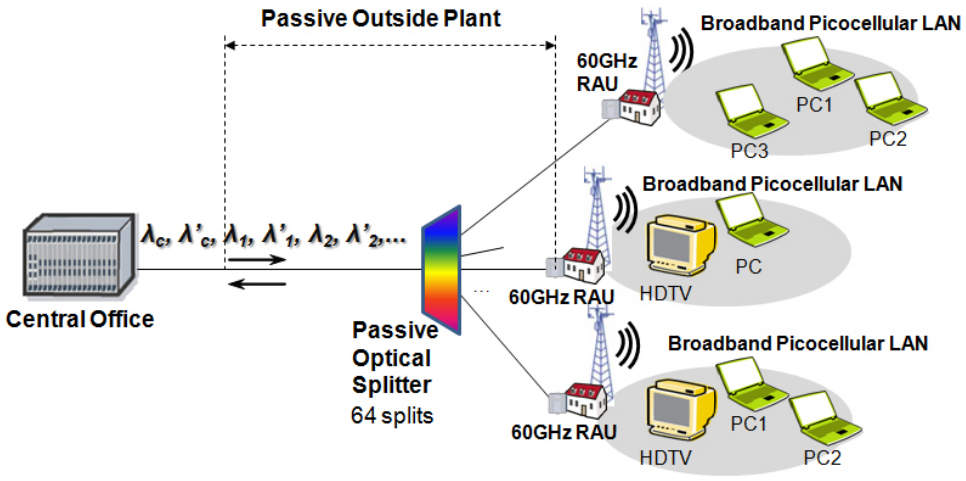

Fig. 3-8: 60GHz RoF over PON network layout.

and for a constant WR ratio of 50%. As can be easily observed, only a slight performance degradation is obtained, primarily being the result of the additional fiber propagation delay emerging due to the considerably longer bus lengths. However, even when the number of RAUs increases from 10 to 128 by a factor of approximately 1000%, throughput is decreased by only 3% and only a small delay increment of 5% is experienced, confirming the highly scalable aspects of the proposed protocol and its tolerance to large number of RAUs.

3.3 60GHz LAN in RoF-over-PON Network Topology

As PON architectures are undoubtedly dominating the field of optical access network architectures providing broadband Fiber-To-The-Home (FTTH) services, 60GHz RoF-over-PON implementations can be envisaged as a viable solution towards equipping residential end-users with broadband wireless service delivery. To this end, this section presents performance evaluation results of the proposed MT-MAC protocol in a RoF-over-PON network scenario with the aim to yield wireless LAN functionality in home environments.

Fig. 3-8 depicts the network layout when a 1:64 PON splitting ratio is used implying that a total number of 64 RAUs are connected to the passive fiber-based network part. Given that our MAC protocol requires wavelength-selectivity only at the antenna site in order to fully support its dynamic capacity allocation procedures, the proposed MAC scheme is fully compatible with the passive nature of PON network necessitating only the deployment of wavelength-tunable RAUs at the end-user site.

The main difference of this RoF-over-PON MAC protocol compared to its already presented version for bus network topology lies in the synchronization of the control channel response pulses that inform the CO about the traffic-requesting RAUs. As RAUs in this PON network layout are now connected to different pieces of fiber lengths after the passive optical splitting stage, the differential path delays between RAUs do not follow a uniform and serial distribution like in the case of a bus topology. In that case, the time intervals considered necessary for ensuring the time-discriminated arrival of response pulses will follow a non-uniform arrangement, as already discussed in Chapter 3.1.1, with the maximum pulse duration being dictated by the minimum of the differential fiber length between two successive RAUs.

Fig. 3-9 presents simulation results carried out for a RoF-over-PON network topology comprising the CO and 64 RAU units with each RAU serving a number of 5 wireless clients. The RAU modules have been considered to be located at randomly chosen different distances from the CO following a uniform distribution between 7km and 13km distance values. The remaining simulation parameters have been the same as in the bus network performance analysis summarized in Table 3-1. Throughput and delay are here again defined as described in Chapter 3.2.

Fig. 3-9(a) and Fig. 3-9(b) display throughput and delay results obtained for load values ranging from 10% up to 100% of the maximum theoretical network capacity, and for three different WR ratio values, namely 30%, 50% and 80%. As can be noticed by the respective behavior of throughput and delay graphs in these two figures, the application of the proposed MAC protocol to a RoF-over-PON architecture yields a network performance similar to the case of the bus architecture, confirming the strongly adaptive character of our MAC scheme to various network topologies. Both throughput and delay follow a pattern similar to the respective curves obtained for the bus topology for a certain WR ratio value, forming again two discrete and different operational regions around a load value close to the available WR ratio. While load remains lower

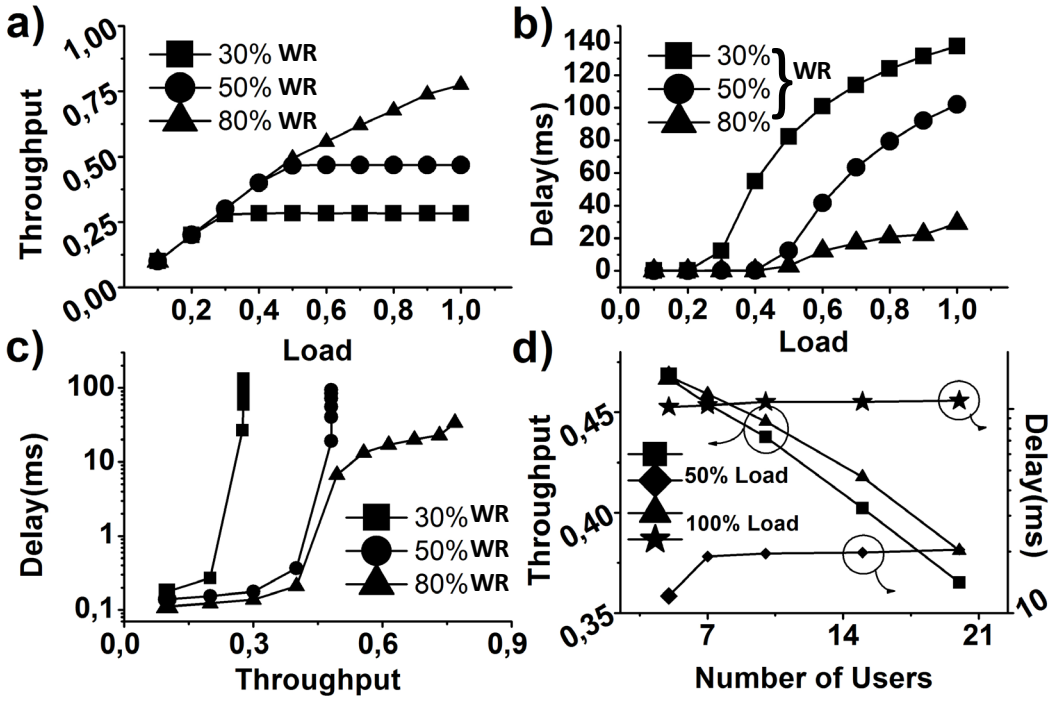

Fig. 3-9: Performance results for a PON network with 64 RAUs (a) Throughput vs. Load for 30%, 50% and 80% WR, (b) End to end packet delay vs. Load for 30%, 50% and 80% WR, (c) End to end packet delay vs. Throughput for 30%, 50% and 80% WR, (d) Throughput and Packet Delay vs. Number of RAUs in the network.

than the WR ratio, throughput increases almost linearly with increasing load whilst delay remains in the μsec range. When the offered load approaches the WR ratio value, throughput begins to saturate whereas delay increases rapidly. Once load exceeds the available WR ratio, throughput remains to a constant saturation value forming a plateau. At the same time, delay continues a slowly increasing course, being always constrained within boundaries below 130msec.

The respective delay versus throughput graph for these 3 different WR ratios is illustrated in Fig. 3-9(c), whereas the protocol's scalability properties for growing number of wireless users per RAU are addressed in Fig. 3-9(d). This figure depicts again only marginally impacted throughput and delay values as the number of users per RAU ranges from 5 to 20 for two different network load conditions (50% and 100%), with WR value being in all cases equal to 50%. Compared to the respective results obtained for the case of the RoF-over-bus network with 128 RAUs, the PON-adapted protocol yields only a 1.8% decrease in throughput and a 4% increase in delay for almost all three WR values. This performance degradation is again mainly experienced as the result of the significantly larger PON network dimensions compared to the fiber lengths

employed in the bus network topology of Chapter 3.2. However, the marginal throughput and delay deterioration indicate the protocol's capabilities to tolerate enhanced fiber propagation delays, whilst confirming its agile character that allows effective adaptation to both bus and PON topologies.

Fig. 3-10 presents the respective MAC protocol performance analysis for more realistic network conditions, considering different load values and different number of wireless clients at every RAU. Fig. 3-10(a) and Fig. 3-10(b) depict throughput and delay results obtained for different load conditions with load mean values ranging from 10% up to 100% of the maximum theoretical network capacity, for variable number of wireless clients per RAU with a mean value of 5, and for four different WR ratio values, namely 30%, 50%, 80% and 100%. The respective delay versus throughput graph is shown in Fig. 3-10(c). Despite the versatility in load and end-user numbers per RAU, throughput and delay performance is similar to the case of RAUs with equal network usage requirements. A minor reduction in throughput and a small increment in delay of 1.5% and 2.8%, respectively, emerge due to the enhanced wireless arbitration procedures at RAUs having an increased number of clients and heavier traffic requests.

The origin of having only a minor performance impairment when only the number of users per RAU is altered without modifying the number of RAUs lies in the absence of any additional optical capacity contentions. This can be verified by the graphs corresponding to the case of 100% WR ratios, where the number of wavelengths equals the number of RAUs so that a complete wavelength is statically assigned to one RAU. To this end, wavelength assignments to the RAU units are carried out only once during the network start-up, whereas for the rest of the network operation only the 2nd Contention Period is actively running. This implies that only the MAC performance in the

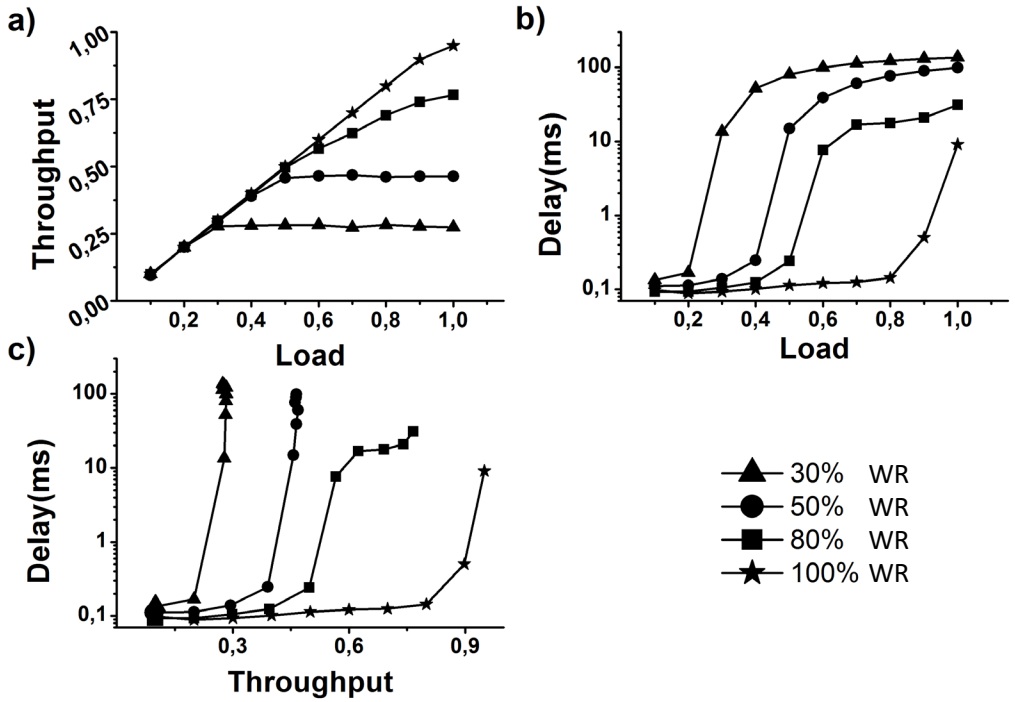

Fig. 3-10: Performance results in a PON network with 64 RAUs with variable number of users per RAU and variable load per RAU conditions: (a) Throughput vs. Load, (b) End to end packet delay vs. Load, (c) End to end packet delay vs. Throughput. All results are shown for 30%, 50%, 80% and 100% WR.

wireless domain affects the total throughput and delay values. As can be noted by Fig. 3-10(a) and Fig. 3-10(b), the absence of any optical capacity contending periods under these "ideal" optical medium conditions yields an almost linear throughput increment proving the low-impact of the wireless traffic arbitration processes. Delay values remain also stably in the μsec range as long as load resides below the available WR ratio value.

Major changes in both the throughput and delay curves are experienced only when the offered load approaches the available WR value for all cases of WR ratios of 30%, 50%, 80% and 100%, showing that wavelength assignment is a higher impact performance factor compared to the wireless capacity arbitration. More specifically, contention in the optical domain has a multiplication effect on the delay experienced by the wireless arbitration tasks, since the complete delay experienced in the wireless domain is in that case transferred also to the next wavelength assignment cycle. The maximum delay value experienced in the 100% WR case in Fig. 3-10(b) is 9 msec, identical to the case of a network with a single RAU, a single available wavelength and 5 wireless users, which is shown in Fig. 3-11.

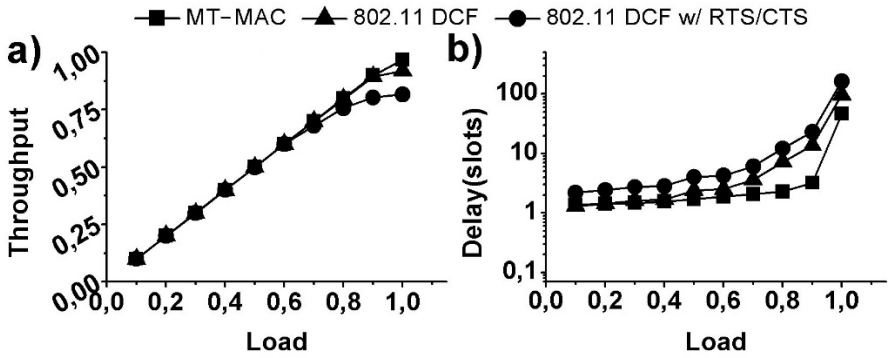

Fig. 3-11: (a) Throughput and (b) Delay results for a single RAU – single wavelength network for the medium transparent MAC and the 802.11 protocol with and without RTS/CTS. Delay is measured as number of data slots allowing for direct comparison between different bit-rate MT-MAC and 802.11 DCF.

In the case of 30% WR or 50%WR values, where the available capacity does not suffice for saturated network conditions, delay reaches an upper limit close to 220msec and 100msec, respectively, being several times larger than the single wireless arbitration delay. This is simply the result of the additional wavelength assignment cycles required for fulfilling the capacity requests, indicating that each cycle acts as a multiplication factor to the wireless contention delay. To this end, a possible acceleration of the 1st Contention Period functions through appropriate RAU and wavelength clustering employing different degrees of wavelength dedication per each RAU cluster could certainly lead to improved network performance.

The scenario of a single RAU-single wavelength network with 5 wireless end-users and 500m CO-RAU distance depicted by Fig. 3-11 provides also an insight into the performance of the combined RRF/DF polling-based approach employed for the wireless traffic arbitration, comparing throughput and delay metrics with respective values obtained for an identical network when a typical 802.11 DCF MAC protocol is used. As can be identified, 802.11 yields slightly decreased throughput and higher delay values when no RTS/CTS mechanism and no HNTs are employed. However, the delay performance is severely degraded compared to the MT-MAC protocol when RTS/CTS is used, as would be certainly required for ensuring HNT-released network operation [52]-[54] especially when shifting to the 60GHz frequency band. Given that the DWA process has a multiplied effect on the delay induced solely by the wireless capacity sharing procedures, the enhanced delay enforced by the Distributed Coordination Function (DCF) of the 802.11 with RTS/CTS appears to be prohibitive for a 60GHz RoF LAN capable of serving latency-sensitive applications. The network parameters used for the 802.11 simulation-based analysis are summarized in Table 3-1.

3.4 Performance Analysis for Gb/s Burst-Mode Traffic Applications

The turn towards 60GHz wireless communications has been mainly driven by modern high-bandwidth applications in combination with the high bandwidth availability in the 60GHz RF spectral band that extends up to 5GHz. 60GHz technology seems to be currently the mainstream solution for providing Gb/s wireless connections in order to cope with the bandwidth demands of recently introduced high speed applications like HD Audio/Video streaming (real time/on demand) or HDTV. This can be also confirmed by the variety of 60GHz standardization efforts like the 802.11ad[21], the 802.15 TG3c[22] and the WirelessHD[23] standards, all of them utilizing 60GHz technology either for WPAN or WLAN high-speed connectivity. Following this rationale, successful operation of the 60GHz RoF MT-MAC protocol even with this type of applications that have extremely low latency requirements is certainly a prerequisite for considering it as a promising approach.

TABLE 3-2: SIMULATION PARAMETERS UNDER BURSTY TRAFFIC MODEL

Slots in *RRF*	10	**Frames in *SF***		10
Air Prop. Delay	0.16μs	**Packet Size (bytes)**	**ACK**	8
Fiber Prop. Delay	1μs= 200m		**DATA**	1500
Average Burst Length	15kbytes or 13.5kbytes		**ID**	64
Data Bitrate	3Gbps		**POLL**	64

The previous sections have presented the MT-MAC's performance assuming Poisson traffic, which is the classic model used to estimate data packet arrivals and has been shown to be very accurate to model arrivals of TELNET, mobile telephony and FTP sessions[81]. However, Poisson traffic is not realistic for video traffic modelling since it lacks correlation properties between packet arrivals[82]. To this end, this section presents performance evaluation results of the proposed MT-MAC protocol for generic traffic characteristics that are present in HD audio or video streaming applications such as the bursty traffic mode. Network traffic at 3Gb/s bit-rates has been provided by using a burst-mode traffic generation model based on a Markov On-Off distribution process with burst sizes exceeding the packet size. The protocol's performance in high-speed burst-mode traffic conditions has been tested for both the bus and the PON network

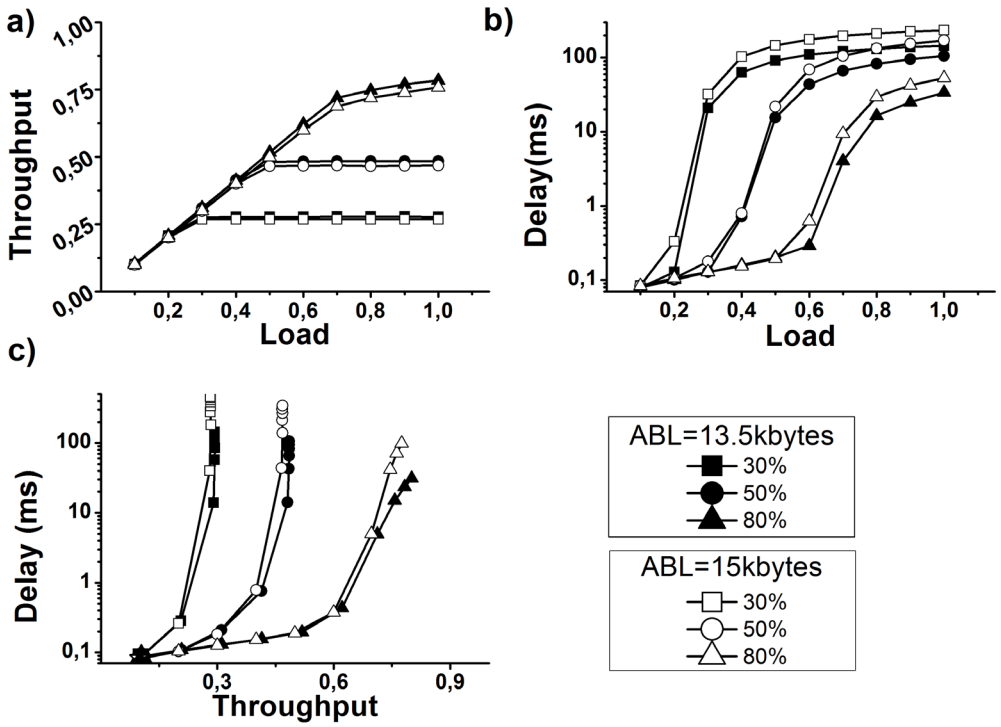

Fig. 3-12: Performance results in a Bus network with 128 RAUs: (a) Throughput vs. Load, (b) End to end packet delay vs. Load, (c) End to end packet delay vs. Throughput Curves with black-filled symbols present the case where the Average Burst Length (ABL) is lower than the Super-Frame Size, whereas curves with white-filled symbols present the case where the ABL exceeds the SuperFrame Size.

configurations using the same network parameters that have been already employed and described in Chapters 3.2 and 3.3 for the bus and the PON topology, respectively. A summary of the simulation parameters used for the protocol's evaluation with the bursty traffic model is provided in Table 3-2.

Fig. 3-12 and Fig. 3-13 show the results obtained in the case of a bus and a PON network architecture, respectively, for two different Average Burst Lengths (ABLs), i.e. 13.5 Kbytes and 15 Kbytes. The two ABL values have been selected so as to evaluate the protocol for both cases of having bursts with a total average duration lower and higher, respectively, than the total duration of the packets included within a single SuperFrame. The 13.5 Kbytes ABL value corresponds to 9 data packets marginally fitting within a single SuperFrame, whereas the 15kbyte ABL value corresponds to 10 data packets, occupying a complete SuperFrame and still requiring an additional packet frame. It should be noted that one frame out of the 10 packet frames employed within a SF serves as the contention frame, so that 9 data packets is the maximum number of usable bandwidth within a single SF.

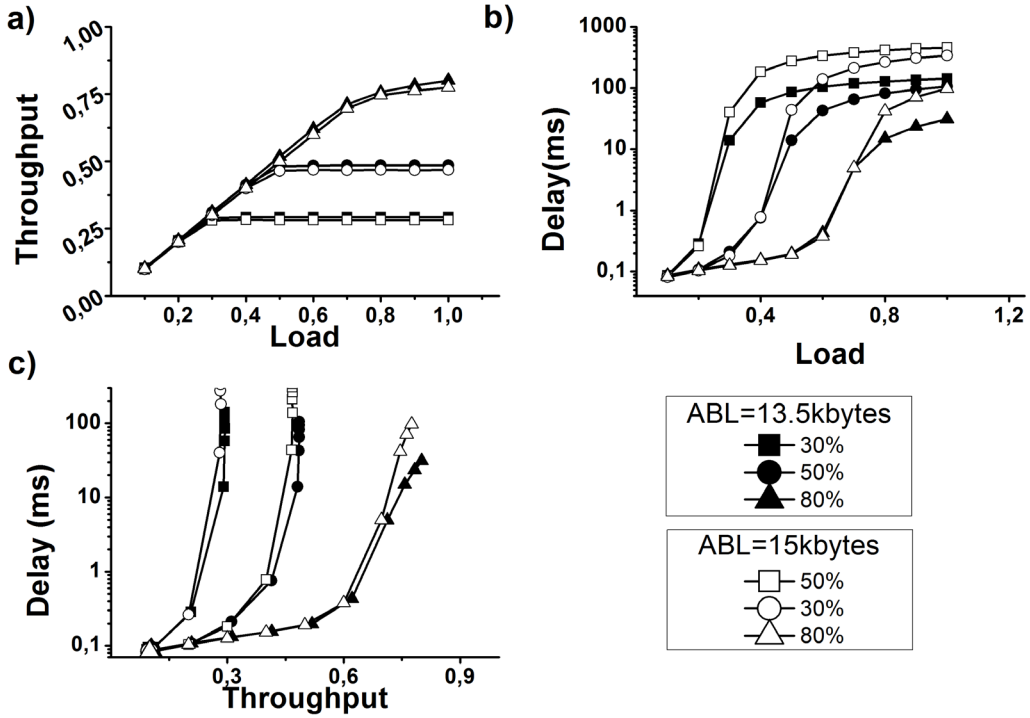

Fig. 3-13: Throughput and delay results in a PON network with 64 RAUs: (a) Throughput vs. Load, (b) End to end packet delay vs. Load, (c) End to end packet delay vs. Throughput Curves with black-filled symbols present the case where the Average Burst Length (ABL) is lower than the SuperFrame Size, whereas curves with white-filled symbols present the case where the ABL exceeds the SuperFrame Size.

Fig. 3-12(a), (b) and (c) display throughput versus load, delay versus load and delay versus throughput, respectively, obtained for a bus RoF network. Fig. 3-13(a), (b) and (c) illustrate the respective graphs for the case of a RoF-over-PON architecture. In both figures, the performance is shown load values ranging from 10% up to 100% of the maximum theoretical network capacity, and for three different WR values, namely 30%, 50% and 80%. The curves formed by the black symbols correspond to the case of 13.5 Kbytes ABL value and the curves formed by the white symbols correspond to the case of 15 Kbyte ABL value.

In both bus and PON network configurations and for both ABL values, the network performs similar to the respective RoF topologies with Poisson traffic, with the WR value comprising the decisive performance factor. Once again, throughput and delay graphs are logically divided into two discrete performance regions: as long as the offered load is lower than the WR value, throughput increases almost linearly and delay remains low. For loads close to the WR value, throughput starts to saturate to a plateau close to the WR and a jump in delay to values greater than 10msec is observed.

However, it is interesting to note that the delay remains constantly below 1msec for a great range of load values lower than the WR value. This is extremely important for latency-sensitive applications like HD video streaming, where strict latency constraints of 2-5 msec have to be satisfied in order to ensure high quality service delivery. Taking into account that this low latency performance is achieved without considering any Quality-of-Service (QoS) guarantee mechanisms in the proposed MAC protocol, improved performance should be expected by employing appropriate optimization processes.

Moreover, delay is significantly lower in the Load<WR region compared to the case of Poisson traffic, whereas it increases more rapidly saturating at a slightly higher level when Load≥WR. Lower delay in the Load<WR region mainly owes to the uneven distribution of traffic among RAUs and wireless nodes in the case of burst-mode operation, since a data burst commences and continues to be provided from the same client until it reaches its end. This results in fewer assignments and de-assignments of wavelengths by the CO and therefore to lower delay values. On the contrary, data generated by a memoryless Poisson model is spread more uniformly across the whole network necessitating more frequent wavelength reallocation procedures. Reversely, in a high load network state, where almost all participating nodes produce traffic with high probability, the situation is completely different and higher delay values are obtained when burst-mode traffic is used compared to Poisson. In burst-mode operation, the high load network conditions yield a bulk production of packets in individual nodes without having the required optical capacity to serve them. To this end, the round-robin polling fashion during the second contention period of the proposed scheme results to higher stays in the buffer. Finally, it should be mentioned that slightly different results are obtained for the two different ABL values. Improved MAC protocol performance with respect to throughput and delay measurements is achieved in the case of 13.5 Kbytes ABL, since in that case the burst size is lower than a SuperFrame and a single wavelength assignment is sufficient for a whole burst delivery.

3.5 Discussion on the benefits of the MT-MAC protocol

The simulation-based performance analysis of the 60GHz RoF-enabled MT-MAC protocol reveals that this scheme is capable of supporting high-bandwidth applications like HD video streaming forming extended reach 60GHz WLAN areas and connecting

even non-LOS wireless devices. High-bandwidth connectivity is ensured in our approach by the RoF technologies that are inherently broadband with proven potential to carry bit-rates up to several Gb/s over several km of optical fiber. Moreover, this MAC protocol enables 60GHz RoF communication directly between the individual end-users and the CO, utilizing the RAU modules just for optical-to-wireless and vice versa conversion purposes. This means that besides forming WLAN networks around each 60GHz Access Point, as targeted within the 802.11ad standard, the proposed scheme yields an Extended WLAN network that incorporates all wireless clients connected to the same CO, even when located at different RAU cells and without direct LOS. LOS is required only between wireless users and at least one RAU in order to successfully yield LAN connectivity. To this end, the 60GHz RoF MT-MAC protocol solution overcomes the bottleneck of 60GHz technology to connect non-LOS wireless devices, allowing for Gb/s 60GHz networks beyond the 10-meter piconet range of the 802.15 TG3c[22] and the WirelessHD[23] standards. A typical example where the MT-MAC protocol can yield significant benefits is the case of a large office building or of a university campus where multiple users in different rooms will certainly require high-speed WLAN connectivity. In that case, a CO can serve as the common network management point utilizing individual 60GHz RAUs in each individual office room or multiple 60GHz RAUs in larger areas, enabling high-speed LAN communication between all wireless clients.

Moreover, the proposed RoF-compatible protocol supports a rather cost-effective 60GHz coverage extension compared to currently considered 802.11ad WLAN protocol solutions. In our scheme, 60GHz RAU units are not required to incorporate any advanced processing functionalities, since all the capacity negotiation and capacity allocation decisions are met at the CO leaving for the 60GHz RAUs the role of simply tuning to the appropriate wavelength and converting the signal into the optical or wireless domain, respectively. As such, even an area larger than the 10-meter range of conventional 60GHz technology currently employed in 802.15 TG3c and WirelessHD piconets can be covered by using multiple 60GHz RAU modules, each one backhauled to the same RoF network. If this scenario had to be accommodated with the 802.11ad protocol[21], then each one of the multiple 60GHz APs would form a separate WLAN so that only clusters of users would belong in the same LAN. At the same time, the cost

of the 60GHz APs would be certainly greater than in the 60GHz RoF case, since each AP would require expensive 60GHz-to-baseband and baseband-to-60GHz down- and up-conversion electronic hardware for enabling the "intelligent" WLAN processing functionalities. On the other hand, the 802.11ad protocol allows for successful WLAN connectivity even in larger areas offering up to 100m wireless range but with Gb/s connectivity provided only for the first 10 meters, beyond which the protocol switches to classic 802.11-compatible 600 Mb/s bitrates[83]. An overview of established WLAN/WPAN MAC protocols compared to the proposed MT-MAC design is provided in Table 3-3.

TABLE 3-3: WLAN/WPAN MAC PROTOCOL OVERVIEW

	Medium-Trans.MAC	**802.11a/b/g**	**WirelessHD**	**802.15TG3c**
medium type	hybrid optical-wireless	wireless	wireless	wireless
wireless frequency	60GHz	2.4 or 5 GHz	60GHz	60GHz
network type	WLAN	WLAN	WVAN	WPAN
Bitrate	3 Gbps	11 or 54 Mbps	4 Gbps	2-3 Gbps
Continuous Link Availability	No	Yes	Yes	Yes
Media Access Mechanism	Contention-based RRFs / polling DFs	PCF /DCF	PSMA/CA Access / TDMA Ch. Allocation	CSMA/CA Access / TDMA Ch. Allocation
RoF compatible	Yes	Yes	No	Not shown

3.6 Conclusive remarks

In this chapter we have introduced the concept of medium transparency in MAC protocols for 60GHz RoF networks demonstrating a MT-MAC protocol that is capable of dynamically allocating both optical and wireless capacity and resources. Medium-transparency relies on two parallel running contention periods with nested dataframe structures requiring wavelength selectivity functions only at the RAU site, allowing in this way for compatibility with completely passive network implementations and for telecom operator transparent fiber-network infrastructures. We have presented extensive performance evaluation results for bus and PON architectures of RoF network topologies, both for Poisson and for burst-mode traffic at bit-rates up to 3Gb/s, confirming in all cases the enhanced potential of our protocol to easily adapt to the network topology whilst providing broadband 60GHz LAN functionality. Finally, our protocol's scalability and its sensitivity to fiber propagation delay have been addressed by evaluating its performance for bus networks with up to 128 RAUs and for PON networks

with up to 64 RAUs and for different numbers of end-users and load conditions. The successful protocol's performance even with Gb/s burst-mode traffic allows for the formation of extended reach 60GHz LAN networks offering LAN connectivity also between wireless devices without LOS, whilst rendering it suitable for high-bandwidth latency-sensitive LAN applications like HD video streaming.

Page intentionally left blank

Chapter 4 The Client-Weighted MT-MAC protocol

Chapter 3 introduced the first available 60GHz RoF WLAN network architecture that employs dynamically reconfigurable bandwidth mechanisms alongside a fully functioning MAC protocol both in the optical and the wireless network parts. The MT-MAC concept demonstrated the successful connectivity between wireless end-users who are served even by different 60GHz RAUs, effectively expanding Gbps-scale mm-wave communication into an extended WLAN area when exploiting the seamless interplay between optical and wireless capacity arbitration processes. More recently, a multi-channel resource allocation scheme relying on the MT-MAC mechanism has been presented towards enriching the mm-wave WLAN environment with handover capability[84]. However, both the MT-MAC protocol mechanism as well as its associated network architecture yield certainly a sub-optimal performance when it comes to more practical network scenarios: it employs a simple Round-Robin algorithm for distributing the optical capacity among the different RAU elements, negating in this way user fairness in the case of uneven user population distributions per RAU. Towards coping with user fairness in 60GHz RoF-based WLANs, we introduce here the Client-Weighted MT-MAC (CW-MT-MAC) protocol mechanism that is specifically designed to provide enhanced user fairness conditions under various network loads.

In this chapter we present an extensive performance evaluation of the CW-MT-MAC protocol, showing that the latter can balance out end-user throughput and delay inequalities, while significantly decreasing and equating the user-perceived packet delay variance even in highly deviating population distributions amongst the network's

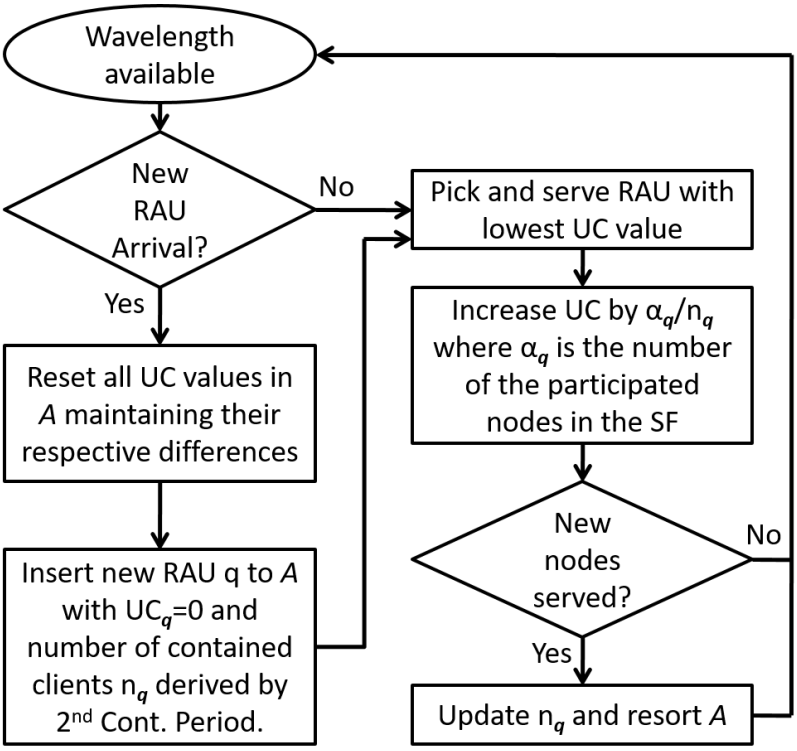

Fig. 4-1: CW-MT-MAC's flowchart.

RAUs, significantly outperforming the MT-MAC protocol with respect to end user fairness.

4.1 The Client Weighted MT-MAC (CW-MT-MAC)

The CW-MT-MAC's enhanced user throughput and consequent delay fairness properties originate from the wavelength distribution algorithm implemented at the CO, taking advantage of the RoF's centralized network architecture that allows the latter to have full knowledge of the active clients residing in every RAU. Instead of the Round Robin Algorithm (RRA) employed so far in the MT-MAC approach of Chapter 3, the proposed CW-MT-MAC pursues a client-based approach to the wavelength-to-RAU distribution when the number of requesting RAUs R exceeds the number of available wavelengths w. The CW-MT-MAC mechanism is designed to distribute capacity based on the projected demand, which is considered analogous to the number of clients requesting traffic. As opposed to the static SF sizes employed by MT-MAT, CW-MT-MAC deploys SFs with variable durations, by assigning a transmission opportunity window (TX_OP) for every user demanding traffic at the specific point in time. For the purpose of choosing the next serviced RAU, CW-MT-MAC utilizes matrix A. Matrix A is always sorted in descending order regarding the number of the contained clients per RAU. In each row, a Utilization Counter (UC_q) indicates the total amount of serving

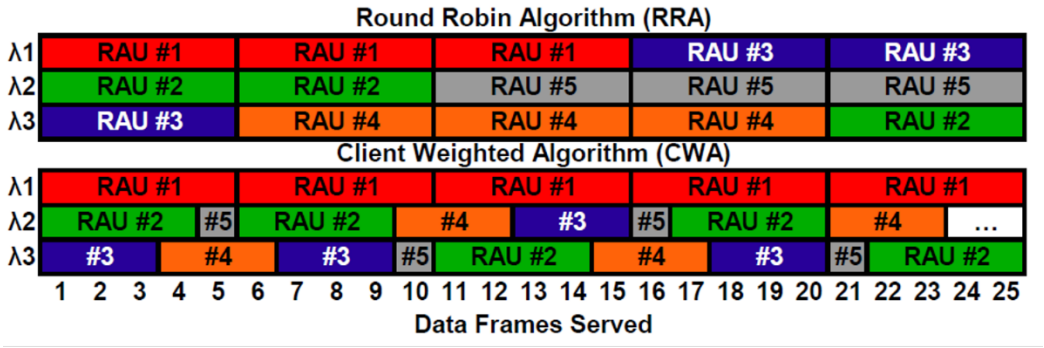

Matrix *A*		
RAU ID	#Clients	*UC*
1	5	5
2	4	5
3	3	4
4	3	4
5	1	4

Fig. 4-2: CW-MT-MACs operation example compared to MT-MAC. Utilization Counter (UC) refers only to the Client Weighted scenario. Different colors correspond to packets originating from different RAUs.

time granted to RAU q. The higher the UC_q, the lowest the priority that RAU q has in the selection process. CW-MT-MAC's flowchart is depicted in Fig. 4-1. When a wavelength becomes available, usually at the end of a SF, the CO checks by means of the 1st Contention Period whether a RAU not present in A has requested a wavelength allocation (i.e. at least one end-user residing in RAU's range has pending data). If so, the CO resets all UC counters before inserting the RAU in A, but preserves their respective differences. For example, if the UC values for RAUs 1, 2 and 3 are (9, 9, 7), with the addition of RAU 4 they become (2, 2, 0) and UC_4 initializes at 0. The latter aims in providing the newly inserted RAU with the maximum priority, enabling the CO to become rapidly acquainted with its properties (i.e. number of active/total nodes) and maintain A correctly updated. To commence the next SF, the CO chooses the RAU with the lowest UC value and, in case of a tie, the RAU with the highest number of active nodes, as the one to be served by the available wavelength. In the case of a second tie, the RAU is chosen in random. The length of the assigned SF in terms of frames is defined as $\alpha_q \cdot TX\_OP$, where α_q is the number of active nodes that are participating in the current SF, and TX_OP is the length of the per user transmission opportunity window measured in polling frames. When the SF ends, UC_q is increased by α_q/n_q, where n_q is the total number of nodes residing in RAU q. The value n_q is accumulatively calculated and updated as time progresses and different users become active within

TABLE 4-1: SIMULATION PARAMETERS			
Fiber Prop. Delay	1 μs/200m	**Air Prop. Delay**	0.16 μs
Slots in *RRF*	10	**ACK Size**	8 bytes
DATA Size	1288 bytes	**ID, POLL Size**	64 bytes
Data Bitrate	1 Gbps	**Buffer Size**	80 pack.
Mean Burst Length	1.5 Kbytes	**Burst Length Std. Deviation**	1,42 Kbytes
CWA TX_OP Size	30 packets	**RRA SF Size**	150 pack.

RAU q. In case α_q equals zero, meaning that the chosen RAU q had no active clients, UC_q is increased by 1, denoting that all users where served. If RAU q remains with no requesting clients for some time, then it is removed from A. It is essential to note here that, due to constraints applied by the Physical Layer, CW-MT-MAC is facing an upper barrier in certain extreme cases regarding the maximum achievable equalization of bandwidth. Even though densely populated RAUs can in theory be granted a larger portion of the available optical capacity, no more than one wavelength can be assigned to a single RAU, thus forming a maximum allocation limit. This limit effectively corresponds to the maximum number of users that can be served by a single RAU before overcoming CW-MT-MAC's operational capacity and is denoted as $n_{MAX} = {}^{z}/_{W}$, where z is the total number of active clients served by the CO. When the number of active nodes residing in a RAU surpasses n_{MAX}, CW-MT-MAC chooses to grant a dedicated wavelength to this RAU element for as long as the above condition applies. In this case, the CW-MT-MAC subtracts the dedicated wavelength and the number of users served by it and functions recursively for the remaining wavelengths and nodes.

Fig. 4-2 illustrates an execution example for 3 available wavelengths, 5 RAUs and a total of 16 users that are unevenly distributed amongst the RAUs as shown in matrix A. The figure depicts the wavelength-over-time allocation of CW-MT-MAC versus the corresponding MT-MAC operation presented in Chapter 3. As can be noted, the MT-MAC equips each RAU with static 5-Data-Frame-long capacity "chunks" for the entire 25-Data-Frame-long running time, irrespective of the number of users served by each RAU. On the contrary, the CW-MT-MAC clearly differentiates and promotes the densely populated RAUs by reserving the wavelengths on a balanced user centric basis

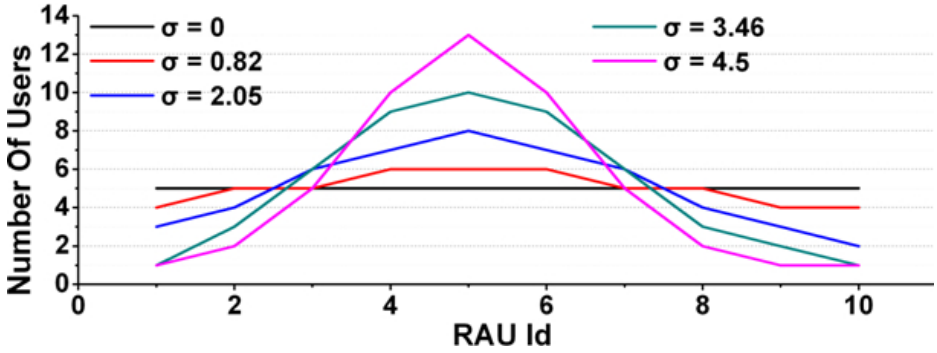

Fig. 4-3 Node population distributions for five different standard deviations

for the same period so as to provide fairness amongst the users, when the later occupy unevenly burdened RAUs.

4.2 Performance Evaluation

This section presents the performance of the client-weighted algorithm when applied on the MT-MAC protocol for a RoF-over-bus topology. The test configuration follows the same topology as the one tested in Chapter 3, comprising 10 RAUs in a bus topology with the distance between the first RAU and the CO equal to 500m and 50m fiber intervals amongst the RAU modules, producing a total network length of 950m. This architecture is compatible with network deployments in indoor domestic or small enterprise environments, where a common CO is considered to serve multiple rooms over a single fiber bus providing a discrete RAU connectivity point to every room. An event-driven simulator was implemented in Java with the full simulation parameters employed being summarized in Table 4-1. The total number of users located in the system equals to 50, distributed using an approximation of the normal distribution properly adjusted to produce discrete values that provides "bell-shaped" populations with mean value $n = 5$ users per RAU. We tested five different user distribution patterns, starting from the least dispersed (uniform) distribution with standard deviation $\sigma = 0$ and gradually migrating to the most dispersed distribution with standard deviation $\sigma = 4.5$, as depicted in Fig. 4-3. In order to stress test the algorithm's functionalities for the whole network length, the users' distributions always abide by the rule of having at least one user per RAU. Furthermore, the channel is considered to operate under ideal conditions and all users are equipped with buffers in order to accommodate generated traffic. Each RAU module is considered to have 3m effective radius. Since the presented framework implies a dynamic capacity allocation scheme, a shortage of wavelengths towards the

number of existing RAUs in the network is always taken into consideration and denoted henceforth as the wavelength availability factor WR. This shortage is imposed by the mm-wave nature of the wireless medium which generally presumes a large amount of very short ranged RAUs serviced by a lesser number of wavelengths either due to scale or due to energy efficiency reasons. In order to better simulate IP traffic, the employed packet generator is based on a bursty traffic model exhibiting long-tail properties, meaning generated traffic is characterized by high deviation from the distribution's mean value of burst length. As presented in detail in Table 4-1, for the current experimental set we considered a mean burst length of 1.5kB, with the employed traffic generation algorithm producing a standard deviation of 1,42kB. Due to this high deviation, the per user TX_OP window was chosen to be 30 frames long (~4kB), so as to be certain that the majority of the generated bursts would fit into a single SF. In accordance, the RRA SF size was set to 150 frames long, a value that was inferred by multiplying the corresponding CW-MT-MAC transmission opportunity window with the users' distribution mean $\mu = 5$.

Fig. 4-4 depicts the protocol's non-saturation performance versus various optical availability factors designated by the WR ratio (Fig. 4-4(a) and Fig. 4-4(b)) , ranging from 0.1 and up to 0.9 as well as versus various traffic loads(Fig. 4-4(c) and Fig. 4-4(d)), ranging from 10% up to 100% of the maxi mum theoretical network capacity. Both CW-MT-MAC and MT-MAC were tested for the most extreme user distribution depicted in Fig. 4-3 with standard deviation σ=4.5. As demonstrated by the respective legends all results in Fig. 4-4(a) and Fig. 4-4(b) can be logically classified into groups depending on the offered load. Accordingly results in Fig. 4-4(c) and Fig. 4-4(d) are clustered based on the respective WR ratio. As can be noted in the 30% load case depicted in Fig. 4-4(a), throughput follows a linear path until it reaches its maximum value when the WR ratio exceeds the offered load, effectively meaning that all traffic is accommodated due to the optical wavelength abundance. The same applies in the curves group depicting the 80% load scenario, with the difference being that linear properties continue for higher loads until again the point where the WR ratio exceeds the offered load. Regarding the MT-MAC/CW-MT-MAC comparison we notice a borderline superiority of the second over first one. Specifically, CW-MT-MAC exhibits a marginal

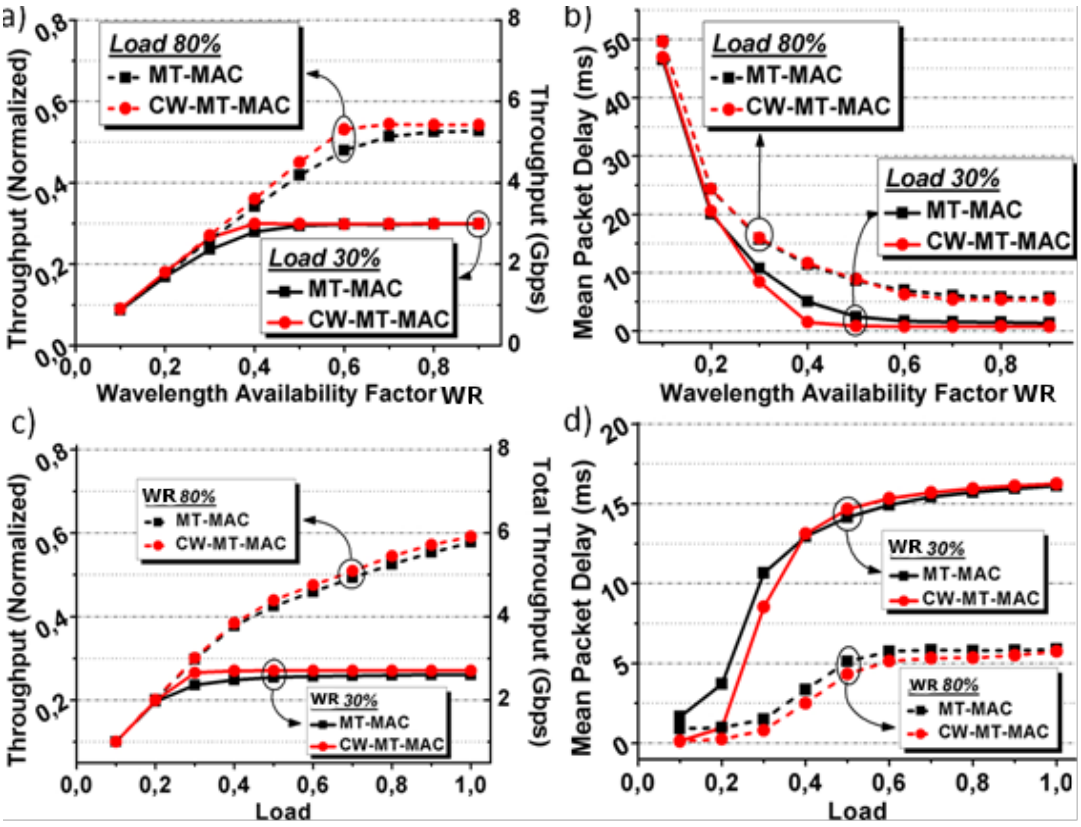

Fig. 4-4: a) Throughput vs. WR b) Delay vs. WR c) Throughput vs. load d) Delay vs. Load

throughput gain in the 30% load scenario, whereas the gain increases and reaches its highest value of 5% in the 80% load scenario. This performance boost is the result of the proportional wavelength assignment mechanism which administers optical capacity not statically but in accordance to the received bandwidth claims. In this way, possible idle times in less crowded RAUs are avoided while the much needed service time is extended in the densely populated areas. This performance agreement is also evident in Fig. 4-4(b) which depicts the mean packet delay. As can be noted, delay outcomes start at very high values while the offered load exceeds the available optical capacity ratio due to the traffic being many times greater than the maximum theoretical capacity achievable by the available wavelengths. However, as the wavelength availability rises, delay follows a decreasing slope, with the curves corresponding to 30% load dropping at higher rates than the high-load 80% scenario. The latter is due to the fact that when increasing the optical capacity, the added number of available slots can serve the small number of generated packets produced in low load conditions in a single SF faster than the high load conditions where a further optical capacity increment is necessary to achieve the same. By comparison it becomes clear that, when population distribution is uneven, CW-MT-MAC manages to attain higher metrics, especially while the WR ratio

remains lower than the offered load, confirming that service balancing can indeed lead to better overall system level performance.

Fig. 4-4(c) and Fig. 4-4(d) illustrate the protocol's behavior versus various traffic loads, ranging from 10% up to 100% for the most extreme user distribution deviation. Performance was tested for two different wavelength availability factors WR, namely 0.3 and 0.8. Fig. 4-4(c) presents the total system throughput versus various load conditions, revealing the linear exploit of the dual-medium while the offered load remains well under the corresponding WR ratio. As load increases beyond the WR point though, throughput stagnates around its saturation plateau, since all traffic beyond that point exceeds the optical capacity available in the system. For instance, at 40% normalized load and 1 Gbps bitrate each RAU receives 400 Mbps aggregated traffic from the wireless nodes. However, with 10 RAUs in the system and 3 available optical wavelengths (30% WR) the optical network has a total capacity of 3 Gbps which is insufficient to serve the aggregated traffic of $10 * 400$ Mbps $=$ 4 Gbps produced by the wireless nodes. This is the reason that in 30% WR throughput saturates around 30% normalized load. Delay outcomes presented in Fig. 4-4(d) remain minimal while load is below WR and increase rapidly when load approaches the later. After the offered load has exceeded WR, delay follows an increasing course before saturating at its maximum value. This delay saturation behavior appears as a direct consequence of the limited buffer space, since at loads higher than the WR ratio multiple packets are dropped and therefore do not contribute to delay metrics, whereas the number of packets that do gain buffer access are constant and produce a constant delay. Regarding the two competing schemes we notice again a marginal performance gain in favor of CW-MT-MAC. This performance thrust highlights that when faced with uneven populations, traffic provision and service distinction are necessary to achieve optimum operation.

Fig. 4-5 offers a more detailed observation of the protocol's performance as the latter is perceived from the user's perspective. In addition, it provides insight on how this performance fluctuates when gradually transitioning from uniform to uneven distribution of the network's nodes. The displayed results show the protocol's performance for both CW-MT-MAC and classic MT-MAC at the user level versus the user distribution's standard deviation σ. The σ-values utilized correspond to the distribution patterns

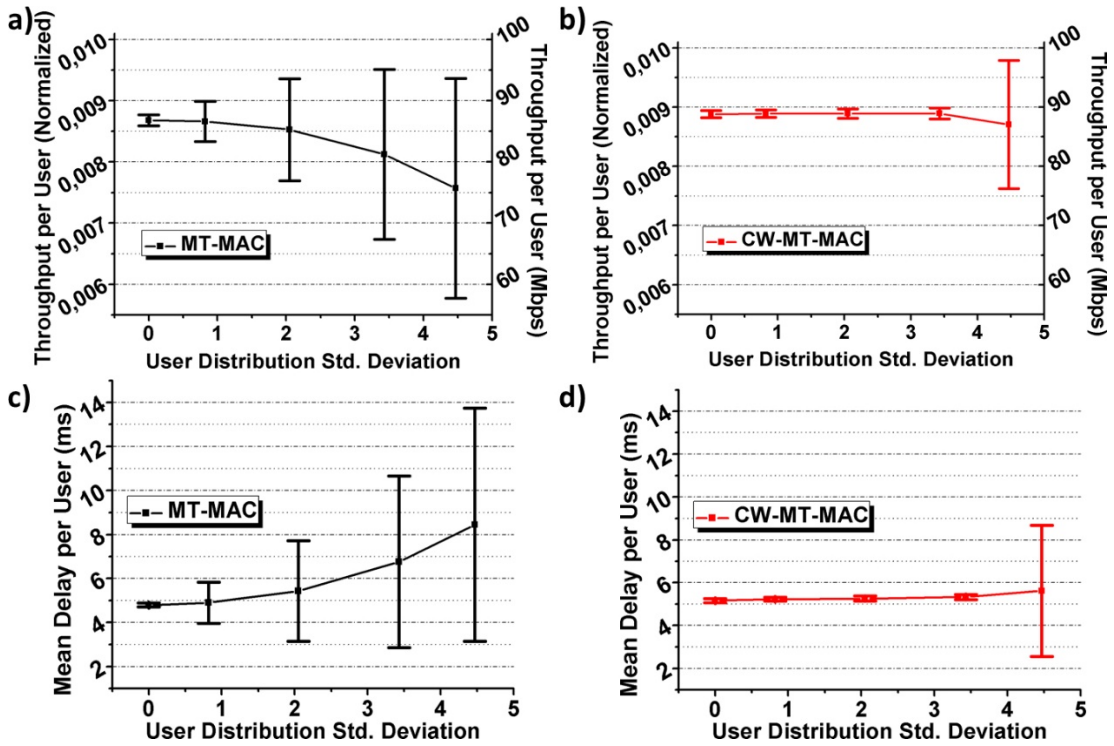

Fig. 4-5: a-b) MT-MAC protocol User Throughput and Mean User Delay Performance with their respective Standard Deviations vs. the User's Distribution Standard Dev. c-d) CW-MT-MAC protocol User Throughput and Mean User Delay Performance with their respective Standard Deviations vs. the User's Distribution Standard Dev.

displayed in Fig. 4-3 and the results are shown for WR=0.5 and 50% traffic load conditions. Fig. 4-5(a) and Fig. 4-5(b) illustrate the mean user throughput and its respective standard deviation for both protocols. As can be noted, not only does CW-MT-MAC achieve higher and more consistent throughput output, but its main advantage lies in the latter's standard deviation, where it exhibits significantly lower deviations compared to the MT-MAC. In agreement to the respective saturation outcomes, MT-MAC's σ-value (Fig. 4-5(a)) approaches zero only for the uniform user distribution pattern, whereas CW-MT-MAC's σ-value (Fig. 4-5(b)) succeeds in remaining zero for the first four user distribution patterns where the number of clients n is always lower than n_{MAX}. When overcoming this point, CW-MT-MAC dedicates a wavelength to all RAUs having $n > n_{MAX}$ clients, which produces inequalities and therefore deviation of throughput. However, CW-MT-MAC clearly retains the edge over MT-MAC by offering the minimum possible deviation and therefore fairer throughput delivery. The above are also reflected and are the reason for the curvature shown in the respective mean user packet delay results displayed in Fig. 4-5(c) and Fig. 4-5(d). In the above it is clear that the CW-MT-MAC's superiority in throughput equalization also drives the advantage of significantly lower delay and their respective σ-values, ergo confirming the proposed

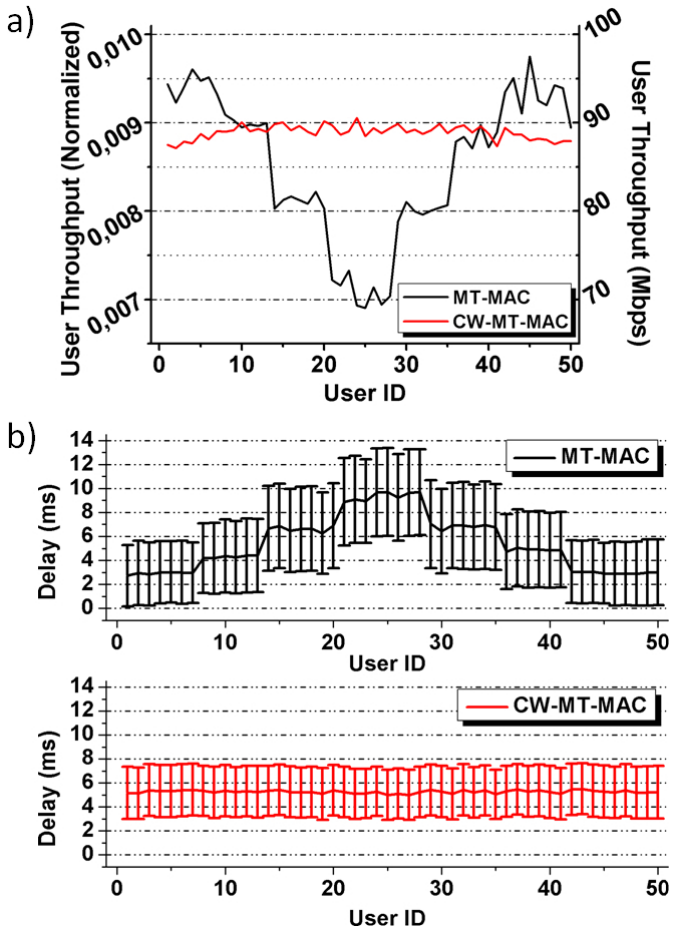

Fig. 4-6 a) User throughput vs. User Id b) User mean packet delay and its standard deviation for each of the 50 users of the network

scheme's increased fairness capabilities. Over all user distributions CW-MT-MAC achieves 69% reduction in the average exhibited throughput standard deviations as opposed to the corresponding MT-MAC values (2.8 vs. 8.9 Mbps) and 72% reduction in the per user packet delay (0.7 vs. 2.5 ms).

A more comprehensive look on CW-MT-MAC's fairness properties internals can be derived by means of Fig. 4-6, which presents the above mentioned metrics for each of the 50 participating users in the bus topology network for the case of σ=2.05, WR=0.5 and 50% traffic load. Fig. 4-6(a) presents the achieved user's throughput where it is clearly evident that MT-MAC exhibits great disproportion regarding capacity allocation and remains heavily depended on the user's distribution. On the contrary CW-MT-MAC manages to level out all service deliverance irrespective of the inequalities inserted into the network from the uneven client distribution. Specifically, the MT-MAC protocol displays an average of 85.3 Mbps per user with σ-value equal to 8.3 Mbps whereas the CW-MT-MAC scheme achieves an average of 88.9 Mbps with σ-value as

low as 0.8 Mbps, thus accounting for ~90% reduction in the user perceived throughput deviation. Fig. 4-6(b) displays the per user mean packet delay and their respective intra-packet delay variation metrics. As can be noted, not only does CW-MT-MAC offer an almost constant delay amongst the participating nodes of the network regardless of the grade of population's dissimilarity but also CW-MT-MAC's observed delay is subject to smaller, strictly uniform and consistent delay variations. Specifically, the MT-MAC's average delay performance is 5.4ms with 3.15ms average standard deviation. On the other hand, CW-MT-MAC manages an average packet delay of 5.3ms with 2.1ms average deviation, thus achieving 32% reduction in the PDV. This fact highlights that CW-MT-MAC is a better fit towards supporting real-time applications, e.g., VoIP, since PDV can be a serious issue affecting delay-restricted applications.

4.3 Conclusive Remarks

We have presented a new user fairness-enabling MT-MAC protocol for the realization of efficient and fair Gbps-range 60 GHz RoF WLAN networks. Fairness is achieved by equipping the protocol with the user-centric Client Weighted Algorithm for the optical capacity arbitration procedures. Rapid improvement on user throughput and delay equalization is demonstrated for various network conditions through simulation performance analysis for different user distribution patterns and loads under specific wavelength availability constraints. Specifically, the CW-MT-MAC scheme has demonstrated almost zero standard deviation for 4 out of the 5 studied user deviations achieving an overall 68% reduction in throughput and 72% reduction in delay standard deviation as the latter is perceived amongst the network's users, thus proving its enhanced user-fairness properties. In addition, CW-MT-MAC achieved 32% reduction in the exhibited intra packet standard deviation performance, highlighting its ability to serve modern delay-restricted applications where PDV remains a major issue.

Page intentionally left blank

Chapter 5 Mathematical Analysis

In this chapter, we demonstrate an analytical model followed by a detailed saturation throughput performance analysis for the MT-MAC protocol described in Chapter 3, assuming ideal channel conditions. The introduced model relies on a two-dimensional (2D) Markov chain approach for calculating the end-user transmission probabilities, taking into account contention for both the optical and the wireless layer resources. An analytic formula for throughput computation is derived and the respective results for different optical resource availability factors and for data rates up to 1 Gbps are found to be in close agreement with simulation-based findings, confirming the validity of the MT-MAC model. Our analysis reveals that the proposed MT-MAC is capable of re-solving contention within a limited time frame, concluding with the optimized duration of consecutive data transmitting frames for maximizing network throughput. This first successful MT-MAC modeling approach indicates that the functional interfacing of the optical and the wireless connection links can yield new and efficient capacity utilization concepts in 60 GHz RoF networks.

5.1 MT-MAC Saturation Throughput analysis

We declare S to be the normalized system throughput, i.e. the ratio depicting the amount of time that the system transmits payload bits to the total amount of communication time. Considering the protocol rules, the above translates directly to the time portion that the system exhibits engaged SF activity, and more specifically to the time portion that the system is located in the DATA_TX period of the latter.

Therefore, S can be defined as:

$$S = \frac{\Pi_{TX} T_{DF}}{\Pi_{CONT} T_{RRF} + \Pi_{TX} T_{DF}} (\Pi_{TX} + \Pi_{CONT}) \rho_{DF}$$

where Π_{TX} is the Steady State Probability (SSP) of the system being in the DATA_TX mode, Π_{CONT} is the SSP of the system being in the 2nd Cont. Period, T_{DF} and T_{RRF} are

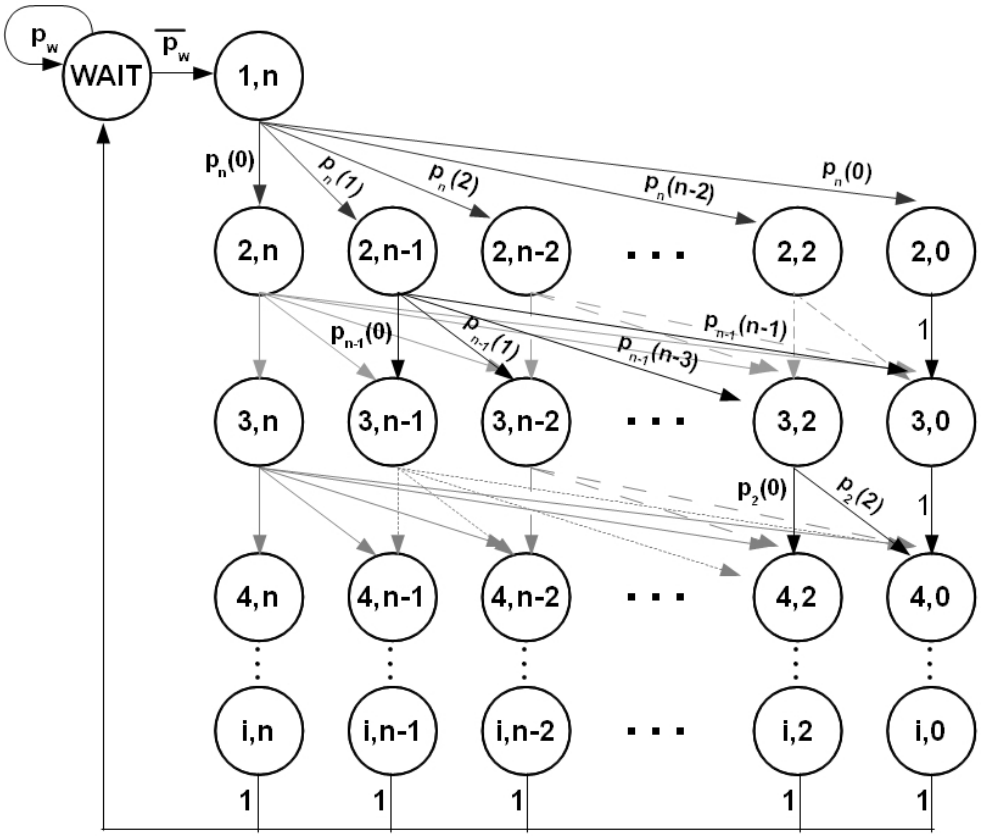

Fig. 5-1: Markov Model from the perspective of a single Remote Access Unit.

the durations of the DF and the RRF respectively, and B is the payload information percentage contained in a DF. The latter is typically defined as $B = L_{DATA}/(L_{POLL} + L_{DATA} + L_{ACK})$ where L_{DATA}, L_{POLL} and L_{ACK} are the size in bytes of the DATA, POLL and ACK packets respectively.

To calculate Π_{TX} and Π_{CONT} we have deployed a two-dimensional (2-D) Markov chain model, depicted in Fig. 5-1, which demonstrates the scheme's operation from the scope of a single RAU. The above model operates under the assumption of ideal channel conditions. In addition, we consider that each RAU contains a constant and finite number of n stations in its radius. Traffic generation follows the saturation model, meaning that each of the n terminals always possesses a packet ready for transmission immediately after transmitting the previous one. Finally, no hidden or exposed terminals phenomena are taken into account, since they are negated by our protocol's centralized topology as it has been mentioned in Chapter 3.

In the following analysis, we consider a fixed number of RAUs R, with each RAU servicing an identical and constant number of wireless nodes. Moreover, we define the total number of available downlink and uplink data wavelength pairs as w. The model's

nomenclature follows the $S_{i,k}$ symbolism, where i stands for the i-th frame of the current SF and k is the number of nodes that are yet to be resolved through means described in the 2nd Cont. Period. It should be noted here that the first state of the Markov chain model, referred as WAIT, represents the optical waiting period, i.e. the state where the RAU does not have an assigned pair of wavelengths yet and is waiting for optical capacity assignment. Each SF contains a number of frames between (i_{MIN}, i_{MAX}), the values of which are immutable and known to the network. These bounds denote the minimum and maximum time duration of the non-interrupted wavelength assignment to every RAU respectively. More specifically, the i_{MIN} and i_{MAX} values reflect the logical restriction that each consecutive wavelength assignment period must be long enough to allow for adequate data transmission without exceeding, however, a certain upper limit, so as to prevent unaffordable delays and inequalities amongst the RAUs.

Contention in the optical domain is resolved by means of a simple round robin algorithm using a step of one RAU at the end of each time quantum, i.e. each RAU holds the same wavelength pair for the amount of time equal to the w/R percentage of the total time. The w/R percentage, meaning the ratio of the number of wavelength pairs available in the system to the number of RAUs serviced by the CO will henceforth be referred as WR, as it has been also referred in the previous chapters. In real non-saturated mode of operation, a phase shift in wavelength re-assignment is not performed unless there are outstanding claims for allocating optical capacity to other non-serviced RAUs. However, in network saturation conditions, as considered in our analysis, the CO acquires a constant demand for optical capacity from all RAUs, implying the exercise of the round robin algorithm in a strictly time-sharing fashion.

The Markov chain model diagram can be logically divided into two areas. The first area is comprised of the state WAIT, whereas the second area is comprised of all the rest states. State WAIT, being representative of the waiting period caused by the assignment/de-assignment of the optical wavelength, effectively controls the length of time that the current RAU lies in idle state. This signifies that its respective SSP is:

$$\Pi_{WAIT} = 1 - {}^{w}/_{R} \tag{1}$$

and by considering the normalizing condition $\sum \Pi = 1$ the sum of the rest SSPs is:

$$\sum_i \sum_k \Pi_{i,k} + \Pi_{1,n} = {}^{W}/_{R} \quad \text{for } i \in [2,n], k \in [0,n]\backslash\{1\} \tag{2}$$

where $\Pi_{1,n}$ is the SSP of the $S_{1,n}$ state and accordingly $\Pi_{i,k}$ represents the SSP of the $S_{i,k}$ state. Once being in the WAIT state the only possible actions are: to remain stationary with probability p_w while awaiting for wavelength assignment, or to enter the $S_{1,n}$ state with probability $\overline{p_w}$ once a wavelength has been assigned. Following this, the wireless nodes served by this RAU enter the 2nd Cont. Period according to the rules of the MT-MAC. All the wireless activity is depicted in the second logical area of the Markov model, which can be further divided into distinct rows and columns: each individual row corresponds to a single frame in the SF, while each column represents the number of nodes that are yet to be resolved in the 2nd Cont. Period. As such, the far-left column signifies the maximum number of unresolved nodes n and the far-right represents the situation where all nodes have been resolved, i.e. the number of unresolved nodes has reached zero. It should be noted that $S_{i,1}$ type of states are not present in the Markov state diagram, given that node collision can only occur when at least two nodes are available for picking the same slot number in the random selection process.

Every state in this second logical area of the Markov model is accessible from all the states of its preceding frame (or previous row) that lie exactly above and on its left. This carries the physical meaning that the number of unresolved nodes can either remain the same or decrease when moving to the next frame. The transition probability from state $S_{i,k}$ to state $S_{i+1,k-x}$ equals to the probability of having x out of a current total of k unresolved nodes making a unique number choice and consequently getting resolved. This probability is provided by the relation [85]:

$$p_k(x) = \frac{(-1)^x m!\, k!}{x!} \sum_{a=x}^{k} \frac{(-1)^a (m-a)^{k-a}}{(a-x)!\,(m-a)!\,(k-a)!} \tag{3}$$

where m is the number of slots the nodes are choosing from i.e. the slots contained in a single RRF, and $k \in [2,n], x \in [0,k]\backslash\{k-1\}$.

A complete summary of all the non-null one-step transition probabilities is provided below:

$$\begin{cases} p\{1,n|0,n\} = \overline{p_w} \\ p\{i+1,k-x|i,k\} = p_k(x) \\ p\{i+1,0|i,0\} = 1 \end{cases} \quad (4)$$

for $i \in [1, i_{max}), k \in [0,n]\backslash\{1\}, x \in [0,k]\backslash\{k-1\}$.

The "0, n" notation in the first part of (4) represents the WAIT state. The third part of (4) denotes that, once reaching a state where all nodes have been resolved, the 2nd Cont. Period is over and the CO initiates the transmission of sequential DFs until the end of the SF. To this end, the states of the form $S_{i,0}$ correspond to effective packet transmission, so that the aggregate probability Π_{TX} of the system residing in DATA_TX is:

$$\Pi_{TX} = \sum_{i=2}^{i_{max}} \Pi_{i,0} \quad (5)$$

Accordingly, all the rest states of the form $S_{i,k}$ for $k \geq 2$ correspond to the 2nd Cont. Period and therefore:

$$\Pi_{CONT} = \sum_{i=1}^{i_{max}} \sum_{k=2}^{n} \Pi_{i,k} \quad (6)$$

All $\Pi_{i,k}$ probabilities including $\Pi_{i,0}$ can be calculated by exploiting the single-step transitions from all possible states in the preceding $i-1$ row. Every SSP is derived by the sum of all the states that reside in the previous frame and on the left, multiplied by the corresponding transition probabilities. To this end, the SSPs for all $S_{i,k}$ states can be expressed as:

$$\Pi_{i,k} = \sum_{a=k}^{n} (\Pi_{i-1,a} \cdot p_a(a-k)) \quad (7)$$

for $i \in [2, i_{max}], k \in [0,n]\backslash\{1\}$.

For $i = 1$, the respective expression describing the transition from the WAIT state to the $S_{1,n}$ is given by:

$$\Pi_{1,n} = \Pi_{WAIT} \cdot \overline{p_w} \quad (8)$$

By utilizing the fact that each of the i frames, independently of its type, is of equal duration we derive that:

$$\Pi_{1,n} = \sum_{k} \Pi_{2,\kappa} = \sum_{k} \Pi_{3,\kappa} = \cdots = \sum_{k} \Pi_{i_{max},k} = {}^{\lambda}/_{(iR)} \tag{9}$$

Using (1), (7) and (8), $\overline{p_w}$ is found to be:

$$\overline{p_w} = \frac{\lambda}{i \cdot (R - \lambda)} \tag{10}$$

By utilizing (2), (3), (4), (8) and (10), equation (7) can be recursively solved yielding all required $\Pi_{i,0}$ values, which can be then used in (5) to enable the calculation of Π_{TX}. Finally, in order to calculate S we also need to specify the T_{RRF} and T_{DF} values. According to the protocol rules T_{RRF} is defined as:

$$T_{RRF} = m(3\delta_{fiber} + 3\delta_{air} + D_{POLL} + D_{ID} + D_{ACK}) \tag{11}$$

where δ_{air} is the propagation delay in the wireless medium and D_{POLL}, D_{ID} and D_{ACK} are the transmission delays of the POLL, ID and ACK packets respectively. Correspondingly T_{DF} is defined as:

$$T_{DF} = 3\delta_{fiber} + 3\delta_{air} + D_{POLL} + D_{DATA} + D_{ACK} \tag{12}$$

where D_{DATA} is the transmission delay of the DATA packet. Eq.(11) and (12) correspond to the time duration of the RRF and DF frames in the general scenario where no packet rescheduling is taking place. In the latter case though, (11) and (12) become:

$$T_{RRF} = 3\delta_{fiber} + m(3\delta_{air} + D_{POLL} + D_{T_{ID}} + D_{ACK}) \tag{13}$$

And

$$T_{DF} = \frac{2\delta_{fiber} + 3\delta_{air} + \Pi_{TX} \cdot i_{max}(D_{POLL} + D_{DATA} + D_{ACK})}{\Pi_{TX} \cdot i_{max}} \tag{14}$$

respectively, where $\Pi_{TX} \cdot i_{max}$ corresponds to the number of DFs in the SF. Notably, if the appropriate values are chosen so that $T_{RRF} = T_{DF}$ then $S = \Pi_{TX} \cdot B$.

5.2 Performance Evaluation

To evaluate the validity of our proposed model, we have produced and compared both analytical and simulation results using our custom made event-driven simulation tool

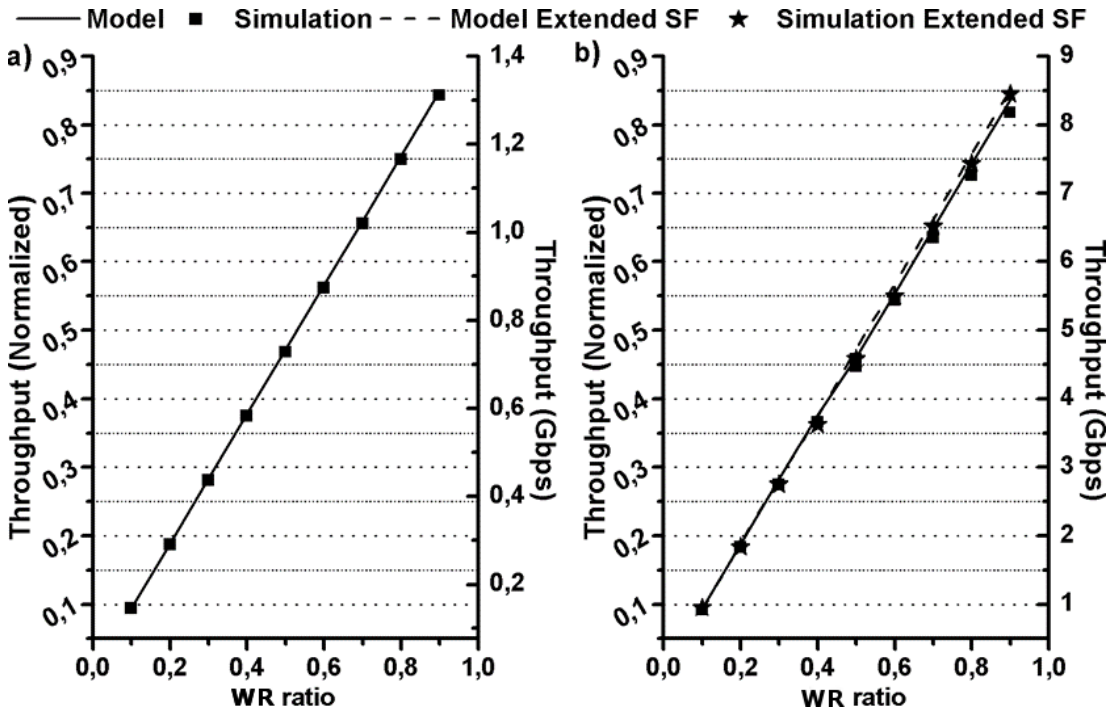

Fig. 5-2: a) Throughput vs. WR ratio performance results for wireless bit-rate of 155 Mbps 5b) Throughput vs. WR ratio performance results for wireless bit-rate of 1 Gbps with standard and extended SuperFrame size.

written in Java. The employed network configuration comprises 10 RAUs in a bus topology, with each RAU servicing 5 end-users under saturation load conditions, as it is schematically depicted in Fig. 3-5. Table 5-1 summarizes the full specification parameters of the simulation run and of the respective analytical model where applicable.

Fig. 5-2 depicts the saturation throughput results obtained by both the analytical model and the respective simulation tool, for different optical capacity availability factors denoted by the WR ratio and ranging from 10% to 90%. Throughput is displayed both in its normalized form as well as in bits per second, taking into account that the maximum possible throughput value corresponds to the case where all employed RAUs can simultaneously transmit data packets at line-rate.

TABLE 5-1: SIMULATION PARAMETERS WITH SATURATION TRAFFIC MODEL			
Fiber Prop. Delay	1μs per 200m	**Air Prop. Delay**	0.16 μs
Slots in *RRF*	10	**ACK Size**	8 bytes
DATA Size	1288 bytes	**ID, POLL Size**	64 bytes
Data Bitrate	155 Mbps	1 Gbps	1 Gbps
Frames in *SF*	500		3200

Fig. 5-2(a) displays throughput for 155 Mbps bit-rate that has been already shown experimentally to allow for successful multi-user connectivity in 60 GHz RoF networks[86]. As it can be noted throughput increases almost linearly and in total accordance to the WR ratio growth. In addition, the theoretically obtained results practically coincide with the simulation-based outcomes experiencing only negligible differences up to a maximum of 1%. The good agreement between theory and simulation confirms the validity of our model, revealing also the almost linear dependency between throughput and WR, which indicates the nearly optimum capacity exploitation offered by the proposed MT-MAC in this dual medium platform. Fig. 5-2(b) displays the corresponding results for the same configuration but at 1 Gbps wireless data rate. As can be noted, the transition to a higher bit rate yields a slightly deteriorated throughput performance of up to 2% when all other network and traffic parameters remain unchanged. This owes mainly to the combined effect of the reduced packet durations obtained as the bit-rate increases and of the fiber propagation delay that remains constant. The RRF duration, as defined in (13), becomes almost independent of the bit-rate since the transmission delays of the relatively small-size POLL, ID and ACK packets are negligible with respect to the fiber propagation delay δ_{FIBER}. This means that the total time required for transmitting all RRFs and completing the 2nd Cont. Period will be almost constant and bit-rate independent, primarily determined by δ_{FIBER} since δ_{AIR} corresponds only to small cell radii. However, this will not be the case for the DFs that have a greater size than the RRFs so that their duration will still depend upon the bit-rate, as can be seen by (14). Having the RRF duration constant and down-limited by the δ_{FIBER} quantity and the DF duration decreasing as the bit-rate increases to 1 Gbps, the ratio of DFs duration within a certain SF will decrease leading to slightly lower throughput values. This can be, however, compensated by increasing the number of DFs incorporated in a SF and this case is also depicted in Fig. 5-2(b). The parallel extension of the SF to a size analogous to the bit-rate increase (i.e. from 500 to 3200 for the 155 Mbps to 1 Gbps transition) renders the RRF induced delays again negligible, owing to the enhanced

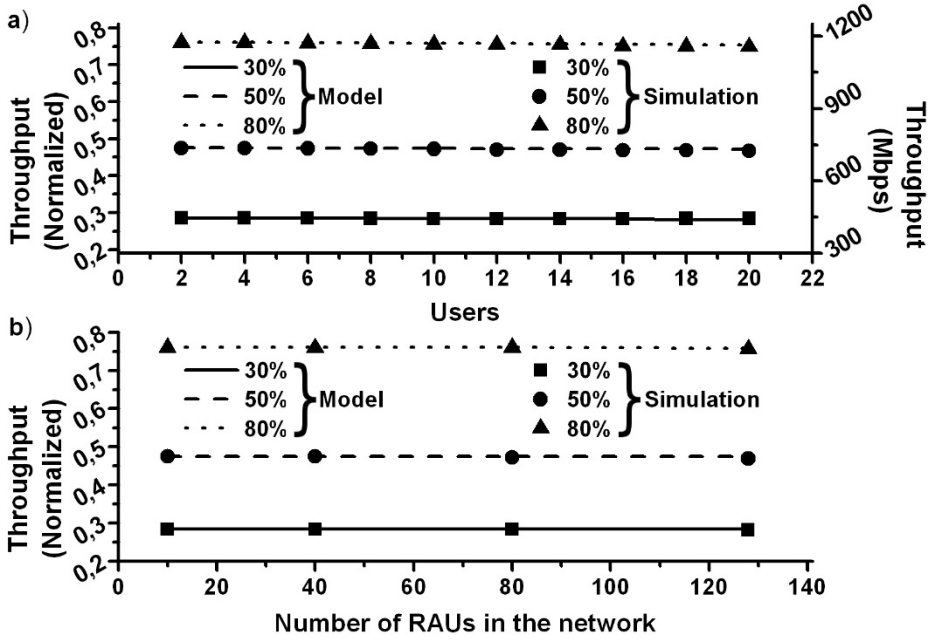

Fig. 5-3: a) Throughput vs. number of users per RAU for 30%, 50% and 80% WR ratio respectively. b) Throughput vs. number of RAUs in the network for 30%, 50% and 80% WR ratio respectively.

number of DFs being transmitted without rerunning the 2nd Cont. Period. In this way, throughput performance recovers to its original metrics.

Fig. 5-3(a) and Fig. 5-3(b) illustrate the protocol's scalability performance for a growing number of nodes per RAU and a rising number of participating RAUs in the network, respectively. Each curve represents one of three distinct WR ratio configurations that were investigated, namely 30%, 50% and 80%. Fig. 5-3(a) elaborates that throughput values remain practically immutable as the number of nodes grows from 2 to 20, displaying only a slight performance degradation of less than 1%. Since the only alternating factor is the number of users, the good scaling performance can only be attributed to the high efficiency of the random choice wireless arbitration process. In order to verify this claim, we carry out additional trials that are depicted later on in Fig. 5-4. Fig. 5-3(b) depicts the throughput performance as the number of RAUs employed in the network increases from 10 up to 128, illustrating the protocol's behavior as the optical round-trip delay multiplies, affecting in principle the RAUs located the farthest from the CO. The RAU modules are considered equally spaced with 50 m inter-RAU fiber intervals, producing a total fiber length between 0.5 and 6.4 km depending on the number of RAUs involved. As can be noted, only a small performance degradation of up to 0.5% appears in the simulation-based curve for a number of RAUs equal to 128, while

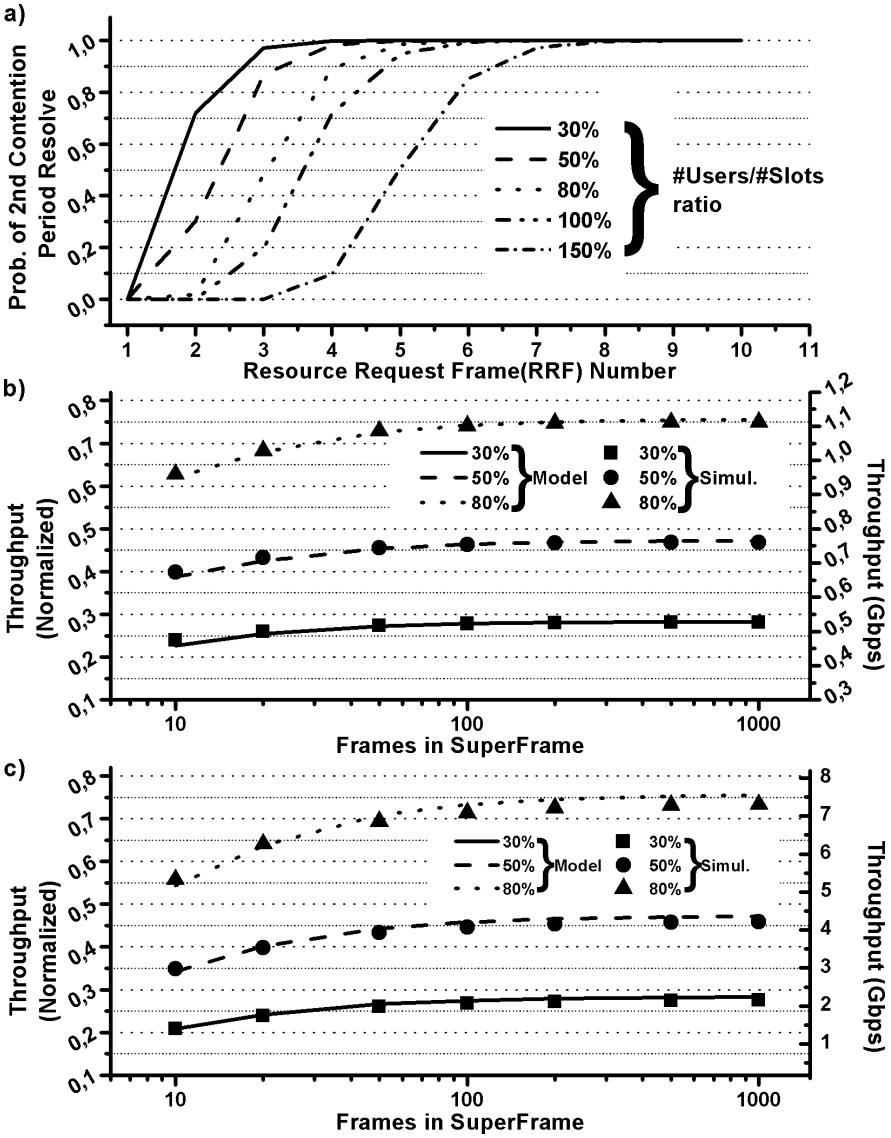

Fig. 5-4: a) Analytical probability results of resolve vs. number of RRFs for different Users/Slots ratios. b) Throughput vs. number of frames in a SF, for different WR ratios at 155 Mbps wireless bit-rate. c) Throughput vs. number of frames in a SF, for different WR ratios at 1 Gbps wireless bit-rate.

the respective curve originating from the mathematical analysis remains constant irrespective of the antennae elements incorporated. This small difference between analysis and simulation owes mainly to the additional fiber propagation delay emerging due to the considerably longer bus lengths as the number of RAUs increases, which is not taken into account in our mathematical model. It is important to note that throughput deliverance remains essentially unscathed even when the number of RAUs escalates by a factor of 1000%, confirming the increased scalability characteristics of the protocol and the optimum exploitation of the underlying infrastructure properties.

The validity of our model allows for its use towards acquiring a more detailed insight into the role of specific MT-MAC protocol parameters and their performance impact.

Fig. 5-4(a) illustrates the effectiveness of the random slot number choice scheme employed in the 2nd Cont. Period; the probability of achieving "resolve" for ranging RRF sequence lengths is computed, assuming 10 slots per RRF and different amount of competing nodes scaling from 3 to 15 (i.e. from 30% up to 150% node/slot ratios). In order to calculate the respective probabilities of 2nd Cont. Period resolutions we employ the 2D Markov chain depicted in Fig. 5-1 in conjunction with Eq.(7). As can be noted by the analytical results, "resolve" probability tends to be 1 at an early stage, essentially meaning that all wireless nodes are effectively resolved after a small number of RRFs. For example, in the case of 3 active nodes and 10 slots/RRF, resolve probability reaches 0.98 after only two RRFs, whereas for 5 active nodes the resolve probability becomes 0.99 after 4 RRFs. The same is true even in the extreme case where the number of nodes greatly exceeds the number of available slots, such as the case of 15 active nodes to 10 slots/RRF, where it can be noted that resolve probability becomes 0.99 after 8 RRFs. The above results indicate that no matter the number of active nodes, the 2nd Cont. Period's duration is always in the scope of single-digit amount of RRFs, thus leading to a quick resolve and in turn benefiting the throughput-producing data exchange period.

Fig. 5-4(b) presents both simulation and analytical results displaying throughput vs. the number of frames per SF for three different WR ratios, namely 30%, 50% and 80%. The produced results correspond to SF durations ranging from 10 to 1000 and a static number of 5 wireless nodes served by each RAU at 155 Mbps bit-rate. As expected, throughput performance increases with i, since the fraction of the 2nd Cont. Period duration becomes relatively insignificant as i rises, so that a greater part of the SF is devoted to the DATA_TX mode and as such to actual data transmission. This can be easily explained by taking into account the fact that the quantity of RRFs required for resolving all wireless nodes is in fact independent of i and as proved above remains minimal. Moreover, throughput tends to reach a saturation point after a certain number of frames, rendering a negligible gain in performance for greater SF sizes. This can be verified by its mere increment of only 0.3% for a frame number enhancement from 500 to 1000, allowing us to establish the number of $i = 500$ frames as a close to optimal SF size with respect to highest throughput performance. Fig. 5-4(c) illustrates the same evaluation for 1 Gbps wireless bit-rate. As it can be observed, throughput follows the same

behavioral pattern as in Fig. 5-4(b), with the only difference being that at 1 Gbps bit-rate the throughput values are lower when the SF is very small in size compared to the respective throughput yields in 155 Mbps. The reason for the latter is again the combined effect of a) the reduced packet durations obtained at the high bit-rate and b) the fact that the fiber propagation delay that remains constant as the SF size increases. As noted before, the RRF duration is almost independent of the bit-rate since the short POLL, ID and ACK packets have negligible transmission delay compared to the fiber propagation delay. This means that the total time required for transmitting all RRFs and completing the 2nd Cont. Period will be almost constant regardless the SF size. However, this is not the case for the DFs since in the latter the majority of time is spent in the Data packet transmission and as such the DFs are heavily depended on the bit-rate. Having the RRF duration constant and down-limited by the fiber propagation time and the DF duration decreasing as the bit-rate increases to 1 Gbps, the ratio of DFs duration within a certain SF will decrease leading to lower throughput values. The latter is confirmed by the extended SF metrics presented in Fig. 5-4(b) where the enhanced DF number compensates the throughput losses. Finally, it can be noted that the analytical results are once again in excellent agreement with the respective simulation-based findings.

The successful MT-MAC protocol modeling provides a number of significant advantages towards turning MT-MAC schemes into reliable and viable approaches for high-bandwidth 60 GHz wireless over fiber network applications. It confirms the protocol's capability of almost optimally handling capacity offered by the two different media, extracting at the same time the optimal network and traffic parameterization conditions. Even more important, it draws the roadmap for effectively merging optical and wireless capacity arbitration algorithms within a single mathematical framework, offering the possibility to alter the complete protocol performance by modifying only the optical or only the wireless arbitration process. By combining this with the centralized topology of the proposed 60 GHz RoF network that consolidates the complete knowledge of all network and end-user parameters into the CO, one can reach highly agile network configurations without requiring any intervention to the hardware infrastructure.

The enhanced agility unleashed by our analytic MT-MAC model can be highlighted in a simple example of different bandwidth sharing strategies. The scheme demonstrated

in Chapter 3 relies on the Round-Robin allocation algorithm in the optical domain, issuing a fairness policy that works on a per RAU basis so that each RAU element enjoys the same amount of throughput. However, as it has been demonstrated in Chapter 4 this can produce important variations on the per node throughput values in case the distribution of wireless nodes among the RAUs experiences severe inequalities. The analytical model presented here can easily reveal how the fairness policy could be shifted with minor modifications to a user-centric mode of operation, where not every RAU but every single user within the entire network should perceive the same level of bandwidth. This kind of policy would demand the transition to an optical arbitration algorithm that allocates wavelengths for time windows directly proportional to the number of active nodes currently residing in each RAU, such as the CW-MT-MAC scheme.

Within the same frame, the same principle could be applied solely in the wireless portion of the network as well towards supporting a more guaranteed service in modern high bandwidth applications with stringent delay requirements, like High Definition video streaming. In that case, the time bandwidth allocation in the wireless arbitration process would not be distributed in equal time portions amongst active nodes, but could be in principle reserved according to specific prioritization criteria depending on the type of traffic requested. As such, requests for real time data would be ranked as higher priority traffic in the polling sequence so as to allocate continuous fractions of bandwidth. This indicates that the MT-MAC protocol can incorporate a plethora of Quality of Service (QoS) schemes following established techniques used in a variety of wireless protocols.

Finally, the centralized knowledge of the entire network configuration can spur new energy reduction concepts for given 60 GHz network performance metrics. As the number of end-users and traffic requests changes, the CO can update its parameter database and determine the minimum number of wavelengths required for sustaining the same level of performance. To this end, it can decide to switch off certain transceiver elements at the CO, enabling constant and high-quality performance while preserving always the minimum possible power consumption levels.

5.3 Saturation Model extension for the CW-MT-MAC protocol

This paragraph presents an enhanced version of the saturation model that was described in the previous section. This version has been properly altered in order to abide by the CW-MT-MAC operational rules. Note that in this paragraph we present only the features that differ from the previous analysis, and as such all the aforementioned equations and the 2D Markov model are still valid unless dictated otherwise.

In the following analysis, we consider again R RAUs sharing w available wavelengths. Each RAU contains n wireless users with z being the total number of users residing in the whole system. The model's nomenclature again follows the $S_{i,k}$ symbolism, where i stands for the i-th frame of the current SF and k is the number of nodes that are yet to be resolved through means of the 2nd Contention Period. It should be noted that the WAIT state represents the optical waiting period, i.e. the state where the RAU does not have an assigned wavelength yet. The Markov chain model diagram depicted in Fig. 5-1 can be logically divided into two areas. The first area is comprised of the state WAIT, whereas the second area is comprised of all the rest states. WAIT, being representative of the waiting period caused by the assignment/de-assignment of the optical wavelength, effectively controls the length of time that the current RAU lies in idle state. This signifies that its respective SSP is:

$$\Pi_{WAIT} = 1 - fw \tag{1}$$

where f is the function determining the allocation of the optical wavelengths. Under MT-MAC operation the w wavelengths are equally distributed among the R RAUs, whereas under CW-MT-MAC operation each RAU receives optical capacity directly proportional to the percentage of the total number of users it holds and therefore f becomes:

$$f = \begin{cases} 1/R & \text{(MT-MAC operation)} \\ n/z & \text{(CW-MT-MAC operation)} \end{cases} \tag{2}$$

Regarding CW mode, we derive that $n \leq z/w$ since $f \cdot w \leq 1$. The latter denotes the upper barrier or maximum number of users $n_{max} = z/w$ per RAU, above which CW-MT-MAC assigns a dedicated wavelength. Once being in the WAIT state the only possible actions are: to remain stationary with probability p_w while waiting for wavelength

assignment, or to enter the $S_{1,n}$ state with probability $\overline{p_w}$ once a wavelength has been assigned. Following this, the wireless nodes enter the 2nd CP according to the CW-MT-MAC rules. All the wireless activity is depicted in the second logical area of the Markov model, which can be further divided into distinct rows and columns: each row corresponds to a single frame in the SF, while each column represents the number of nodes that are yet to be resolved in the 2nd CP. As such, the far-left column signifies the maximum number of unresolved nodes n and the far-right represents the situation where all nodes have been resolved, i.e. the number of unresolved nodes has reached zero. The expression describing the transition from state WAIT to state $S_{1,n}$ is:

$$\Pi_{1,n} = \Pi_{WAIT} \cdot \overline{p_w} \tag{3}$$

By (3) and the fact that each of the i frames, independently of its type, is of equal duration we derive that:

$$\Pi_{1,n} = \sum_{k} \Pi_{2,\kappa} = \sum_{k} \Pi_{3,\kappa} = \cdots = \sum_{k} \Pi_{i,k} = {}^{f \cdot w}/_{i} \tag{4}$$

Using (1), (3) and (4), $\overline{p_w}$ is found to be:

$$\overline{p_w} = \frac{f \cdot w}{i \cdot (1 - f \cdot w)} \tag{5}$$

In the case of CW-MT-MAC employment (5) translates to:

$$\overline{p_w} = \frac{n \cdot w}{i \cdot (z - n \cdot w)} \tag{6}$$

whereas in the case of RRA it becomes:

$$\overline{p_w} = \frac{w}{i \cdot (R - w)} \tag{7}$$

Finally, in order to calculate throughput S we need to specify Π_{TX}, Π_{CONT}, T_{RRF} and T_{DF} values, that are directly depended on (1) and (3) as well as on the specifics of the wireless access control scheme as they have been analyzed in the previous section.

Fig. 5-5(a) depicts the saturation throughput results obtained by both the analytical model and the respective simulation tool for the CW-MT-MAC scheme, for various

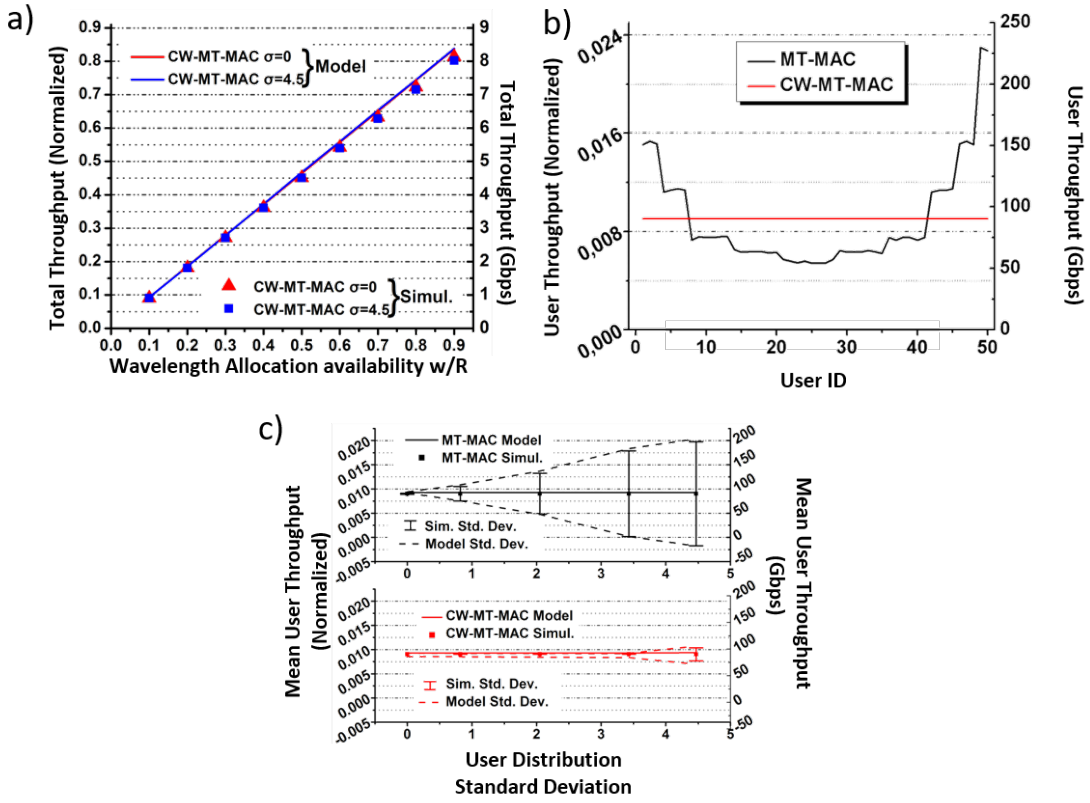

Fig. 5-5: a) User throughput vs. w/R ratio b) Throughput per user for all participating users of the network c) User throughput and its standard deviation vs. the user distribution standard deviation.

optical capacity availability factors denoted by the WR ratio, ranging from 0.1 to 0.9 and for the two most extreme distributions with σ=0 and σ=4.47, respectively. As can be noted the curves and symbols practically overlap each other, denoting that in saturation conditions CW-MT-MAC exhibits equal performance at the system level, irrespective of the client distribution pattern. In addition, Fig. 5-5(a) displays the excellent matching existing between the analytical results and the respective simulation-based findings, experiencing only negligible differences up to a maximum of 3%. This good agreement between theory and simulation confirms the validity of the model, revealing also the linear dependence existing between throughput and the optical availability ratio WR. CW-MT-MAC yields an efficiency rate of almost 92% (throughput to load), a fact that is indicative of the nearly optimum capacity exploitation in this dual-medium platform.

Fig. 5-5(b) presents the average throughput for each of the 50 participating users in the network, when the later are spread out using the distribution with σ =2.05. As can be

clearly observed, CW-MT-MAC manages to level out all throughput deliverance irrespective of the inequalities inserted into the network from the uneven client populations. In comparison, classic MT-MAC exhibits great disproportion regarding capacity allocation where the majority of clients residing in crowded RAUs receive less-than-average throughput opportunities, whereas the small fraction of clients that are in less-occupied areas receive up to four times greatest share. The above behavior undermines the network's efficiency as a whole, since users residing in different RAUs perceive a highly variating resource availability depending on their current location.

This variation can be more fully visualized in Fig. 5-5(c) where the mean throughput per user as well as its standard deviation for all distribution patterns of Fig. 4-3 and for WR=0.5 is depicted. As can be noted, the mean throughput remains constant regardless of the clients' distribution, but the case is totally different when coming to the standard deviation of the later, where CW-MT-MAC exhibits significantly lower throughput deviations compared to MT-MAC. MT-MAC's standard deviation values equal zero only in the case of the uniform user distribution pattern, and increase rapidly as the users get unevenly distributed amongst the system's RAUs, showing the latter's inefficiency towards accommodating irregular populations in RoF networks. On the other hand, CW-MT-MAC's σ-values remain zero for the first four user distribution patterns where the number of clients n is always lower than $n_{MAX} = 10$. When overcoming this point, CW-MT-MAC dedicates a wavelength to all RAUs having $n > n_{MAX}$ clients, which produces inequalities and therefore deviation of throughput. However, the latter always delivers the best possible throughput uniformity, offering a clear advantage and fairer throughput delivery.

5.4 MT-MAC delay analysis

5.4.1 Non saturation delay analysis

For the delay analytical model, we consider an MT-MAC network consisting of the CO, w wavelength pairs and R RAUs connected to the CO through an optical fiber of length L km. The network is utilizing an optical bus topology and the inter-RAU fiber interval is l km, i.e. the first RAU is L km away from the CO, the second RAU is $L + l$ km away from the CO, etc. Data packets are assumed to follow a Poisson arrival pro-

cess with bit rate of λ Mbits/s and a fixed size of B bits. Traffic is assumed to be symmetric, meaning that all clients introduce the same load into the network. The fiber transmission links provide 1 Gbit/s of bandwidth to each RAU which is shared amongst the wireless terminals serviced by each RAU. All RAUs are considered to serve the same number of clients n and therefore the symmetric traffic property applies in the RAU domain as well. We declare T_{cycle} to be the cycle time defined as the time between the start of two successive data transmission windows for a fixed RAU.

Since the MT-MAC operates under fixed service we can derive an accurate estimation of the cycle duration. To do that we need to specify the duration of the SF T_{SF} and the waiting period T_{WAIT}. T_{WAIT} refers to the time that a RAU has no assigned wavelengths either due to lack of pending traffic or due to wavelength time sharing amongst the network's RAUs. T_{SF} is equal to the sum of the duration of the SCP T_{SEC} and the data transmission period T_{DATA}. The first is comprised of one mandatory RRF followed by optional RRFs in case the first does not suffice in resolving the clients that request channel access. According to the MT-MAC rules the duration of the RRF frame T_{RRF} is defined as:

$$T_{RRF} = 3\delta_{FIBER} + s(3\delta_{AIR} + T_{POLL} + T_{ID} + T_{ACK}) \quad (1)$$

where δ_{AIR} is the propagation delay in the wireless medium, m is the size of the slots pool that the clients choose a random number from and T_{POLL}, T_{ID} and T_{ACK} are the transmission delays of the POLL, ID and ACK packets respectively. On the other hand, T_{DATA} is defined as the time it takes to transmit several sequential DFs plus the corresponding POLL and ACK frames. In the fixed service regime, the number of sequential DFs that is granted per RAU is immutable and always equal to P_{MAX}. DF's duration T_{DF} is defined as:

$$T_{DF} = \frac{2\delta_{FIBER} + 3\delta_{AIR} + P_{MAX}(T_{POLL} + T_{DATA} + T_{ACK})}{P_{MAX}} \quad (2)$$

where T_{DATA} is the transmission delay of the DATA packet. Based on the above we define T_{SF} as:

$$T_{SF} = T_{RRF} + P_{MAX}T_{DF} \quad (3)$$

Notice that at this point we consider only one RRF per SF. As described before, due to the MT-MAC rules this is not the only possibility since it could take more than one RRFs for the 2nd Cont. Period to resolve. Later on, a corrective factor will be added to account for that event, but at this point only the mandatory RRF is taken into account. Having defined T_{SF}, $T_{cycle}$is calculated as:

$$T_{cycle} = \frac{R}{w} T_{SF} \tag{4}$$

Since the cycle time is constant, the system can be considered at discrete moments that are apart T_{cycle} seconds as depicted in the example provided in Fig. 3-4.

We define $Q(t)$to be the queue size of a RAU at time $t * T_{cycle}$. $Q(t)$ is a discrete homogeneous Markov chain, which means that $Q(t)$ depends on the "past" states $(Q_0, Q_1, \dots, Q_{m-1})$ only through the present and is independent of t. Therefore, we are able to define transition probabilities and a transition matrix as it has been similarly done in [87]:

$$p_{i,j} = \Pr[Q(t+1) = j | Q(t) = i] \tag{5}$$

$$P = \begin{pmatrix} p_{0,0} & p_{0,1} & p_{0,2} & \cdots & p_{0,M} \\ p_{1,0} & p_{1,1} & p_{1,2} & \cdots & p_{1,M} \\ p_{2,0} & p_{2,1} & p_{2,2} & \dots & p_{2,M} \\ \vdots & \vdots & \vdots & \ddots & \vdots \\ 0 & 0 & 0 & \dots & p_{M-1,M} \\ 0 & 0 & 0 & \dots & p_{M,M} \end{pmatrix} \tag{6}$$

The transition probabilities are given below:

$$p_{i,0} = \sum_{k=0}^{P_{MAX}-i} e^{\left(-\frac{\lambda}{B} T_{cycle}\right)} \frac{\left(\frac{\lambda}{B} T_{cycle}\right)^k}{k!} \tag{7a}$$

for $i \leq P_{MAX}$,

$$p_{i,j} = e^{\left(-\frac{\lambda}{B} T_{cycle}\right)} \frac{\left(\frac{\lambda}{B} T_{cycle}\right)^{\mathrm{P_{MAX}}+j-i}}{P_{\mathrm{MAX}} + j - i} \tag{7b}$$

for $i \geq 0, j > 0$ and $j - i \geq -P_{\mathrm{MAX}}$,

$$p_{i,j} = 0 \tag{7c}$$

for $i, j \geq 0$ and $j - i < -P_{\mathrm{MAX}}$.

Equation (7a) states that it is only possible for a queue to send all its packets in one transmission window if the number of Poisson generated packets is equal or smaller than the maximum transmission window. This probability is given by the sum of probabilities of having no more packet arrivals than the maximum transmission window. The general probability of having a transition of i packets in the queue at an instant t to j packet at instant $t + 1$ in a cycle period is equal to the probability of generating exactly $P_{\mathrm{MAX}} + j - i$ packets and is given in (7b). Equation (7c) is a special case of (7b) and it states that if j is smaller than $i - P_{MAX}$ then $p_{i,j}$ is zero since that transition would require a transmission window greater than P_{MAX}. In order to be able to derive results we must set the upper limit M of the buffer size. This limits the dimension of the matrix P,causing the sum of the elements of all the lines to be less than one, which contravenes the mandatory property of a Markovian matrix. This problem is alleviated by defining the last element of each row of matrix P as:

$$p_{i,M} = 1 - \sum_{j=0}^{M-1} p_{i,j} \tag{8}$$

In order to find the stationary probabilities of queue sizes, a linear system of equations must be solved.

$$\pi P = \pi \tag{9}$$

$$\sum_{i=0}^{M} \pi_i = 1 \tag{10}$$

where π is the vector defining the probabilities of the queue sizes ranging from 0 to M in the steady state. The average queue size $\hat{Q}$ at the end of each transmission cycle is:

$$\hat{Q} = \sum_{i=0}^{M} \pi_i i \tag{11}$$

In order to derive the average queue size Q in the continuous time domain we must add the terms that account for the packets that have been produced during the 2nd Cont.

Period that precedes each SF and the packets that are born in between the discrete moments, i.e. T_{cycle} intervals. For calculating the average number of RRFs that will take place at the beginning of each SF we deploy the same two-dimensional (2-D) Markov chain model, depicted in Fig. 5-1, which demonstrates the 2nd Contention Period again from the perspective of a single RAU. The model follows the $S_{i,k}$ naming convention, where i stands for the i-th RRF frame of the current SF and k is the number of clients that are yet to be resolved by means of the 2nd Cont. Period. For each SF there is an upper limit i_{MAX} denoting the maximum number of RRFs that can take place within a single SF. Beyond that limit, the data transmission period commences with the clients that have been resolved, whereas any unresolved terminals will retry during the next SF.

The 2nd Contention Markov chain can be logically divided into distinct rows and columns. The first row corresponds to the initial state of the 2nd Cont. Period where all wireless clients are unresolved, whereas each individual row after that corresponds to a single RRF in the SF, i.e. the 2nd row corresponds to the 1st RRF, the 3rd row to the 2nd RRF and so forth. Each column represents the number of clients that are yet to be resolved in the 2nd Cont. Period. As such, the far-left column signifies the maximum number of unresolved clients n and the far-right represents the situation where all users have been resolved, i.e. the number of unresolved users has reached zero. It should be noted that $S_{i,1}$ type of states are not present in the Markov state diagram, given that node collision can only occur when at least two users are available for picking the same slot number in the random selection process.

The initial steady state probabilities are set based on the stationary distribution of queue sizes π:

$$\begin{cases} S_{0,0} = \pi_0 \\ S_{i,0} = \pi_{i,} \text{ for } 0 < i < n \\ S_{n,0} = \sum_{i=n}^{M} \pi_i \text{ for } i \geq n \end{cases} \quad (12)$$

The transition probability from state $S_{i,k}$ to state $S_{i+1,k-x}$ equals to the probability of having x out of a current total of k unresolved clients making a unique number choice and consequently getting resolved. This probability is provided by the equation:

$$p_k(x) = \frac{(-1)^x s!\, k!}{x!} \sum_{a=x}^{k} \frac{(-1)^a (s-a)^{k-a}}{(a-x)!\,(s-a)!\,(k-a)!} \tag{13}$$

for $k \in [2, n], x \in [0, k] \backslash \{k-1\}$.

A complete summary of all the non-null one-step transition probabilities is provided below:

$$\begin{cases} p\{i+1, k-x | i, k\} = p_k(x) \\ p\{i+1, 0 | i, 0\} = 1 \end{cases} \tag{14}$$

for $i \in [1, i_{\max}), k \in [0, n] \backslash \{1\}, x \in [0, k] \backslash \{k-1\}$. The second part of Eq.(14) denotes that, once reaching a state where all nodes have been resolved, the 2nd Cont. Period is over and the CO initiates the transmission of sequential Data Frames until the end of the SF duration.

The steady state probabilities of type $S_{0,k}$ (with k>0) form the Cumulative Distribution Function (CDF) of the numbers of RRFs that are necessary for completing the 2nd Cont. Period. Since the number of RRFs is an integer, we obtain the Probability Mass Function (PMF) from the CDF by means of subtraction. In turn, the PMF is used to derive the average number of RRFs N_{RRF} necessary to complete the 2nd Cont. Period. N_{RRF} is used to calculate the average number of packets that have been produced during the 2nd Cont. Period:

$$Q_{RRF} = \frac{\lambda}{B}(N_{RRF} - 1) T_{RRF} \text{ for } N_{RRF} \geq 1 \tag{15a}$$

$$Q_{RRF} = 0 \text{ for } N_{RRF} = 1 \tag{15b}$$

Notice that in (15a) 1 was subtracted from N_{RRF}, since in the initial calculation of T_{cycle} the first RRF, which is mandatory, was already included.

To finalize the transition of the average queue size from the discrete to the continuous time domain we must account for the average number of packet arrivals that occur in between the T_{cycle} intervals. Because Poisson arrivals are uniformly distributed in time, the average queue size in continuous time will be equal to the average queue size ex-

TABLE 5-2 DELAY ANALYSIS SPECIFICATIONS

PARAMETER	SYM-	VALUE
Number of Wavelengths	w	3-10
Number of RAUs	R	10
Fiber Length between CO and 1st	L	200m-
Packet arrival rate at the RAU	λ	0.1-1 Gbps
Fixed Transmission Window	P_{MAX}	30
Fiber propagation delay	δ_{FIBER}	1μs =
Slots in RRF	s	10
Number of clients per RAU	n	5
RAU range	-	10m
Air propagation delay	δ_{AIR}	0,032μs
Number of RRFs per SF	N_{RRF}	Variable
Wireless Data Bitrate	-	1 Gbps
ACK Size	B_{ACK}	8 bytes
DATA Packet Size (at the MAC	B	1500
POLL Size	B_{POLL}	64 bytes
ID Size	B_{ID}	64 bytes

actly in the middle of the discrete cycle intervals, i.e. the middle of the cycle.

$$Q_{mid} = \frac{\lambda}{B}\frac{T_{cycle}}{2} \tag{16}$$

The average queue size in continuous time Q is given by the following sum:

$$Q = \hat{Q} + Q_{RRF} + Q_{mid} \tag{17}$$

By means of Little's law, which states that the average number of packets in a stable system is equal to their average arrival rate multiplied by their average waiting time in the system, we yield the average waiting time or delay D:

$$D = Q * \frac{B}{\lambda} \tag{18}$$

5.4.2 Performance Evaluation

This section presents the performance of the proposed analytical model and evaluates its accuracy by comparing the delay values against the respective results obtained by the non-saturation simulation platform employed in Chapter 3 and Chapter 4. The results produced here correspond to a network configuration comprising 10 RAUs in a bus topology, serviced by w optical wavelength pairs each offering 1Gbps backhaul capacity as it is schematically depicted in Fig. 3-5. Table 5-2 summarizes the full specification parameters of the simulation run and of the respective analytical model where applicable. Performance is tested for various load conditions, wavelength availabilities, fiber lengths, transmission window sizes and data packet sizes. In this chapter load values correspond to the aggregated Poisson arrivals of all the wireless terminals per RAU and are presented in a normalized scale compared to the wireless channel capacity, ranging from 10% (100Mbps) up to 95% (0.95Gbps). Wavelength availability is referred as WR and is displayed as a percentage, i.e. for 10 RAUs and 3 wavelengths WR is 30%, whereas for 10 RAUs and 8 wavelengths WR is 80%. The different WRs allow the study of the RoF system under dynamic operative conditions where the engagement of the optical resources is assigned on the fly based on the desired service level. Simulation results are displayed with the use of a circle symbol and represent the average of 100 runs while the protruding capped vertical lines signify the 95% confidence interval, meaning that 95% of the produced simulation values fall within this interval.

c) Performance vs. Load

Fig. 5-6 displays the packet delay versus various load conditions for four different WRs namely 30%, 50%, 80% and 100%. For all the above scenarios, we witness that delay values start and remain very low (sub 0.5ms) until the point that the network enters its saturation regime. Note that for each of the different presented WRs, the saturation point is not constant, i.e. 30% WR the network saturates around 30% (300Mbps) offered load per RAU, whereas for 80% WR the saturation point is around 80% (800Mbps) of generated traffic. This comes as a direct effect of the backhauling capability of the presented network, since the latter depends on and is limited by the number of wavelengths available to the network. By means of Fig. 5-6(a) it is evident that delay

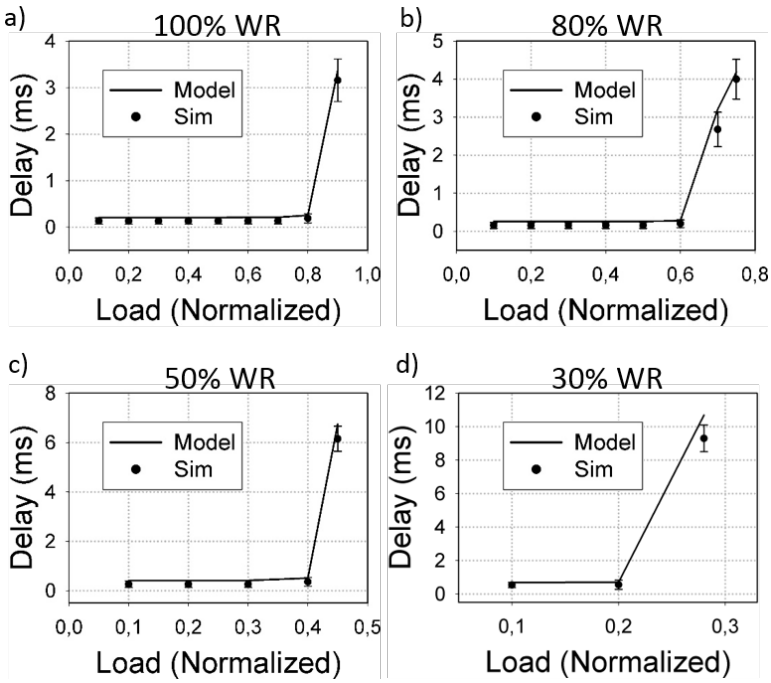

Fig. 5-6 Delay vs. Normalized load for 10 RAUS and (a) 10 wav. (100% WR) (b)8 wav. (80% WR) (c) 5 wav. (50% WR) and (d) 3 wav. (30% WR).

values start off in the sub 0.4 millisecond range and remain very low as long as the per RAU load is under 80% (800Mbps). In this area we also notice that the theoretical results practically coincide with the average values of the respective simulation runs. When the offered load approaches the maximum theoretical wireless channel capacity, delay values increase rapidly as the packets remain longer in the buffer queue awaiting transmission. In this area we note also small deviations between the average simulation and the analytical results. This discrepancy is explained by the fact that near the maximum theoretical wireless channel bitrate the average arrival rate approaches the system's capacity, resulting in the queue becoming unstable and therefore susceptible to small variations caused by the probabilistic Poisson traffic. However, even in these high load conditions the analytical results are within the 95% confidence interval of the simulation runs. The same curvature applies in the delay performance for every tested WR, as depicted in Fig. 5-6(b)-(d), with the only changing factors being the load value at which the network experiences saturation conditions, for reasons previously explained, and the absolute delay value that each configuration reaches in the congested areas. The latter happens due to the fact that the lack of wireless capacity in the low WR ratios forces each client to wait longer periods for the wavelength assignment to take place, thus introducing further delays.

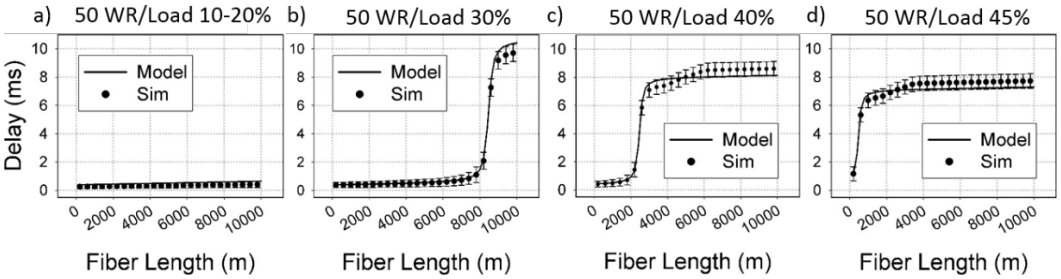

Fig. 5-7 Delay versus the length of the optical part of the network for 10 RAUs and 5 wavelengths (50% WR) (a) for 10-20% normalized load (b) 30% norm. load (c) 40% normalized load (d) 45% norm. load.

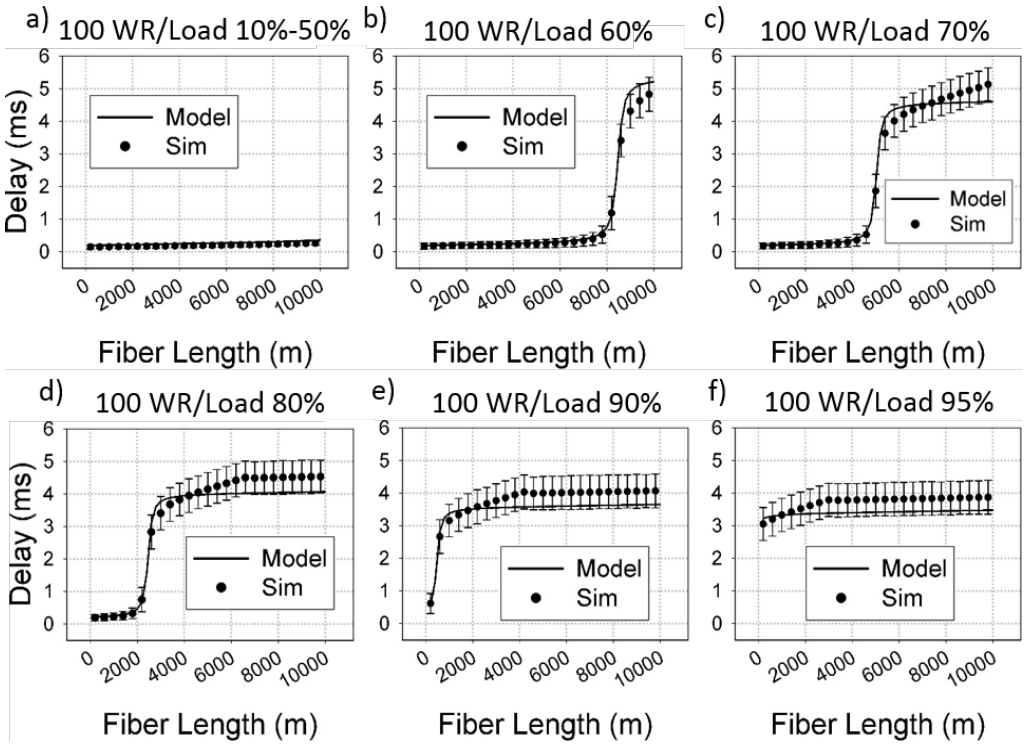

Fig. 5-8 Delay versus the length of the optical part of the network for 10 RAUs and 10 wavelengths (100% WR) (a) for 10-50% normalized load (b) 60% norm. load (c) 70% normalized load (d) 80% norm. load (e)90% norm load (f) 95% norm. load

d) Performance vs. Fiber Length

Fig. 5-7 and Fig. 5-8 present the packet delay performance versus various fiber lengths ranging from 200m up to 10km for two WRs, namely 50 and 100%, and for normalized load generation ranging from 10% up to 95% for 100% WR and 45% for 50% WR. As can be noted in the 100% WR case displayed in Fig. 5-8, for low and medium load conditions ranging up to 50% of normalized load (Fig. 5-8(a)) delay values are very low and always in the sub 0.5ms range for all tested fiber lengths up to 10km. The produced results display only a very small and linear performance degradation taking place amongst the shorter and longer tested network ranges. This shows that when there is high optical capacity availability, the MT-MAC protocol is capable of tolerating long

fiber hauls and is able to achieve optimum delay values as long as the offered network load does not exceed 50% of the maximum theoretical normalized value. Again here it can also be seen that the analytical and the simulation results coincide perfectly for all derived values of fiber length, since the network does not enter its saturation regime which would cause buffer depletions and instability in the queue. At higher load conditions, such as the case depicted in Fig. 5-8(b) representing the 60% offered network load, the MT-MAC protocol fails to maintain the low latency properties in long fiber lengths. Specifically, when the fiber length exceeds 8km, delay values increase rapidly, as the larger cycle times effectively lead to more packet births than the amount of data frames that can be serviced by the static transmission window. This fact also attributes for the small discrepancy between the analytical and the mean value of the simulation results, since the system operates at capacity forcing data packets to wait multiple cycle times before transmission, therefore resulting in an unstable system. However, the analytical results are always within the 95% confidence interval of the simulation results exhibiting the excellent match between simulation and theory. The same behavior is also evident in Fig. 5-8(c)-(f) that display the delay results for normalized loads ranging from 70-95% respectively. The only alternating factor is the maximum fiber length that can be tolerated for each load value, i.e. at 70% load, the maximum fiber length within which the MT-MAC protocol exhibits low delay properties is around 5km, at 80% the saturation point drops to 2km and at 90% load the maximum fiber length drops to 400m. In the extreme scenario of 95% load, depicted in Fig. 5-8 (f), the network appears saturated even for the smallest fiber lengths, effectively denoting the upper limit where the MT-MAC's remote arbitration scheme is capable of delivering fast service to the end users.

Regarding the 50% WR ratio, a similar performance pattern is observed for low load values (up to 20% Fig. 5-7(a)), with delay being constantly in the sub 0.5ms region for all tested network ranges up to 10km. As the ingress load increases however (Fig. 5-7 (b)-(c)), the network enters its saturation regime at high fiber lengths. As in the previous scenario, the specific length where the increased cycle time causes the network to saturate is based on the offered network load, ranging from 8km in the case of 30% load down to 200m in the extreme scenario of 45% load. In is also noteworthy that in the

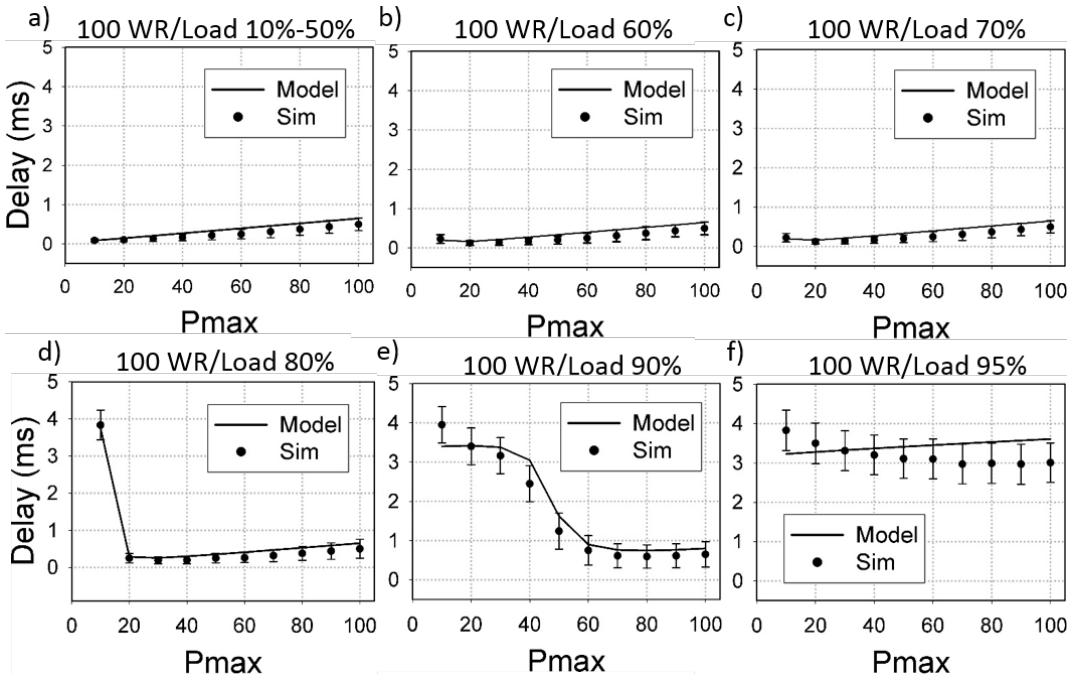

Fig. 5-9 Delay versus the length of the transmission window Pmax for 10 RAUs and 10 wavelengths (50% WR) (a) for 10-50% normalized load (b) 60% norm. load (c) 70% normalized load (d) 80% normalized load (e) 90% normalized load (f) 95% normalized load

50% WR scenario the actual delay is greater compared to the case of 100% WR, due to the fact that wavelength sharing causes added delays as the RAUs are forced to wait approximately 50% of the system time for a wavelength assignment.

e) Performance vs. Transmission Window Size Pmax

One of the most crucial parameters that define the performance of the fixed service regime is the size of the transmission window $P_{\max}$. To this end the proposed analysis can be employed to derive the optimum window size based on the available WR and the respective load conditions. Fig. 5-9 and Fig. 5-10 present the packet delay performance of the hybrid MT-MAC protocol versus $P_{\max}$ for two different WR ratios, namely 50 and 100%, and for various normalized load conditions ranging from 10% up to 95% for the 100% WR case and 45% for the 50% WR case.

Fig. 5-9 presents the case of the 100% WR versus the $P_{\max}$ value ranging from 10 up to 100 packets per static window assignment. As can be seen in Fig. 5-9 (a), while the offered load ranges from 10% up to 50%, delay values remain very low and increase linearly with $P_{\max}$ at a very low rate. The reason for the slow performance deterioration

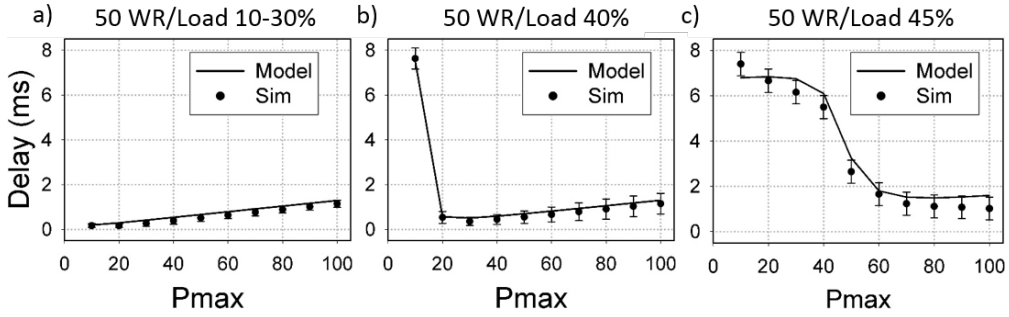

Fig. 5-10 Delay versus the length of the transmission window Pmax for 10 RAUs and 5 wavelengths (50% WR) (a) for 10-30% normalized load (b) 40% norm. load (c) 45% normalized load

is that in low traffic conditions a large transmission window size leads to underutilization of the wireless channel, since the initial polling sequence constructed at the beginning of the SF is larger than the number of packets waiting in the nodes' buffers. This directly translates to unused transmission opportunities when the nodes' buffers are depleted. Moreover, larger transmission windows lead to larger cycle times and therefore to less frequent executions of the 2nd Cont. Period which, according to the MT-MAC rules, is responsible for constructing the polling sequence in the CO. This forces the inactive users that did not partake in the last 2nd Cont.Period to wait longer periods until the beginning of the next SF, thus introducing further delays into the network. As load increases (Fig. 5-9(b)-(d)), we observe that the delay performance is no longer linear to $P_{\max}$, but instead very small $P_{\max}$ values (i.e. 10) exhibit higher delays than larger $P_{\max}$ values (i.e.20). Once the delay reaches its global minimum, linearity is reestablished and any further increase in the transmission window results in a small rate linear increment of the delay, similarly to the low-medium traffic conditions depicted in Fig. 5-9(a). This behavior is caused by the fact that for very small $P_{\max}$ values, the transmission window no longer suffices for all packets to be transmitted, thus a part of the outstanding traffic is forced to wait for the next transmission opportunity that will take place in the following SF. When load increases even further (Fig. 5-9(e)), incoming traffic greatly exceeds the capacity of the transmission window causing high delays and instability in the queue which results in the exhibited difference between the theoretical and simulation results. As $P_{\max}$ increases however, delay values decrease and the system's utilization factor drops below 1, resulting in the theoretical results to be well within the 95% confidence interval, once again proving the excellent matching between

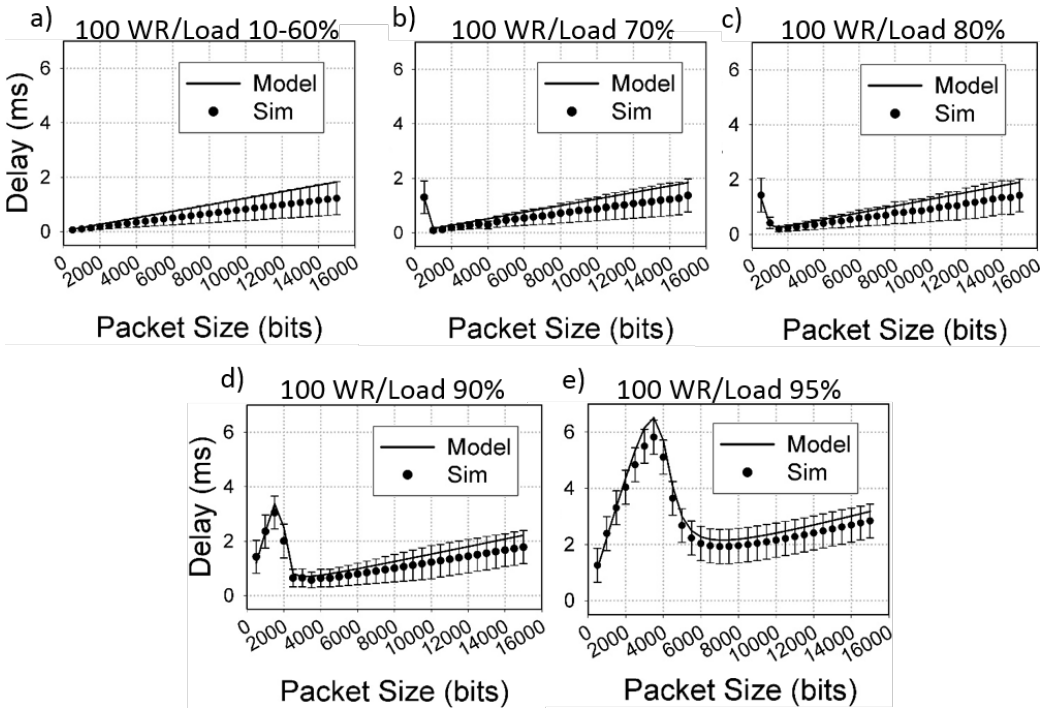

Fig. 5-11 Delay versus the length of the transmission window Pmax for 10 RAUs and 5 wavelengths (50% WR) (a) for 10-30% normalized load (b) 40% norm. load (c) 45% normalized load

the theoretical analysis and the simulation. Finally, in the extreme case of 95% normalized load depicted in Fig. 5-9 (f), the system resides in unstable saturation conditions for all the tested values of $P_{\max}$, therefore exhibiting high delay values and a higher degree of mismatch between the theoretical and simulation results.

In the 50% WR scenario depicted in Fig. 5-10, we note that the system exhibits the same overall behavior with the difference being that the system enters saturation regime in lower normalized load values and produces higher absolute delay values as opposed to the 100% WR scenario. The latter is again attributed to the fact that the RAUs are inactive for a significant portion of the system time while waiting for wavelength assignment, thus contributing towards higher delay values.

f) Performance vs. the Data Packet size

Fig. 5-11 and Fig. 5-12 present the MT-MAC's delay performance versus the size of the Data Packet at the MAC layer for two WR ratios, namely 50 and 100%, and for various normalized load conditions ranging from 10% up to 95% for the 100% WR case and 45% for the 50% WR case. The tested Data Packet sizes range from 500 up to 15000 bytes per packet. Fig. 5-11 presents the scenario of 100% WR. By means of Fig. 5-11(a) we observe that in low load conditions the increment of the Data Packet size

leads to a small rate linear increment in the derived delay. This is due to the fact that the larger the data packet size the more time it takes for a packet to reach the head of the polling sequence and initiate transmission. A further increment of the offered traffic above 60% of the maximum theoretical capacity (Fig. 5-11(b)-(c)) creates a phenomenon similar to the previous section, meaning that very small packet sizes cause the network to perform worse than greater packet sizes. This is due to the fact that for very small payload sizes the generated traffic exceeds the capacity of the packet and therefore data has to be split into several packets. The increased number of packets reduces the protocols efficiency since it also increases the overhead of the actual transmission due to the additional headers and signaling requirements, therefore resulting in higher latencies. However, we also notice that once the packet size grows large enough to accommodate the produced traffic, delay values drop until they reach their minimum value, signifying the optimum packet size for the specific load/WR conditions. Beyond this optimum value any further increment causes the delay to increase at a low rate for the same reasons as the ones presented in Fig. 5-11(a). The very high load scenarios presented in Fig. 5-11(d) and (e) follow a different curvature than the rest of the load conditions. Specifically, in both figures delay values start low, then rapidly increase until they reach a maximum value, and in turn drop before resuming the normal linear behavior that was evident in the previous figures. In order to justify this behavior, we include Table 5-3 that presents the average normalized throughput values and packet drops percentages as they were derived by the simulator. Normalized throughput values have been calculated as the number of data packets that were correctly delivered per

TABLE 5-3 THROUGHPUT VALUES IN PACKET SIZE VS DELAY ANALYSIS

P. Size	Load 90%		Load 95%	
(bytes)	TH	PD	TH	PD
500	0.692	23.0%	0.692	27.2%
1000	0.818	8.50%	0.818	14.0%
1500	0.871	3.35%	0.871	7.86%
2000	0.890	0%	0.899	3.70%
2500	0.892	0%	0.918	2.82%
3000	0.900	0%	0.930	1.01%
3500	0.890	0%	0.937	0.33%
4000	0.891	0%	0.944	0%
4500	0.897	0%	0.945	0%

TH: Average Normalized System Throughput (0-1)
PD: Average Packet Drop Percentage (0%-100%)

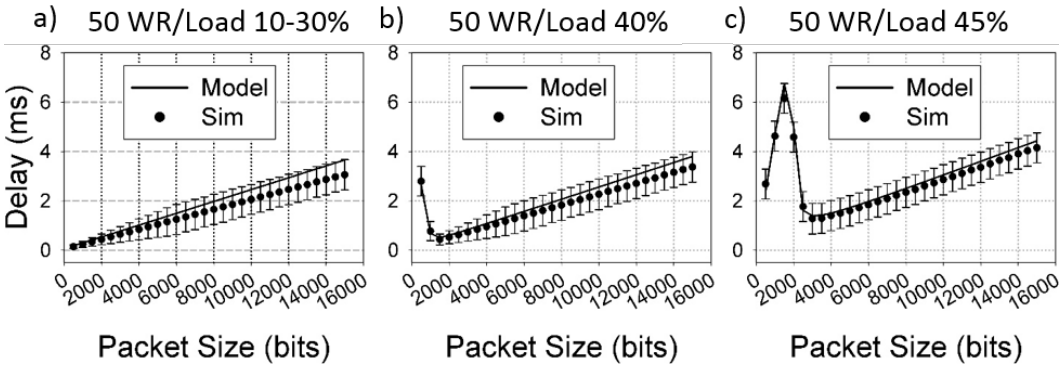

Fig. 5-12 Delay versus the Data Packet size for 10 RAUs and 5 wavelengths (50% WR) (a) for 10-30% normalized load (b) 40% norm. load (c) 45% norm. load.

time slot, with a time slot being equal to the time required for a data packet to be transmitted. As it can be seen in the left-most portion of the Fig. 5-11(d) and (e), while the delay slope is increasing, throughput values are less than the corresponding normalized load since the network exhibits packet losses. The latter effectively means that the system services less packets than the ones that are generated and therefore delay values are counted as lower, since the packets that succeed in entering the buffer are serviced faster while the discarded packets are not taken into consideration when measuring the system's delay performance. To this end, as long as the packet drops are more than zero, the delay measurements appear lower due to the assumption that the buffer's capacity is finite. While the packet size increases and packet drops approach zero, delay increases since the measurement process accounts for a greater percentage of the generated packets, therefore becoming more accurate. Finally, when packet drops become zero, the curvatures of the results resume a path similar to the ones presented in Fig. 5-11(b)-(c). Note here that, due to the increased load, the packet size must increase to 4000 bytes for the system to experience zero losses in 95% traffic, whereas 2000 bytes suffice for 90% load. Again here we notice that the theoretical results are always within the 95% confidence interval of the corresponding simulation results.

Fig. 5-12 presents the same study for 50% WR ratio. Upon examination we notice that the results follow the same curvature, with the only differences being that the absolute delay values are higher than the corresponding results of 100% WR and increase at a higher rate. The latter is attributed to the fact that insufficient packet sizes and the consequent data segmentation into multiple MAC layer packets has a more detrimental effect when the end nodes have to wait for wavelength assignment before being polled to transmit.

5.5 Concluding Remarks

In this chapter we have firstly presented an analytical model for calculating saturation throughput for the MT-MAC protocol. The analytical throughput model was accompanied by a detailed saturation throughput performance analysis, assuming ideal channel conditions. The presented model relies on a two-dimensional (2-D) Markov chain approach for calculating the end-user transmission probabilities, taking into account contention for both the optical and the wireless layer resources. An analytic formula for throughput computation was derived and the respective results for different optical resource availability factors were found to be in close agreement with simulation-based outcomes, confirming the validity of the MT-MAC model. Secondly we have presented a delay model that enables the computation of end to end packet latency under non saturation conditions, successfully confirming respective simulation results for different numbers of optical wavelength availability ratios, network loads, fiber lengths and transmission window sizes. The theoretical results were found to be in excellent agreement with respective simulation-based findings and always within the 95% confidence interval. This first successful MT-MAC modeling approach indicates that the functional convergence of the optical and the wireless connection links can yield new and efficient capacity and resource utilization concepts in 60 GHz RoF networks, equipping 60 GHz high-speed applications with high-level agile operational frameworks.

Page intentionally left blank

Chapter 6 Architectural Aspects and PON synergy

The previous chapters have presented the MT-MAC protocols' operation on top of generic topologies. However, in order to qualify for commercial and deployed fiber systems, it is imperative for the RoF approaches to be tested and compared to already deployed architectures and well-established infrastructural paradigms. In the fiber domain, a series of advantages such as cost effectiveness, energy savings, service transparency, and signal security over all other last-/first-mile technologies have established the PONs as the by far predominant and most widely used optical fiber architecture[88]. This forces all possible future Fiber-Wireless (FiWi) solutions to strive for PON compatibility[89], and as such dictates the need for a detailed comparative study on the inter-play between the extended MT-MAC-enabled WLAN networks and deployed PON systems.

In this chapter, we present an extensive study on the formation, convergence and interfacing of various 60GHz Gigabit WLAN over GPON architectures. Two possible network scenarios are investigated for the establishment of extended range mm-wave WLANs, the first one being based on a recent standardization effort and the other on a recent promising research outcome: i) the Radio-and-Fiber (R&F) scenario termed as "GPON-plus-802.11ad", which considers several 802.11ad routers attached to equally numbered ONUs employing the GPON network as the fiber backhaul infrastructure and ii) the RoF scenario termed as "MTMAC-over-PON", which substitutes GPON's Optical Network Units (ONUs) with RAUs while GPON's Optical Line Terminal (OLT) facilities get upgraded so as to operate under the MT-MAC paradigm. Extensive simulation-based throughput and delay results are obtained for a plethora of network scenarios, revealing the dependence and denoting the benefits and shortcomings of the above architectures on several network planning parameters: the load of the network,

the number of available optical wavelengths, the percentage of intra-LAN and Internet-destined network traffic as well as the PON's total fiber length.

In addition, driven by the above findings we study for the first time to the best of our knowledge a hybrid RoF/R&F architecture under the scope of mm-wave communications. This multi-tier mixed architecture, termed as "GPON-plus-MT-MAC", considers a short-length MT-MAC (RoF) network in a bus topology attached to a GPON ONU that serves the intra-WLAN or intra-cell communication demands, whereas any inter-cell claims are forwarded by the MT-MAC CO to the GPON network through an existing CO/ONU interface. The results derived by GPON-plus-MTMAC's extensive performance evaluation confirm that the latter architecture combines the properties of the MTMAC-over-PON and the GPON-plus-802.11ad approaches, balancing their trade-offs in an optimal manner.

6.1 RoF and R&F architectures for mm-wave communications

In RoF systems, the Central Office (CO) modulates RF signals onto an optical carrier which in turn travels over an analog fiber link towards simple RAU (Optical/Electrical/Optical + Antenna) modules. RoF's centralized architecture allocates all network complexity to the CO and thus overall implementation and operational costs drop while handover and operational-maintenance procedures become simpler. Moreover, the use of simplified RAUs enables the physical expansion of the network dimensions with spatiotemporal centralized resource allocation. However, the added distance that wireless signals must propagate through the (usually) several kilometers long interleaved fiber can cause significant problems in the operation of the wireless MAC protocols (i.e. timeouts etc.) thus limiting the maximum physical reach of the network. The latter becomes increasingly a problem in the 60GHz domain since timeout constraints are even stricter, thus further decreasing the maximum network length. In addition, the remote nature of centralized control becomes a bottleneck in a volatile wireless environment where frequent link establishments dictate the exchange of control packets that are otherwise optional in wired networks. RoF implementations inherently operate as backhauling architectures since packets traverse the entire network. This can be beneficial for packets destined towards Internet destinations, as the former travel faster by remaining at the MAC layer thus avoiding the delays produced by higher layers like the IP. However, the opposite is true for packets destined to close proximity nodes since

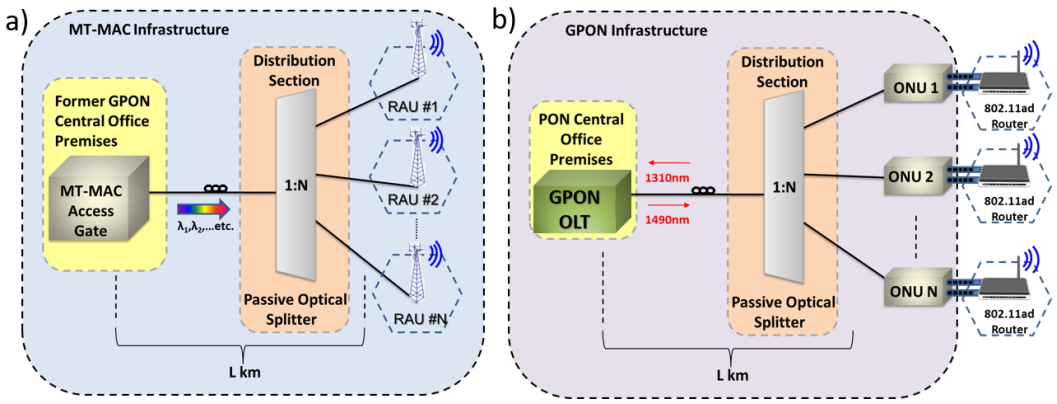

Fig. 6-1 (a) The MT-MAC-over-PON architecture (b) the GPON-plus-802.11ad architecture

they will be indiscriminately forwarded to the CO and therefore acquire significant delay overheads.

In R&F systems, discrete optical and wireless networks are merged in order to form one single integrated network that utilizes different optical and wireless MAC protocols. This means that intra WLAN traffic does not propagate towards the optical network and distributed as well as client-to-client ad hoc connections avoid the fiber's extra propagation delays. This feature also alleviates all wireless MAC restrictions from the optical portion of the network such as the maximum fiber length. However, within the context of the 60GHz communications, providing large scale coverage would require massive active equipment installations, which in turn translates to higher costs and lower energy efficiency. In addition, the range of mm-wave WLANs (<10m as specified in 802.11ad) requires the physical presence of the nodes within a very confined area and is therefore impractical for broad adoption.

This chapter attempts a head-to-head comparison between the predominant RoF and R&F FiWi specifications in order to determine the optimal conditions and identify the trade-off points for a variety of network conditions so as to function as a future guide for the upcoming 60GHz hybrid optical/wireless network implementations. Both tested RoF and R&F architectures utilize tree-based PON infrastructures, since the latter are generally considered the strongest candidate for widespread deployments. Fig. 6-1(a) depicts the Radio-over-Fiber approach operating under the MT-MAC paradigm termed as the MTMAC-over-PON architecture. In this scenario, an MT-MAC Access Gate (MTAG), that includes the necessary hardware resources for generating the RoF optical channels, is placed at the location of a conventional GPON OLT. The OLT is in turn

connected to an Optical Distribution Network (ODN) with L km length that employs a 1:N passive splitter. ODN's fibers terminate in the RAUs that provide the mobile users with 60GHz wireless connectivity. By transferring all functionalities to the CO and substituting the active Access Points (APs) units with RAUs the MT-MAC architecture forms an extended range WLAN that bypasses the inherent limitations of the 60GHz medium in a cost-effective way. Moreover, the MT-MAC scheme employs a dynamic wavelength allocation algorithm that assigns optical capacity only to RAUs with active wireless clients and therefore permitting the physical reach extension of the RoF network by allowing the deployment and operation of a greater number of antenna units with fewer optical resources. This way a MT-MAC architecture with N RAUs and w available wavelengths offers N 60GHz wireless channels to the users, w of which can function concurrently, whereas data backhauling is operated in an w-channel WDM PON fashion.

Fig. 6-1(b) displays the Radio & Fiber architecture, termed as the GPON-plus-802.11ad approach. As mentioned before, this approach stems from the well investigated subject of FiWi integration as the latter has been extensively presented in the literature, with the majority of work revolving around EPON/GPON integration with WiMAX/LTE/DOCSIS[36]-[39] or 802.11[40] and mesh networks[41],[42]. The GPON-plus-802.11ad architecture is comprised of N 802.11ad Access Points (ADAPs) that are bridged to equally numbered ONUs and consequently backhauled through GPON's ODN. The employed GPON network features 2.5Gbps Down- and 2.5Gbps Up-link capabilities whereas the ONU-ADAP communication is handled by their common protocol translation interface that mainly consists of the GPON Encapsulation Method (GEM) scheduler and the GEM classifier. The GPON-plus-802.11ad network offers N continuously operating 60GHz wireless channels to the users alongside buffering and local routing functionality (packets travelling to intra-cell destinations stay within the MT-MAC portion of the network), whereas only the packets that head to destinations residing in other ADAPs of the network are traversed through the GPON infrastructure.

TABLE 6-1. SIMULATION PARAMETERS			
GPON-plus-802.11ad		**MT-MAC-over-PON**	
RTS	160 bits + PHY Header	ID Packet Size	64 bytes
CTS	208 bits + PHY Header	POLL Packet Size	64 bytes
ACK	112 bits + PHY Header	1st Cont. Policy	Static Interval
G-PON downlink	2.5 Gbps	1st Cont. Interval	5ms
G-PON uplink	2.5Gbps	RRF size Policy	Flexible
SIFS	3 μs	Minimum RRF Slots	3
DIFS	13 μs	SuperFrame Size Policy	Gated
Slot time σ	5 μs	Data Serving Policy	Round Robin
Min CWsize (CW_{min})	16	ACK Policy	Immediate
Max CW size (CW_{max})	480	Number of wavelengths	Variable
Common Specifications			
Control PHY header		40 bits	
SC PHY header		64 bits	
MAC Header		320 bits	
Data Packet Payload		2000bytes	
Nr. of ONUs		32	
Control PHY Rate (MCS0)		27.5 Mbps	
SC PHY Rate (MCS4)		1155 Mbps	
SC PHY Range		6.5 m	
G-PON fiber Length		L = 10 km	

6.2 Performance evaluation

In order to assess the performance of RoF versus R&F 60GHz WLAN formations we perform a comparative evaluation of the MT-MAC-over-PON network versus the GPON-plus-802.11ad network. Both configurations are based on a 10km long PON network with 1:32 splitting ratio. In the GPON-plus-802.11ad network, each of the ONUs is attached through the G-PON/802.11ad interface to an ADAP, whereas in the MT-MAC-over-PON network, the PON fibers terminate directly in RAUs. Both radios provide a $6.5m$ radius mm-wave coverage, therefore each of the network configurations provides $32 * \pi * 6.52 \approx 4245m^2$ of 60GHz service area. Every ADAP or RAU unit services 5 randomly placed clients in its range and sector scanning is employed prior to the first packet exchange with a specific client in order to enable the required directionality in the transmission. For the communication part we focus on the uplink transmission direction. Regarding the 802.11ad, every non-AP STA contends for its transmission opportunities (TXOPs) based on the Distributed Coordination Function (DCF) operation. To obtain results for the GPON-plus-802.11ad we implemented an event-driven simulator based on the Pamvotis 802.11 WLAN simulator[90] that was extended to support 802.11ad and GPON operation, whereas for the MT-MAC network an event-driven simulator was implemented in Java. The full list of simulation parameters is presented in Table 6-1.

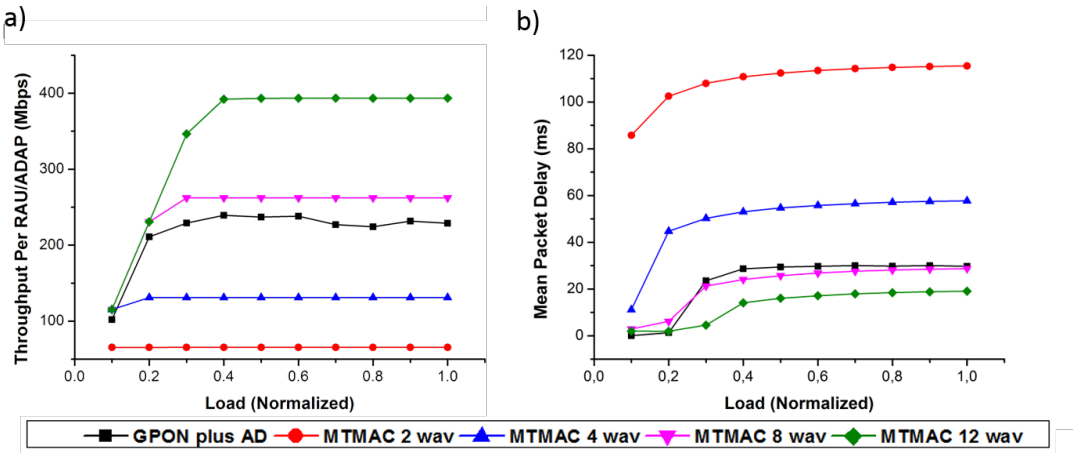

Fig. 6-2 Delay Throughput and Delay for 80/20 traffic (80% stays within the cell).

6.2.1 Dependency on traffic load

Fig. 6-2 and Fig. 6-3 illustrate the architectures' performance behavior versus various intra/inter-cell traffic shapes and load conditions. The generated load ranges from 0.1 up to 1 packet generation per timeslot per RAU/ADAP where the timeslot is defined as the transmission delay of a single data packet for the given data channel rate. Two traffic shapes are considered: i) traffic shaped under the under the traditional 80/20 rule[91], meaning that 80% percent of the traffic is destined for intra-WLAN destinations whereas 20% of the traffic goes beyond the local subnet and heads to GPON's CO (Fig. 6-2) and ii) the more modern 20/80 rule meaning that 20% percent of the traffic is destined for intra-WLAN destinations whereas 80% of the traffic goes heads to GPON's CO (Fig. 6-3). In this chapter we employ the above distinction in order to categorize traffic based on the backhauling requirements relative to existing PON infrastructures for interfused optical/wireless networks. The term intra-WLAN is interpreted as intra-cell in order to maintain a clear comparative platform between the different architectures, whereas the cell is defined as the 60GHz radio service area provided by a single RAU or ADAP. The 80/20 ratio is studied because it closely describes the usual mm-wave applications such as cable replacement scenarios, e-Health applications as well as highly-secure enterprise networks that restrict Internet traffic. On the other hand, the 20/80 ratio represents other type of applications such as server farms and/or other web based computing scenarios where most of the data exchange is between service providers (ISPs, cloud computing, cloud storage companies etc.) and their customers.

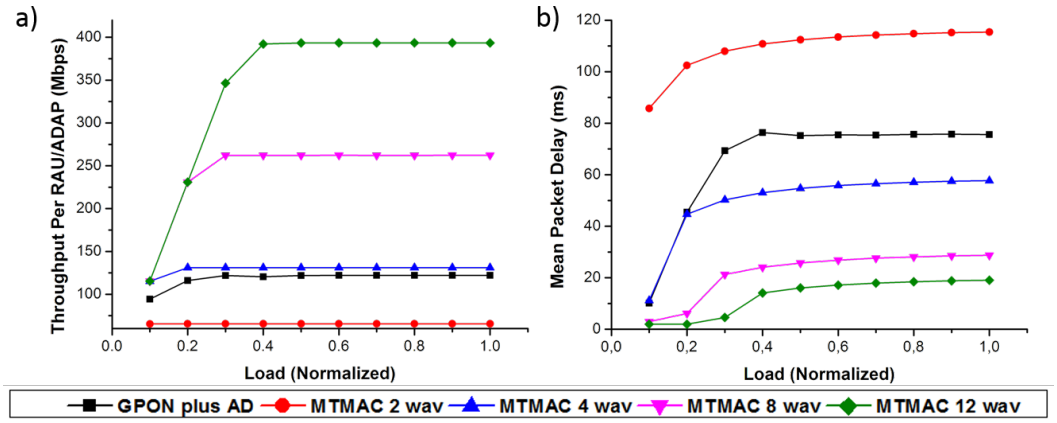

Fig. 6-3 Throughput and Delay for 20/80 traffic (80% heads to destinations outside the cell).

As can be observed in Fig. 6-2(a) (80/20 traffic ratio), the GPON-plus-802.11ad throughput curves increase with load until the point that throughput reaches its saturation plateau. For the RoF architecture represented by the MT-MAC-over-PON scenario we note that for low wavelength availability, such as 2 wavelengths, throughput appears already saturated even for 10% traffic load conditions (0.1 packet/slot/RAU), since all packets have to traverse the entire network length (10 km in this scenario) both in the uplink and downlink direction for the establishment of the communication link and the data exchange. This adds up to significant delays, especially for the packets that head towards nearby intra-cell destinations. However, by employing the MT-MAC's inherent capability to utilize a larger set of optical wavelengths, the MT-MAC-over-PON can operate in a WDM-PON fashion causing throughput values to rise as more wavelengths are added, up to the point where the MTMAC-over-PON's performance surpasses that of the GPON-plus-802.11ad network. As can be witnessed in Fig. 6-2(a), with 8 employed wavelengths the MTMAC-over-PON manages to match and in addition to surpass the GPON-plus-802.11ad's performance by an average of 16%. This throughput improvement escalates even further to an average of 75% for 12 wavelengths. The witnessed performance increment stems from the higher number of optical wavelengths that in turn leads to less time-consuming wavelength (de)allocation activities as well as longer SuperFrame lengths therefore increasing the protocol's efficiency. Therefore, the performance improves with increasing number of wavelengths and the protocol's saturation capacity is extended to higher load values. Going beyond 12 wavelengths will further increase the saturation point to higher load conditions and also provide additional performance gap between the MTMAC-over-PON and GPON-plus-

802.11ad architectures. The proportional relationship of optical resources to the maximum achieved throughput also indicates that the support of specific application types is subject to the number of available optical wavelengths, i.e. resource-heavy applications will demand higher optical capacity to be adequately supported. However, it becomes evident that a broad range of application services can be supported by employing the necessary number of available wavelengths. Delay values, depicted in Fig. 6-2(b) for the same configuration, follow an ascending path as load increases before becoming essentially stable at the point where throughput saturates. Beyond throughput's saturation point any excessive packet arrivals become immediately dropped after birth due to buffer overflow. Note here that measured delay refers only to the packets that get delivered, whereas dropped packets are excluded from the above metric.

Fig. 6-3(a) and Fig. 6-3(b) present the same results but for traffic shaped under the more modern 20/80. Here, throughput and delay values follow the same curvature as in Fig. 6-2(a) and Fig. 6-2(b) with the difference that GPON-plus-802.11ad's performance drops significantly lower, whereas MTMAC-over-PON's corresponding performance remains unchanged. Specifically, GPON-plus-802.11ad's throughput saturation value drops from ~250Mbps to ~125Mbps per ADAP. This performance degradation is caused by the quadrupled extra-cell traffic that places a heavy burden upon GPON's limited uplink capacity, where only one wavelength is employed towards servicing the upstream traffic from all ONUs, therefore causing buffer overflows and packet drops in the GPON/ADAP interface.

This section provides a head to head comparison regarding the performance of the two tested architectures versus load for various optical capacities (2,4,8 and 12 wavelengths) and also displays how the RoF and R&F architectures compete against each other. In this work we are not proposing a specific number of wavelengths to be used universally since the criteria for this selection span across multiple decision factors such as desired service level, hardware cost, energy efficiency, upkeep costs etc. This work focuses on the individual as well as the comparative performance aspects of the tested RoF and R&F architectures supporting VHT wireless over optical communication and to identify the optimal architecture given the relevant network parameters.

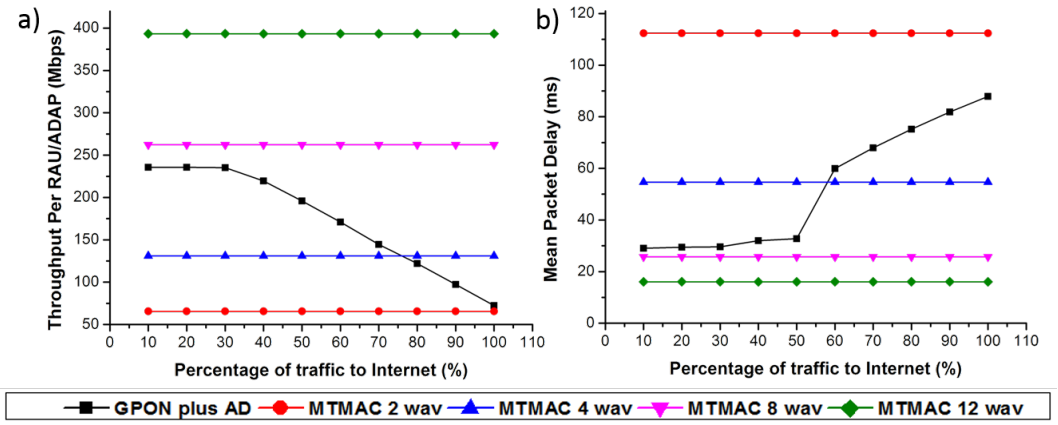

Fig. 6-4 Throughput and Delay versus percentage of traffic heading towards Internet destinations

6.2.2 Dependency on percentage of intra/inter-cell traffic ratio

To gain a more detailed insight into the impact of the intra/inter-cell traffic ratio, Fig. 6-4(a) and Fig. 6-4(b) focus on the performance under various inter- and intra-cell traffic shapes ranging from 10% up to 100% of traffic heading towards internet destinations. The results are shown for a constant load generation of 0.5 packets per slot time per RAU/ADAP. As can be seen in Fig. 6-4(a) and Fig. 6-4 (b), the MT-MAC-over-PON's throughput and delay performance remains constant regardless of the intra/inter LAN traffic ratio fluctuations and depends solely on the number of available wavelengths, since packets have to traverse the whole network irrespective of the traffic shape. On the other hand, GPON-plus-802.11ad's throughput values remain constant only while the ratio of Internet-heading traffic is lower that 30%, whereas beyond that point, throughput drops almost linearly due to congestion in the single wavelength GPON backbone. The same is true for delay performance depicted in Fig. 6-4(b) where the average packet delay remains almost stable while the extra-cell traffic is lower than 30%, but increases soon after, reaching its maximum value of 88ms when all traffic heads beyond the cell. Notably the equilibrium point regarding the two architectures' throughput performance varies depending on the number of the MT-MAC available wavelengths. For instance, for 2 available wavelengths the equilibrium point is set around 100% of the traffic heading beyond the cell, whereas for 4 wavelengths this value drops to 75%. Beyond 4 wavelengths there is no equilibrium point since MT-MAC-over-PON surpasses the performance of 802.11ad-plus-GPON for all traffic shapes. This is due to the fact that when increasing the number of wavelengths, the MT-MAC-over-PON architecture essentially operates in a WDM-PON fashion, therefore

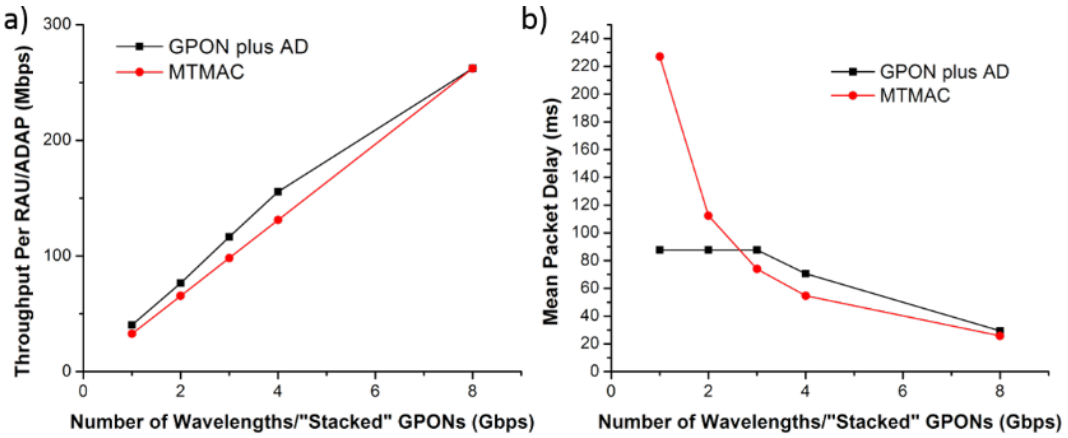

Fig. 6-5 Throughput and Delay versus number of available wavelengths in the MT-MAC-over-PON scenario or Stacked GPONs in the GPON-plus-802.11ad scenario

gaining a significant advantage in data backhauling towards the existing single wavelength GPON implementations. However, when traffic demands concern mostly intra-cell destinations (left-most part of Fig. 6-4(a) and (b)), GPON-plus-802.11ad manages to achieve the same performance with only a single wavelength in the optical backbone due to the close proximity of the ADAP with the wireless clients, making it very efficient for very short range applications. We also observe that for the same throughput values the MT-MAC-over-PON architecture exhibits lower delays with their respective difference progressively increasing as the inter-cell ratio rises.

6.2.3 Dependency on the optical capacity

To better understand the role of the optical wavelength availability Fig. 6-5 displays the relation between performance and optical capacity for both competing architectures. Regarding GPON-plus-802.11ad we consider a variable number of "stacked" GPON networks with 1.25 Gbps down and uplink capacity. The "stacked" GPON solution is one of the dominant candidate technologies according to the NG-PON2[92] paradigm, where multiple GPON sub-networks share the same optical distribution infrastructure by employment of Wavelength Division Multiplexing (WDM) mechanisms. As far as the MT-MAC-over- PON architecture is concerned, Fig. 6-5's x-axis depicts the number of available optical wavelengths, each one having a capacity equal to that of the wireless channel (1.155 Gbps). The results are shown for a constant load generation of 0.5 packets per slot time per RAU/ADAP. As has been expected both architectures benefit greatly from the increase of the optical availability in terms of throughput (Fig. 6-5(a)) as well as delay (Fig. 6-5(b)). Specifically, in the MT-MAC-over-PON case,

throughput increases linearly with optical capacity whereas delay decays at an exponential rate, proving the direct relationship between the MT-MAC architecture's performance and the wavelength availability. Regarding the GPON-plus-802.11ad network, throughput performance increases with optical capacity (Fig. 6-5(a)). The increment rate is linear at lower optical capacities, where the GPON part of the network is the main communication bottleneck. However, throughput's increment rate drops as more GPONs are stacked on the fiber portion of the network, since the bottleneck gradually shifts from the fiber backhaul to the wireless portion of the network. Notably, the wireless bottleneck phenomenon does not appear in the RoF architecture, since the system will continue to derive gains until there is a 1:1 relationship between the number of wavelengths and the RAUs present in the network. Beyond that point no further performance increment is possible since no more than one wavelength can be assigned to every RAU. Note that the produced throughput is derived based on the optical capacity scale (depicted as the x-axis) which is 1.25Gbps for the GPON-plus-802.11ad and 1.15Gbps for the MT-MAC-over-PON network, thus giving an advantage to the former in terms of absolute throughput performance displayed in Mbps. Regarding the average packet delay (Fig. 6-5(b)), delay remains constant at lower optical capacities where the optical part of the network experiences saturation, since GPON's design enables a steady service delivery rate for the packets that fit into the offered buffer space. At higher optical capacities the communication bottleneck shifts from the optical network to the wireless domain, causing a decrease in the delay as more stacked-GPON facilities are added into the network.

6.2.4 Dependency on fiber length

In the interest of future Long-Reach PON (LR-PON) applications, Fig. 6-6 reviews the performance of both architectures versus the length of the Optical Distribution Network (ODN), ranging from 5 km up to 40 km of fiber. The results are shown for a constant load generation of 0.5 packets per slot time per RAU/ADAP, whereas in order to produce results relative to the ODN size, 100% of the generated traffic is considered to target internet destinations. As can be noted in Fig. 6-6(a) the GPON-plus-802.11ad architecture sustains only minor throughput performance degradation as the fiber length

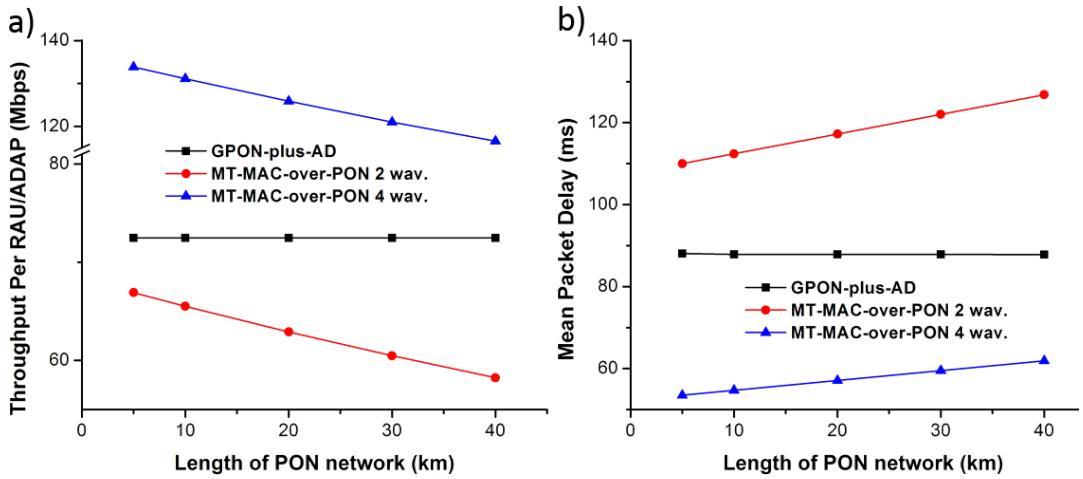

Fig. 6-6 Throughput and Delay versus length of PON network

increases whereas the MT-MAC-over-PON architecture is strongly affected and its performance is shown to be decreasing with the ODN size. This performance drop is attributed to the added delays introduced in the contention periods of the MT-MAC protocol that burdens the remote arbitration scheme in increased fiber lengths. On the other hand, the employment of the purely optical GPON protocol in the backhaul of the R&F architecture allows the latter to operate more efficiently in longer lengths, since packet transmission solely through cable is more robust and the usual time-consuming functions present in the wireless domain such as Collision Avoidance and/or ACK mechanisms are omitted. The same performance behavior is evident in the delay values as well (Fig. 6-6(b)) where it can be observed that in the MT-MAC scenario delay increases with distance whereas in the GPON-plus-802.11ad case delay remains relatively constant. This effect highlights the drawback of remote arbitration scheme employed by the MT-MAC protocol and its inherent weakness to operate in great fiber lengths for the reasons described in Chapter 6.1, whereas it displays the benefit of employing a multi-tier architecture such as the GPON-plus-802.11ad when it comes to LR-PON deployment.

6.2.5 MT-MAC-over-PON vs. GPON-plus-802.11ad comparative summary

The direct comparison of the two tested architectures reveals several aspects regarding the operation and the respective differences of the RoF and R&F paradigms concerning the formation of next-generation converged wireline and wireless networks. As described by the results, the GPON-plus-802.11ad architecture (R&F approach) operates very efficiently when the majority of traffic demands heads towards intra-cell destinations due to the close proximity of the ADAPs to the wireless clients that leads to local

and therefore faster traffic arbitration. In addition, the distinction between the wired and wireless domain offers two significant advantages: i) it allows for shortest communication paths when nodes reside within the same cell area and ii) it avoids time-consuming operations in the optical part of the network that are necessary in the wireless links, like the ACK mechanism, since optical MAC protocols (such as GPON's MAC operation) have been specifically designed and optimized for fiber links. This provides a clear advantage over the RoF approaches such as the MT-MAC protocol that cannot distinguish between the wired and wireless transmission part of the wireless packets and therefore have to employ stricter MAC standards over the whole network length. However, the benefits of the GPON-plus-802.11ad approach come at the cost of massive active AP equipment, a parameter that becomes of greater importance when referring to the very-short range (<10m) mm-wave communications, deeming such installations as impractical for massive deployment.

The MT-MAC-over-PON architecture enables the formation of extended range 60GHz WLANs by shifting all intelligent operations to one single, easily manageable and upgradable location, while coverage is provided through simple RAU modules. MT-MAC's dynamic wavelength allocation mechanism provides also the framework for interactive network control by shifting resources to active RAUs while withdrawing capacity from silent ones. In addition, the remote physical location of the MTAG acts as a natural relay for inter-cell traffic making the RoF scheme more effective for the modern 20/80 telecom paradigm as it has also been shown by the results. Nonetheless optical capacity abundance through WDM techniques as well as relatively short fiber lengths are a restricting technical necessity in order to achieve nominal network operation.

6.3 GPON-plus-MT-MAC hybrid RoF/R&F architecture

RoF architectures lack some of the critical features of the R&F implementations, such as fast access resolution in the wireless domain, local routing capabilities and long reach PON support. On the other hand, R&F architectures require massive active equipment installations, which in turn produce higher deployment, maintenance and upgrade costs as well as lower energy efficiency, factors that become increasingly severe in the dense

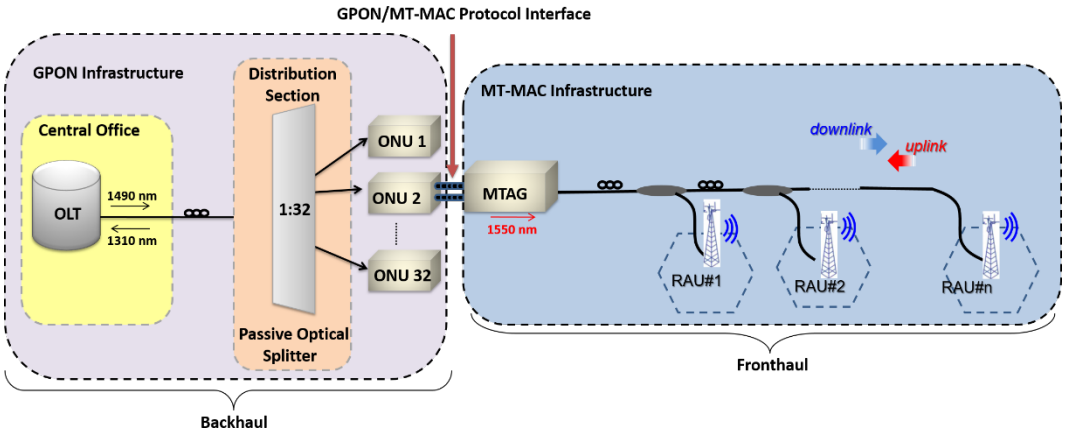

Fig. 6-7 The hybrid RoF/R&F multi-tier architecture "GPON-plus-MT-MAC".

mm-wave antenna deployment scenarios. To this end, this work studies the conjoined performance of a hybrid RoF/R&F architecture termed as the "GPON-plus-MT-MAC" approach, a multi-tier scheme that combines the properties of both the RoF and R&F network topologies, such as the flexibility and cost-effective WLAN extension properties of the RoF MT-MAC scheme along with the long-reach and traffic discrimination capabilities of the GPON-plus-802.11ad network. As shown in Fig. 6-7, the GPON-plus-MT-MAC approach splits the network into two counterparts: i) the GPON that covers the majority of the network, usually employing a several kilometers long fiber and ii) the short range MT-MAC network that offers the wireless access in the users premises. This distinction follows the current backhaul/fronthaul differentiation paradigm that is predominant in Cloud-RAN/5G research efforts. The hybrid GPON-plus-MT-MAC scheme allows the overall architecture to offer quick WLAN access control due to the close proximity of the MTAG to the RAUs and also provide fast and efficient multi-km long backhaul capabilities for connection with the service providers. This way the hybrid scheme establishes the level of performance displayed by R&F architectures but without the massive Access Point installations and also without the fiber length limits imposed by RoF architectures. In the GPON-plus-MT-MAC specification the MT-MAC network lies in a bus topology with the CO being attached to a short length fiber that is connected to a series of RAUs. The CO communicates with a conventional GPON ONU, with the protocol translation taking place at their interface. The CO-ONU interface undertakes the task of encapsulating MT-MAC Data Frames (MTDFs) destined for points outside the WLAN directly into the GPON Encapsulation Method (GEM) frame format, whereas it re-routes packets destined for intra-WLAN destinations. In turn the ONU buffers the GEM frames as they arrive, and transmits them at

specific time slots defined at the Upstream Bandwidth map (UB map) by the OLT, according to GPON's operational rules. Depending on its size, each MTDF is mapped either to a single frame or fragmented into multiple GEM frames. By occupying a single ONU for the same wireless coverage area, the GPON-plus-MTMAC approach offers great flexibility in the design and possible extension of the currently deployed fiber PONs to enter the FiWi era, since the latter architecture can offer multiple wireless area coverage while enabling the concurrent operation with other services already linked to GPON's ONUs.

The rest of this section presents the comparative performance evaluation of the GPON-plus-MT-MAC architecture versus the GPON-plus-802.11ad and the MT-MAC-over-PON networks. All configurations are again based on a 10km long PON network with 1:32 splitting ratio. In the GPON-plus-MT-MAC network, the CO is attached through a fiber bus to 32 RAUs with 13m of intra-RAU fiber interleaves, creating a RoF network with 416m of total fiber length, that offers the same coverage area as the RoF and R&F architectures studied in the previous section (≈4245m2). The CO communicates with one of the GPON's ONUs through the G-PON/MTMAC interface. The GPON-plus-802.11ad network follows the same specifications as presented in the previous section. In order to provide a fair comparison with the R&F and RoF architectures the ONU's buffer size have been set to hold the maximum number of packets that can be provided by the wireless clients. This is calculated as the sum of the buffers of the served clients multiplied by the percentage of traffic that is heading towards the OLT, i.e. 80% or 20% based on the traffic generation pattern. Considering 2000 bytes per packet this is equal to 12Mbytes of buffer space for the 20/80 traffic and 3Mbytes for the 80/20 traffic. The full list of the tested configurations depicted in the rest of this section is:

- The GPON-plus-AD depicted in Black.
- The GPON-plus-MTMAC for:
    - 2 wavelengths depicted in Red.
    - 4 wavelengths depicted in Blue.
    - 8 wavelengths depicted in Purple.
    - 12 wavelengths depicted in Green.
- The MT-MAC-over-PON for:

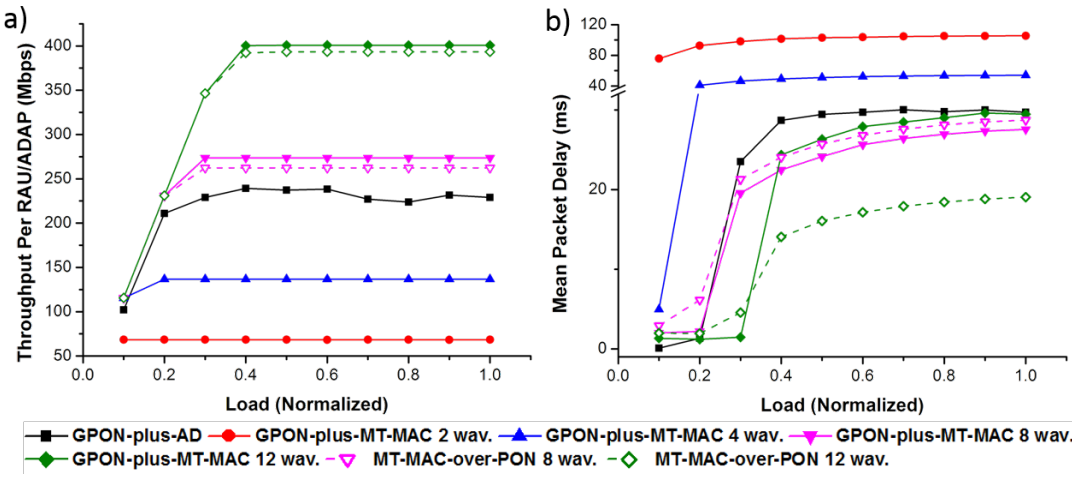

Fig. 6-8 Throughput and Delay for 80/20 traffic (80% stays within the cell).

- 8 wavelengths depicted in Purple with dotted line.
- 12 wavelengths depicted in Green with dotted line.

6.3.1 Dependency on traffic load

Fig. 6-8 illustrates the architectures' performance behavior versus various intra/inter-cell traffic load conditions. The generated load ranges from 0.1 up to 1 packet generation per timeslot per RAU/ADAP. Fig. 6-8(a) and Fig. 6-8(b) display the derived throughput and delay results respectively for traffic that follows the traditional 80/20 rule, meaning that 80% percent of the traffic is destined for intra-cell destinations whereas 20% of the traffic goes beyond the local subnet and heads to GPON's CO. Throughput values follow the same track as with the corresponding results presented in Fig. 6-2. Specifically, it can be witnessed that throughput values rise with load until the point where no more packets can get through and thus throughput reaches its saturation value. For the GPON-plus-MTMAC architecture, this saturation point depends on the number of employed optical wavelengths, and fluctuates from <0.1 packet/slot/RAU for 2 wavelengths up to 0.4 packets/slot/RAU for 12 wavelengths. In the case of 2 employed wavelengths, the GPON-plus-MTMAC architecture appears to be throughput saturated in all the range of tested load volumes meaning that the majority of the produced traffic gets dropped in the MT-MAC portion of the network due to buffer depletion. However, by taking advantage of the MT-MAC's inherent operational capability to support a variable number of wavelengths, we can increase the optical capacity of the fronthaul portion thus significantly improving the overall network performance. In our test setup we notice that when 8 wavelengths are employed, the GPON-plus-MTMAC outperforms the GPON-plus-802.11ad architecture by an average of 20%, a

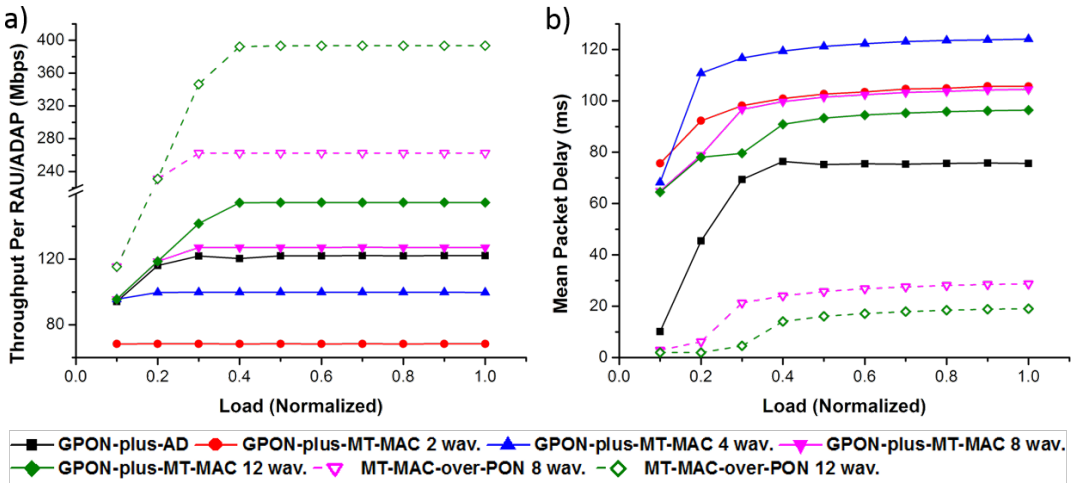

Fig. 6-9 Throughput and Delay for 20/80 traffic (80% heads to destinations outside the cell).

performance enhancement that is also 4% higher to the respective MT-MAC-over-PON value. This effect takes place because the addition of more wavelengths results in higher fronthauling bandwidth which in turn surpasses the ADAP's capacity and therefore produces higher throughput values. Delay results depicted in Fig. 6-8(b) start at a low point and increase rapidly when the offered load approaches throughput's saturation point. When load exceeds the saturation point delay values remain almost constant, since the excessive packets get dropped due to buffer overflow and are thus discarded from the delay metric. Regarding the GPON-plus-MT-MAC architecture, when load exceeds 0.4 packets per slot per RAU, delay values for the 12 wavelength set up are greater than the ones corresponding to 8 wavelengths. This is due to the fact that the increment from 8 to 12 wavelengths increases throughput and decreases delay in the MT-MAC subsection of the combined network, but on the other hand this higher throughput directly adds to GPON's load and therefore its delay. Since the delay increase in GPON is greater than the corresponding drop in the MT-MAC subsection we notice the phenomenon that the increase in MT-MAC's optical capacity causes increase in the overall mean packet delay. The same reason also accounts for the fact that, above the saturation point, the MT-MAC-over-PON architecture exhibits lower delay that the GPON-plus-MT-MAC network, although the former performs marginally worse in the throughput domain compared to the later.

Fig. 6-9(a) and Fig. 6-9(b) present the same results but for traffic shaped under the more modern 20/80 rule, meaning that 80% of it is destined beyond the cell's subnet, whereas

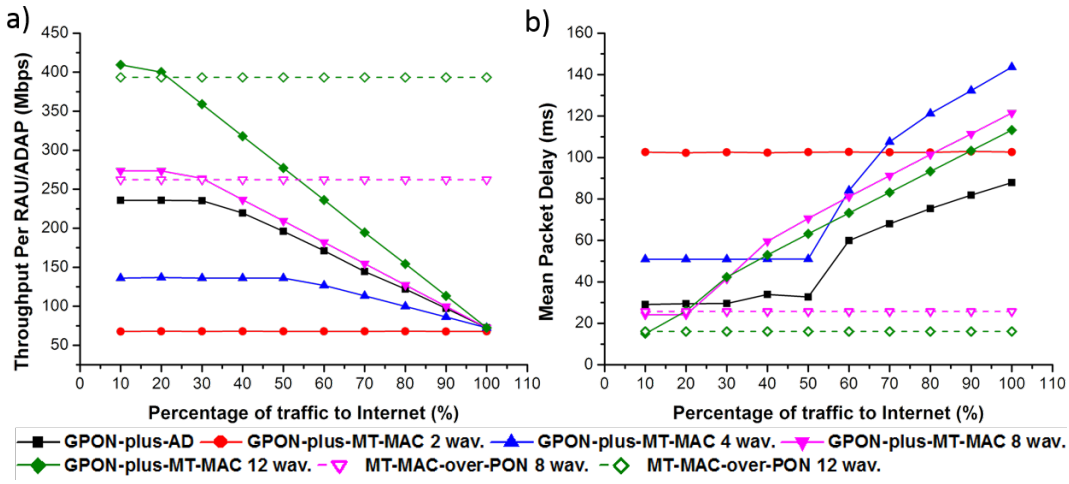

Fig. 6-10 Throughput and Delay versus percentage of traffic heading towards Internet destinations.

only 20% in intended for intra-cell destinations. Here, throughput and delay values follow again the same curvature as in Fig. 6-8(a) and Fig. 6-8(b) but now the two architectures that employ GPON for backhauling (GPON-plus-MT-MAC and GPON-plus-802.11ad) exhibit less throughput and higher delay values, since the massive amount of uplink traffic faces the limited capacity of the single wavelength GPON network and thus a significant portion of the offered load gets discarded at the GPON-RAU/ADAP interface due to buffer overflow. However, by comparing these two architectures we notice that the results maintain the same performance ratio regarding the optical wavelength availability as in the case of the 80/20 traffic. A significant point risen by Fig. 6-9 is that the GPON-plus-MTMAC and GPON-plus-802.11ad architectures are negatively affected by the increase of extra-cell traffic, since both of them rely on the limited-capacity GPON for backhauling of data. Due to that, the backhauling capabilities of the two GPON-based architectures are limited to the GPON capacity (2.5Gbps in our simulations), whereas the MT-MAC-over-PON is a WDM scheme and therefore can employ a higher number of wavelengths which translates in higher backhauling capacity. However, in the traditional scheme 80/20 traffic model where the majority of the produced traffic stays within the cell, the opposite is true, since the remote arbitration of the MT-MAC-over-PON architecture creates intolerable delays, a problem that is not encountered in the other two architectures where the access mechanism is located closely to the wireless nodes.

6.3.2 Dependency on percentage of intra/inter-cell traffic ratio

Fig. 6-10 provides a better insight regarding the hybrid architectures' performance versus the ratio of intra/inter-cell traffic with the results being shown for a constant load generation of 0.5 packets per slot time per RAU/ADAP. Regarding the GPON-plus-MT-MAC architecture, throughput and delay results follow the same trajectory as the GPON-plus-802.11ad network, meaning that throughput values drop and delay values rise while the percentage of traffic that heads beyond the cell increases. As it is depicted in Fig. 6-10(a), throughput's highest point is located on the left-most portion of the graph when the majority of traffic heads towards intra-cell destinations while its absolute value is depended on the tested configuration. Throughput values remain relatively steady as the percentage of traffic that heads outside the cell increases, until GPON reaches its maximum service capacity. Beyond GPON's saturation point, throughput decreases gradually since all excess traffic gets immediately dropped at the interface due to buffer overflow. The lowest throughput value of ~72Mbps per RAU/ADAP is derived for 100% of inter-cell traffic and it is common for all of the tested configurations since it corresponds to GPON's uplink capacity divided by the number of RAUs/ADAPs (32 in this case). As described in the previous section, given the specific PON configuration, the GPON-plus-MT-MAC architecture requires at least 8 wavelengths (1/4 of the total number of RAUs) to be able to overcome GPON-plus-802.11ad's performance. Delay values depicted in Fig. 6-10(b), abide in general to the following curvature: remain steady while throughput remains steady, increase rapidly when the intra/inter-cell traffic is nearing the GPON's saturation point and increase with steady rate after the latter point. The specific x-points notating the three distinct regions described above depend on the configuration (i.e. the number of employed wavelengths). As it is evident in Fig. 6-10 throughput and delay results can be divided into two categories. On one side are the GPON backhauled architectures that are negatively affected by the increase of the extra-cell traffic due to GPON's limited capacity. On the other side is the MT-MAC-over-PON architecture that exhibits steady performance, regardless of the network size since all performance aspects of the latter remain independent of the intra/inter-cell traffic ratio, due to indiscriminate packet backhauling. This fact highlights once again that when the majority of the traffic is destined for backhauling, RoF implementations offer higher performance due to RoF's inherent

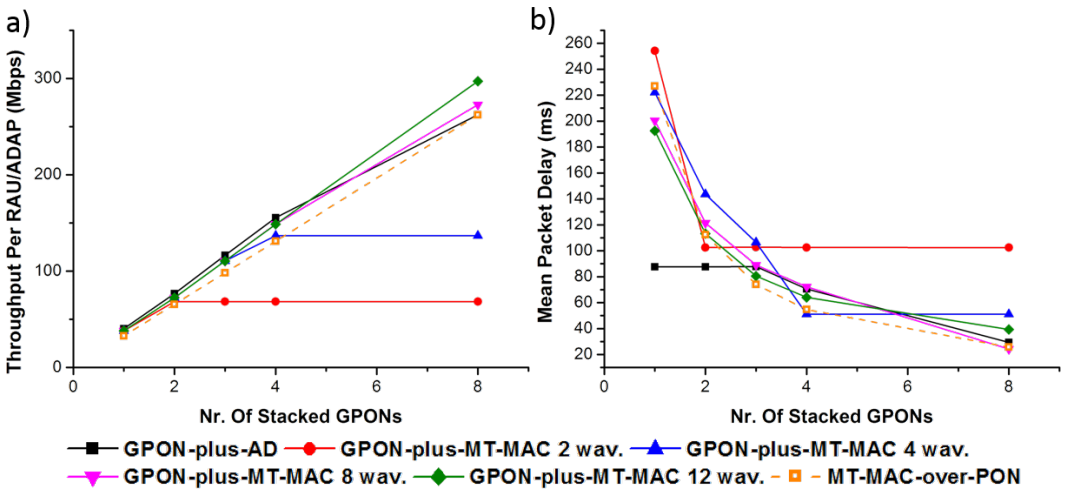

Fig. 6-11 Throughput and Delay versus number of available wavelengths in the MT-MAC-over-PON scenario or Stacked GPONs in the GPON-plus-802.11ad scenario.

backhauling nature, whereas in high intra-cell traffic conditions the hybrid RoF/R&D architecture yields better results.

6.3.3 Dependency on the optical capacity

In order to fully comprehend the role of the optical resource availability Fig. 6-11 displays the relation between performance and optical capacity for the considered FiWi architectures. Regarding the GPON backhauled schemes we considered a variable number of "stacked" GPON networks with 1.25 Gbps down and uplink capacity respectively, whereas specifically for the GPON-plus-MT-MAC architecture each of the curves depict a different optical capacity value in the MT-MAC portion of the network. As far as the MT-MAC-over-PON architecture is concerned, Fig. 6-11's x-axis depicts the number of available optical wavelengths, each one having a capacity equal to that of the wireless channel (1.155 Gbps). The results are shown for a constant load generation of 0.5 packets per slot time per RAU/ADAP. As can be noted, all architectures benefit greatly from the increase of the optical availability in terms of throughput (Fig. 6-11(a)) as well as in terms of delay (Fig. 6-11(b)), however not all in an identical manner. On one hand, we observe that the MT-MAC-over-PON's throughput values increase purely linearly since the addition of wavelengths results in RAUs getting more optical capacity and longer transmission windows and thus causing a linear increase in the overall system's bandwidth. On the other hand, for the two architectures that employ GPON as the backhauling solution, throughput values increase linearly with each addition in the GPON stack only up to the point that any further increase causes no further performance enhancement and throughput stagnates. The latter happens because

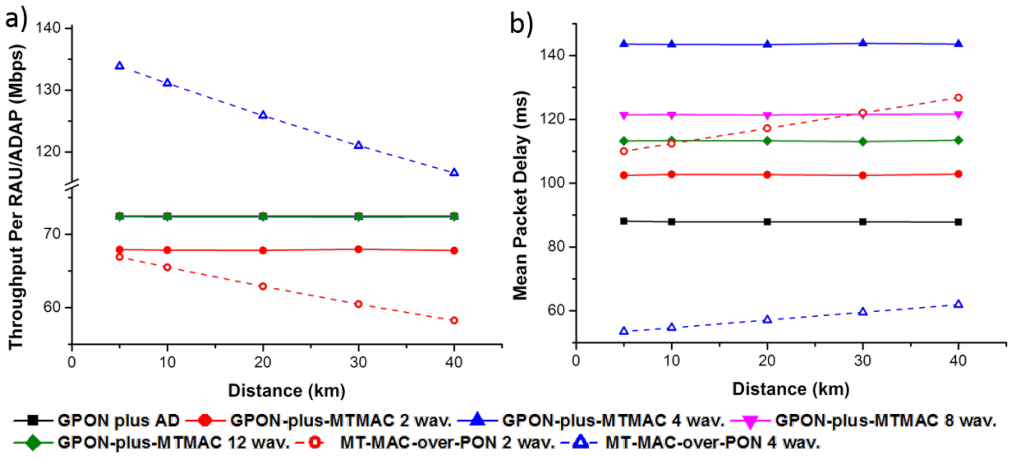

Fig. 6-12 Throughput and Delay versus length of PON network.

the GPON-plus-MT-MAC and GPON-plus-802.11ad architectures are actually comprised of two separate networks and thus any additional GPON stack affects only a portion of the network. When the GPON capacity increases to a large extend, the bottleneck factor shifts from the GPON to the 802.11ad/MT-MAC portions of the architecture and thus throughput and delay values stabilize around the values that are produced by the latter networks. The same trend can be seen in the delay results depicted in Fig. 6-11(b) where we witness the exponential decline of the mean packet delay while more wavelengths are added to the GPON backhaul, up to the point where delay stabilizes and equals the delay produced by the 802.11ad or MT-MAC parts of the network. Results also reveal that GPON-plus-802.11ad retains an advantage over the GPON-plus-MT-MAC for less than 8 available wavelengths due to the local arbitration scheme in the wireless part of the network which directly benefits the delay values. However, given enough optical capacity availability the MT-MAC manages to alleviate the performance difference and provide greater throughput and lower delay values while maintaining the advantage of the flexible, future-proof and cost-efficient architecture.

6.3.4 Dependency on fiber length

Regarding Long-Reach PON applications, Fig. 6-12 reviews the performance of all the architectures versus the distance of the ODN length, ranging from 5km up to 40km of fiber. The results are shown for a constant load generation of 0.5 packets per slot time per RAU/ADAP, whereas in order to produce results relative to the ODN size, 100% of the generated traffic is considered to target internet (extra-cell) destinations. As Fig. 6-12(a) depicts, both GPON-based configurations exhibit static throughput values for

all attested ODN lengths. The latter is due to the fact that GPON's T-CONT1 mode of operation employed here is based on unsolicited periodic permits granting fixed payload allocations and therefore throughput is unaffected by the ODN length. The produced throughput values range from around 68Mbps for the GPON-plus-MTMAC architecture employing 2 wavelengths to approximately 72Mbps for all the rest GPON-based architectures. Since all generated traffic is considered to extra-cell destinations, and therefore is routed towards GPON, the produced throughput results correspond to GPON's uplink capacity divided by the number of RAUs/ADAPs (32 in this case). The small discrepancy between the 2 wavelengths GPON-plus-MTMAC architecture and the other architectures stems from the fact that for 2 employed wavelengths the GPON-plus-MTMAC's throughput is capped by the MT-MAC portion of the network instead of the GPON portion as it is for all the other cases. Compared to the analysis carried out in section 6.2.4, it is shown here that the multi-tier GPON-plus-MTMAC architecture alleviates the drawback of the MTMAC-over-PON scheme that suffered performance losses in great fiber distances due to the remote arbitration of the wireless medium. Regarding the respective delay results depicted in Fig. 6-12(b), we notice again that the GPON-based architectures produce a relatively steady delay since the only alternating factor is the propagation delay which is very small (4.9μs per added km) compared to the delay produced due to transmission and access control that is in the order of 100ms. Another significant point is that the GPON-plus-MT-MAC scheme exhibits greater delay than the GPON-plus-802.11ad architecture for the same throughput values (Fig. 6-12(b)). This is due to the fact that besides the GPON delay, packets get served continuously by the 802.11 Access Points, whereas in the GPON-plus-MTMAC scheme transmission is intermitted by intervals when clients wait for wavelength assignment in the RAU. However, GPON-plus-802.11ad's superiority at this point comes at the cost of the active access point equipment, making it a severely inefficient way to provide wide 60GHz coverage given the very restricted (<10m) range of the specific medium. Finally, it is noteworthy that the MT-MAC-over-PON network's performance, which was introduced in Section 6.2.4 and again displayed here for comparative reasons, yields superior performance when 4 or more wavelengths are employed compared to the single-wavelength GPON backhauled architectures, therefore making it also a valid candidate for Next-Generation PONs when multi-wavelength resources are available.

TABLE 6-2 SUMMARY OF PREVAILING CONDITIONS FOR EACH ARCHITECTURE

Metric			MT-MAC-over-PON	GPON-plus-802.11ad	GPON-plus-MT-MAC
Traffic Shape	Modern 20/80 rule	High Inter-ONU Traffic	√	X	X
		High Inter-Cell Traffic			√
	Classical 80/20 Rule	High Intra-Cell Traffic	X	√	
Optical Backhaul Capacity Requirements			HIGH	LOW	LOW
PON fiber length tolerance			LOW	HIGH	HIGH
Area of Wireless Coverage per PON ONU			LOW	LOW	HIGH

6.3.5 The GPON-plus-MT-MAC architecture and overall performance evaluation

The performance results reveal the nature and specific characteristics of the hybrid RoF/R&F GPON-plus-MT-MAC architecture towards the formation of a multi-tier architecture. As constituted by the respective results the GPON-plus-MT-MAC scheme operates very efficiently under the 80/20 traffic ratio improving the performance gain of the MT-MAC-over-PON scheme by an average of 4%. In addition, the distinction of the wired and wireless portion of the network allows the GPON-plus-MT-MAC architecture to operate for longer fiber backhaul lengths thus being able to cooperate with future generation LR-PONs. Finally, the latter architecture is the most suitable for future FiWi extensions of currently deployed PONs since it occupies only a fraction of the GPON's ONUs therefore enabling concurrent utilization with already existing GPON services.

Table 6-2 summarizes the architectures' overall comparison results displaying the conditions on which each one prevails or is mostly well suited for. According to the presented results, the MT-MAC-over-PON architecture is suitable for high inter-cell traffic but requires high optical availability and operates efficiently only for short fiber lengths. GPON-plus-802.11ad is predominant in high intra-cell traffic, low optical availability in the optical PON backhaul and is very efficient for great fiber distances such as the case of LR-PONs, but at the expense of acquisition and employment of active AP equipment. The GPON-plus-MTMAC architecture optimally combines the advantages of both architectures and is highly efficient in increased intra-cell traffic, low optical availability in the optical backhaul, can operate effectively in long fiber distances and captures only one ONU per each deployed RoF network.

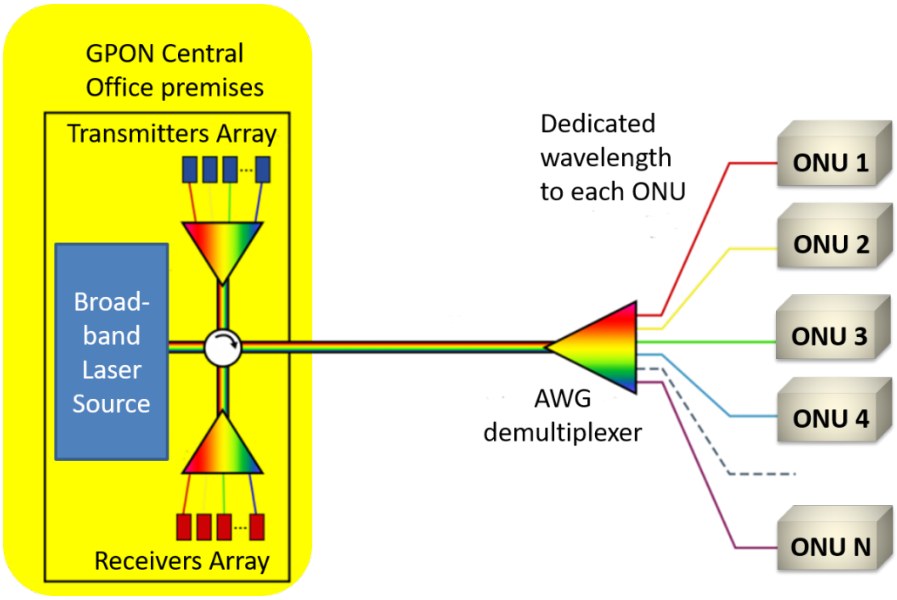

Fig. 6-13 A WDM GPON architecture.

6.3.6 WDM-PON operation under the NG-PON2 paradigm

Throughout this chapter we have considered the TWDM-PON or "PON Stacking" paradigm as the major solution towards providing a Next Generation PON compatible functionality. This choice was based on the fact that the TWDM-PON scheme has been formally submitted and approved by the FSAN community as the primary solution for NG-PON2 since it is less disruptive and less expensive than other approaches, primarily due to the reuse of existing components and technologies[93]. However, in the open topic of the NG-PON2 formation and standardization there have been several proposals concerning the WDM-PON approach which presumes a dedicated wavelength channel to each optical network unit. Fig. 6-13 presents a WDM GPON architecture where the GPON's CO employs a multi-wavelength source and an array of transmitters and receivers each one carrying its own data stream. Each transmitter modulates a distinct wavelength and in turn all wavelengths get propagated through the fiber towards the ONUs. Instead of a splitter, the WDM GPON employs an Arrayed Waveguide Grating multiplexer that has the capability of statically and passively routing each wavelength to a distinct output port. Therefore, each ONU receives a static assignment of a dedicated wavelength for uplink and downlink traffic. In this way, the WDM GPON paradigm transforms the PON to an uncontested delivery line with static transmission/propagation delays. Due to the dedicated nature of the optical capacity, every ONU receives N times more capacity than in the TWDM-PON scenario, where N is the splitting ration

of the AWG multiplexer. This provides a manifold increment of the traffic limit imposed by the optical backhaul, thus establishing the wireless network as the predominant performance factor, given that the aggregated wireless traffic is lower than the average uplink service rate. In case the aggregated arrival rate from the wireless network is greater than the capacity of the optical backhaul, then the PON becomes again the bottleneck and sets the upper limit to the throughput of the conjoined optical/wireless network. Regarding the three architectures reviewed in this work, the transition to a WDM-PON operation would impact performance in the following ways:

a) GPON-plus-802.11ad:

In this case, the backhaul WDM-PON network will immediately propagate the data packets to the OLT as soon as they arrive on the head of the ONU buffer, since no contention is taking place. Given a Poisson generation model traffic, the above translates to small or zero queuing delays in the ONU as long as the mean aggregated arrival packet rate from the wireless 802.11ad access point λ_{AD} is less than the maximum packet service rate R_{ONU} supported by the WDM-PON. Above R_{ONU} the queue becomes unstable and any excess traffic is dropped. Therefore, in the R&F scenario all packets that arrive at the ONU will be immediately forwarded to the OLT provided that $\lambda_{AD} < R_{ONU}$, whereas the aggregated delay of the packets arriving at the OLT will be the sum of the delay produced by the 802.11ad network (MAC functions and corresponding transmission/propagation delays) plus the transmission/ propagation delays of the optical network (no access control and queuing delays). For all values of λ_{AD} that are less than R_{ONU} the optical throughput will rise linearly with load since there is no contention access and all uplink timeslots are available for transmission. If λ_{AD} approaches or exceeds R_{ONU} the optical throughput will enter the saturation zone and any further increment will cause excess packets to be dropped at the ONU. Compared to the TWDM-PON, the absence of contention for uplink traffic as well as the dedicated optical capacity in the WDM-PON results in higher throughput and lower delays in the unified R&F network for the packets that are destined towards the OLT.

b) MT-MAC-over-PON:

In the case that the MT-MAC protocol has a 1:1 wavelengths to RAUs ratio, then each RAU has a permanently assigned wavelength and no contention will take place in the optical domain (termed as 1st contention in the MT-MAC operation). This creates an

effect similar to the previous case and as a consequence all delays and throughput limitation caused by the sharing of the optical resources is alleviated. In this configuration throughput is limited by the MAC functions in the wireless domain (termed as 2nd contention period) and the respective transmission/propagation delays in both the optical and wireless domains. Therefore, as long as the aggregated traffic of all wireless clients λ is lower than the maximum capacity offered by the optical wavelength $R_{\max}$, throughput will rise linearly and delay will be the sum of the transmission/propagation delays in both the optical and wireless domains. If λ is in the vicinity or higher than $R_{\max}$ then throughput will enter its saturation regime and any additional traffic will be dropped from the wireless clients' buffers. Overall, compared to the classic MT-MAC approach where optical wavelengths are limited, graphs are expected to follow the same curvature but offer higher throughput results and lower delays. The above have already been reported in Chapter 3 where a 1:1 wavelength/RAU ratio in the MT-MAC has already been tested and presented.

c) GPON-plus-MT-MAC:

In the case of the hybrid RoF-plus-R&F approach, replacing the TWDM-PON with a WDM-PON offers the same advancement as in the case of GPON-plus-802.11ad, meaning that any performance hindering and added delays caused by the sharing of the uplink wavelength are alleviated due to the dedicated optical wavelengths in the backhaul. The multiplication of the per ONU optical capacity due to the dedicated wavelength association as well as the lack of time consuming access control mechanism in the uncontested medium causes the immediate throughput increment and significant drop in the delay values. Specifically given that λ_{MT-MAC} is the aggregated packet arrival rate at the ONU-MTAG interface and R_{ONU} is the service rate of the WDM-PON ONU, if $\lambda_{MT-MAC} < R_{ONU}$ the throughput in the optical part of the network will rise linearly with the load and delay will be very low. If λ_{MT-MAC} is close or greater than R_{ONU} then the throughput of the WDM-PON will enter the saturation regime and all excess traffic will be dropped at the ONU buffer. Therefore, the adoption of the WDM-PON infrastructure multiplies the R_{ONU} as well as enables the use of simpler access control mechanisms and will yield better performance and lower delay values in the cases where $\lambda_{MT-MAC} < R_{ONU}$.

6.4 Conclusive remarks

In this chapter we have presented an extensive study regarding the network planning and formation of 60GHz Gigabit WLAN enterprise networks over existing GPON infrastructures. Three possible architectures where studied: i) the RoF approach MT-MAC-over-PON, ii) the R&F approach GPON-plus-802.11ad and iii) the hybrid RoF/R&F GPON-plus-MT-MAC approach that combines the properties of both the aforementioned architectures. Extensive simulation results were presented revealing the dependence of the 60GHz enterprise network performance on several network planning parameters: the load of the network, the number of optical wavelengths being available to the network, the percentage of intra-LAN and Internet-devoted network traffic and the PON's total fiber length. Results have shown that the MT-MAC-over-PON architecture is suitable for high inter-cell traffic but requires high optical availability and short fiber lengths. The GPON-plus-802.11ad is predominant in high intra-cell traffic, low optical availability and operates efficiently even for great fiber distances but at the expense of acquiring and operating abundant active AP equipment. The GPON-plus-MTMAC architecture optimally combines the advantages of both architectures being highly efficient in increased intra-cell traffic, low optical availability as well as in the case of long fiber distances. Moreover. the latter architecture is the most suitable for future FiWi extensions of currently deployed PONs since it offers increased freedom and flexibility regarding the network planning.

Page intentionally left blank

Chapter 7 Conclusions and future work

This chapter completes the dissertation by summarizing our main contributions, while also providing some potential research lines for future investigation. In particular, Section 7.1 contains the most significant concluding remarks of our research, while Section 7.2 outlines the open research issues related to our contributions.

7.1 Thesis conclusions

The main research contribution presented in this thesis revolves around the concept of medium transparency in MAC protocols when applied to converged RoF networks. In Chapter 3 we demonstrated the rules and operation of the MT-MAC protocol. This MAC protocol is the first of its kind to be able to dynamically allocate both optical and wireless capacity and resources. The notion of medium-transparency relies on two parallel running contention periods with nested dataframe structures. Hardware wise, the MT-MAC operation is based on wavelength selectivity functions implemented at the RAU site, thus allowing for compatibility with completely passive optical distribution network implementations and for telecom operator transparent fiber-network infrastructures. By taking advantage of the RoF architecture that allows the CO to act as a relay, the MT-MAC protocol forms extended reach 60GHz WLAN networks offering connectivity also between wireless devices that are attached to different RAUs and have no LOS. To examine the performance of the MT-MAC protocol we have presented extensive evaluation results for both bus and PON architectures of RoF network topologies, both for Poisson and for burst-mode traffic at bit-rates up to 3Gb/s, confirming in all cases the enhanced potential of our protocol to easily adapt to the network topology whilst providing broadband 60GHz WLAN functionality. The derived results confirmed the successful performance even under Gb/s burst-mode traffic, a fact that renders the MT-MAC suitable for high-bandwidth latency-sensitive WLAN applications like HD video streaming. The proposed MAC protocol was found to utilize almost all

of the available bandwidth, since in all tested cases throughput increased almost linearly with the offered load as long as load resided within the WR ratio. When load exceeded the WR value, throughput reached its constant saturation limit. At the same time, delay values remain in the μsec range when load is below the WR value and increase rapidly when load approaches WR, however always being below 100msec. We have also evaluated the MT-MAC's performance for bus networks with up to 128 RAUs, showing that throughput decreased by 3% and delay increased by 5% compared to the 10 RAU setup, and for PON networks with up to 64 RAUs, showing a 1.8% decrease in throughput and a 4% increase in delay compared to the 10 RAU PON network, confirming the highly scalable aspects of the proposed protocol and its tolerance to large number of RAUs. Finally, in order to assess the wireless arbitration process, we have conducted simulation evaluations for 2 up to 20 nodes per RAU, showing that for a 1000% increase in the node population the protocol exhibited only a 10% throughput reduction, due to the longer duration wireless arbitration process.

In Chapter 4 we have presented an updated version of the MT-MAC protocol, termed as Client-Weighted MT-MAC. This MAC protocol was specifically designed to address fairness issues where each RAU receives a wavelength assignment for time proportional to the amount of active users that are served by it. To this end, fairness is achieved by equipping the protocol with the user-centric Client Weighted Algorithm for the optical capacity arbitration procedures. The tests that were carried out by means of simulation showed rapid improvement on delay equalization for various network conditions through simulation performance analysis for different user distribution patterns and loads under specific wavelength availability constraints. Specifically, the CW-MT-MAC scheme achieved almost zero standard deviation for 4 out of the 5 studied user deviations achieving an overall 68% reduction in throughput and 72% reduction in delay standard deviation as the latter is perceived amongst the network's users, thus proving its enhanced user-fairness properties. In addition, CW-MT-MAC achieved 32% reduction in the exhibited intra packet standard deviation performance, highlighting its ability to serve modern delay-restricted applications where Packet Delay Variation remains a major issue.

In Chapter 5 we have presented two analytical models for calculating saturation throughput and non-saturation delay for the MT-MAC protocol. The proposed saturation model is based on a two-dimensional (2-D) Markov chain for calculating the end-

user transmission probabilities, taking into account contention for both the optical and the wireless layer resources. The analytic formula for throughput computation and the respective performance evaluation for various network conditions were found to be in close agreement with simulation-based outcomes, confirming the validity of the MT-MAC model. Secondly in the same chapter we presented an analytical model for calculating the end to end delay of the MT-MAC. The presented analytical model enabled the calculation of packet delay under non saturation conditions, successfully validating the respective simulation results for various numbers of optical wavelength availability factors, network loads, fiber lengths, transmission window sizes and data packet payloads. In non-saturation conditions the theoretical results were found to be in the subms region and in excellent agreement with respective simulation-based findings. In saturation conditions the theoretical results exhibited small variations compared to the respective simulation outcomes which are nonetheless always within the 95% confidence interval. The above confirm that the employment of Medium Transparent MAC protocols is compatible and allows the derived results to function as a roadmap towards the efficient incorporation of the MT-MAC scheme into the envisioned era of 5G mm-wave small cell networks.

In the final chapter of this thesis (Chapter 6) we presented an extensive study regarding the network planning and formation of 60GHz Gigabit WLAN enterprise networks when the latter are deployed over existing GPON infrastructures. Three possible architectures where studied: i) the RoF approach MT-MAC-over-PON, ii) the R&F approach GPON-plus-802.11ad and iii) the hybrid RoF/R&F GPON-plus-MT-MAC approach that combines the properties of both the aforementioned architectures. Extensive simulation results were presented revealing the dependence of the 60GHz enterprise network performance on several network planning parameters: the load of the network, the number of optical wavelengths being available to the network, the percentage of intra-LAN and Internet-devoted network traffic and the PON's total fiber length. Results have shown that the MT-MAC-over-PON architecture is more suited for high inter-cell traffic since it requires high optical availability and short fiber lengths. The GPON-plus-802.11ad is predominant in high intra-cell traffic, low optical availability and operates efficiently even for great fiber distances but at the expense of acquiring and operating

abundant active AP equipment. The GPON-plus-MTMAC architecture optimally combines the advantages of both architectures being highly efficient in increased intra-cell traffic, low optical availability as well as in the case of long fiber distances. Moreover. the latter architecture is the most suitable for future FiWi extensions of currently deployed PONs since it offers increased freedom and flexibility regarding the network planning.

7.2 Future Work

The main contributions presented in this dissertation can be followed by several new research lines for future investigation. The main open topics with respect to the MT-MAC protocols are:

- Wavelength assignment in the MT-MAC and CW-MT-MAC protocols is done in a round-robin fashion where the wavelengths are shared in the time domain amongst the system's RAUs. Although it is not possible to assign more than one wavelengths to each RAU, it is technically possible to assign one wavelength concurrently to multiple RAUs. This would allow the sharing of a single wavelength amongst RAUs that have low or complementary traffic characteristics. The benefits of that operation would be manifold. For instance, the RAUs will maintain an active connection to the CO for the majority of the time and the assignment/de-assignment procedures will be carried out more sparsely. This would directly lead to better delay performance since packets will be transmitted faster and there will be less need for buffer space since the RAUs will stay unconnected for less time.

- In the current formation of the MT-MACs, all packets belong to the same category priority, meaning that there is no distinction made between packets that belong to delay sensitive streams and best effort communications. To this end it would be beneficial to incorporate a priority queue system in the MT-MAC. This would allow for further gains and better support of priority traffic, leading to higher Quality-of-Service and quality experience from the user's side.

- Due to telecommunication industry's economy of scale, the sharing of infrastructure among different service providers is becoming a necessity of business in the telecom world. Because of the above, it is fundamental to incorporate

infrastructure sharing capabilities in every next generation converged FiWi proposed architecture, such as the MT-MAC. To this end, we plan to update the MT-MAC mechanisms in order to allow scheduling amongst various RF service providers that will lease capacity through a centralized scheme depended on each operator's current capacity needs and level of service.

- The joint operation of priority queuing and multiple RAU wavelength assignment would raise a series of interesting questions on how to decide what is the optimum way to perform the RAU clustering, i.e. which RAUs should be grouped together under the same wavelength. This implies that a possible optimal clustering algorithm would take into consideration not only the load of each wireless terminal but also the QoS category of the served traffic. For instance, a clustering algorithm would try to match high QoS delay sensitive applications, such as video streaming, with best effort traffic in order i) not to overload a single wavelength with more traffic that it can handle and ii) any sudden high-QoS traffic increments will be accommodated by being "absorbed" by the best-effort traffic where delays are more tolerated.

- In CW-MT-MAC the fairness properties of the protocol are being carried out on the basis of the number of active clients per RAU. As it has been demonstrated, this operation carries significant performance gains and thus it incentivizes the extension of the employed model from a client-based approach to a queue-based approach. The latter would signify that instead of employing the number of active clients to assign transmission window slots, the CO would also request the number of packets in the queue and will carry out a more precise estimation of the appropriate window size for every RAU.

- The end-to-end delay analysis currently considers the fixed service regime employed by the MT-MAC protocol. However, it would be useful to devise an analytical delay model for the CW-MT-MAC protocol as well. CW-MT-MAC's operation resembles the gated service regime, where each client is given a transmission window equal to the number of packets that it currently contains in its buffer. In the CW-MT-MAC case, that operation would take the number of ac-

tive terminals per RAU into account. Such an analytical model for the converged FiWi CW-MT-MAC protocol would grant a much more detailed insight on the internal operations of the gated service in a hybrid network.

- With the vast deployment of 4G networks, as well as the 5G vision of totally interconnected devices, the energy consumption is growing at a staggering rate, which carries a heavy environmental impact and results in high operation expenditure for wireless service providers. The current MT-MAC protocols described in this thesis have not been optimized for low energy devices or eco-friendly operation. To this end it would be beneficial to upgrade the MT-MAC's algorithm of operation in order to allow the wireless nodes or the CO to enter sleep cycles in order to reduce their energy footprint. In addition, given the MT-MAC protocol's inherent capability to employ a variable number of wavelengths, it is useful to consider a joint energy/wavelength optimization scheme where the CO will turn on the optimal number of optical transceivers in a dynamic manner in order to match the current load of the network and reduce energy waste.

- Software-Defined Networking (SDN) is an emerging architecture that is dynamic, cost-effective and adaptable to fast changing conditions, making it ideal for the high-bandwidth, dynamic nature of today's applications. SDN's principle relies on decoupling the network control and forwarding functions enabling the network control to become directly programmable. To this end it is useful to implement MT-MAC mechanisms that will be able to set-up, manage and optimize various aspects of the converged FiWi SDN network infrastructure such as (i) support for sliceable bandwidth variable transponders offering multiple modulation formats, (ii) wavelength and wireless carrier aggregation and (iii) spectrum sharing. In this way the MT-MAC will enable support for network slicing functionalities that will be executed in parallel and on top of the common FiWi physical infrastructure.

- Finally, any actual implementation of the MT-MAC and CW-MT-MAC protocols in real devices would be an important step ahead. So far, we have evaluated the protocols' performance using detailed analytical probabilistic models

(mainly based on Markov theory) and by means of extensive simulation experiments. However, the employment of the protocol rules in real testbeds would reveal unidentified weaknesses, while it would allow for a better and more complete performance assessment.

Page intentionally left blank

References

[1] Gartner report “Market Share: Devices, All Countries, 4Q15 Update”, available at: https://www.gartner.com/doc/3213117

[2] Statcounter’s Report, available at: http://gs.statcounter.com/#all-comparison-ww-monthly-201308-201408

[3] “Cisco Visual Networking Index: Global Mobile Data Traffic Forecast Update, 2015–2020 White Paper”, Feb 01 2016, Document ID:1454457600805266, available at: http://www.cisco.com/c/en/us/solutions/collateral/service-provider/visual-networking-index-vni/mobile-white-paper-c11-520862.html

[4] V. Jungnickel et al., "The role of small cells, coordinated multipoint, and massive MIMO in 5G," in IEEE Communications Magazine, vol. 52, no. 5, pp. 44-51, May 2014.

[5] P. Mogensen et al., "Centimeter-Wave Concept for 5G Ultra-Dense Small Cells," 2014 IEEE 79th Vehicular Technology Conference (VTC Spring), Seoul, 2014, pp. 1-6.

[6] N. Bhushan et al., "Network densification: the dominant theme for wireless evolution into 5G," in IEEE Communications Magazine, vol. 52, no. 2, pp. 82-89, February 2014.

[7] B. Bangerter, S. Talwar, R. Arefi and K. Stewart, "Networks and devices for the 5G era," in IEEE Communications Magazine, vol. 52, no. 2, pp. 90-96, February 2014.

[8] P. Demestichas et al., "5G on the Horizon: Key Challenges for the Radio-Access Network," in IEEE Vehicular Technology Magazine, vol. 8, no. 3, pp. 47-53, Sept. 2013.

[9] N. Ghazisaidi, M. Maier, C. Assi, "Fiber-wireless (FiWi) access networks: A survey", IEEE Commun. Mag., Vol.47, No.2, pp.160-167, Feb. 2009

[10] N. Ghazisaidi and M. Maier Fiber-Wireless (FiWi) Networks: Challenges and Opportunities IEEE Network, vol. 25, no. 1, pp. 36-42, Jan./Feb. 2011

[11] H. Al-Raweshidy and S. Komaki, editors, Radio over Fiber Technologies for Mobile Communications Networks, Norwood: Artech House, 2002.

[12] IEEE 802.3ah Ethernet in the First Mile Study group IEEE 802.3ah Draft2.0 2003.

[13] ITU-T G.984.2 Gigabit-capable Passive Optical Networks (G-PON) (2006) Amendment 1: Appendix III

[14] O. Andrisano, V. Tralli, and R. Verdone, “Millimeter Waves for Short-Range Multimedia Communication Systems,” Proc. IEEE, vol. 86, no. 7, pp. 1383-1401, July 1998.

[15] P. Smulders, “Exploiting the 60 GHz Band for Local Wireless Multimedia Access: Prospects and Future Directions,” IEEE Commun. Mag., pp. 140-147, Jan. 2002.

[16] J. R. Forrest, “Communication Networks for the New Millennium,” IEEE Trans. Microwave Theory Tech., vol. 47, no. 12, pp. 2195-2201, Dec. 1999.

[17] F. Giannetti, M. Luise and R. Reggiannini, “Mobile and Personal Communications in the 60 GHz Band: A Survey,” Wireless Personal Commun., pp. 207-243, Oct. 1999.

[18] A. Cooper, “Fibre/radio for the Provision of Cordless/Mobile Telephony Services in the Access Network,” Electronics Letter , vol. 26, pp. 2054–2056, November 1990.

[19] H. Ogawa, D. Polifko, and S. Banba, “Millimeter-Wave Fiber Optics Systems for Personal Radio Communication,” IEEE Trans. Microw. Theory Tech. , vol. 40, pp. 2285–2293, December 1992.

[20] H. Schmuck, R. Heidemann, and R. Hofstetter, “Distribution of 60 GHz Signals to more Than 1000 Base Stations,” Electronics Letter, vol. 6, pp. 59–60, January 1994
[21] IEEE P802.11 ad, http://www.ieee802.org/11/Reports/tgad_update.htm
[22] IEEE 802.15 TG3c, http://www.ieee802.org/15/pub/TG3c.html
[23] WirelessHD, http://www.wirelesshd.org/
[24] IEEE, P802.11ay task group, http://www.ieee802.org/11/Reports/tgay_update.htm
[25] H. Ogawa, D. Polifko and S. Banba, “Millimeter-Wave Fiber Optics Systems for Personal Radio Communication,” IEEE Trans. Microwave Theory Tech., vol. 40, no. 12, pp. 2285-2293, Dec. 1992.
[26] R. Braun, G. Grosskopf, D. Rohde, and F. Schmidt, “Low-Phase-Noise Millimeter-Wave Generation at 64 GHz and Data Transmission Using Optical Sideband Injection Locking,” IEEE Photon. Technol. Lett., vol. 10, no. 5, pp. 728-730, May. 1998
[27] G. H. Smith and D. Novak, “Broadband millimeter-wave Fiber-radio network incorporating remote up/down conversion,” Microwave Symposium Digest, IEEE MTT-S, vol. 3, pp. 1509-1512, Jun. 1998.
[28] K. Kitayama and R. A. Griffin, “Optical Downconversion from Millimeter-Wave to IF-Band Over 50-km-Long Optical Fiber Link Using an Electroabsorption Modulator,” IEEE Photon. Technol. Lett., vol. 11, no. 2, pp. 287-289, Feb. 1999.
[29] K. Kitayama, A. Stoehr, T. Kuri, R. Heinzelmann, D. Jaeger and Y. Takahashi, “An Approach to Single Optical Component Antenna Base Stations for Broad-Band Millimeter-Wave Fiber-Radio Access Systems,” IEEE Trans. Microwave Theory Tech., vol. 48, pp. 2588-2594, Dec. 2000.
[30] T. Kuri, K. Kitayama, and Y. Takahashi, “60-GHz-Band Full-Duplex Radio-On-Fiber System Using Two-RF-Port Electroabsorption Transceiver,” IEEE Photon. Technol. Lett., vol. 12, no. 4, pp. 419-421, Apr. 2000.
[31] G. H. Smith, D. Novak, and C. Lim, “A millimeter-wave full-duplex Fiber-radio star-tree architecture incorporating WDM and SCM,” IEEE Photon. Technol. Lett., vol. 10, pp. 1650-1652, Nov. 1998.
[32] H. Harada, K. Sato and M. Fujise, “A Radio-on-Fiber Based Millimeter-Wave Road-Vehicle Communication System by a Code Division Multiplexing Radio Transmission Scheme,” IEEE Trans. Intelligent Transport. Sys., vol. 2, no. 4, pp. 165-179, Dec. 2001.
[33] U. Gliese, S. Norskow, and T. N. Nielsen, “Chromatic Dispersion in Fiber-Optic Microwave and Millimeter-Wave Links,” IEEE Trans. Microwave Theory Tech., vol. 44, no. 10, pp. 1716-1724, Oct. 1996.
[34] N. Ghazisaidi and M. Maier Fiber-Wireless (FiWi) Networks: Challenges and Opportunities IEEE Network, vol. 25, no. 1, pp. 36-42, Jan./Feb. 2011
[35] N. Ghazisaidi, M. Maier, and C. M. Assi, “Fiber-Wireless (FiWi) Access Networks: A Survey,” IEEE Commun. Mag., vol. 47, no. 2, Feb. 2009, pp. 160–67.
[36] Madamopoulos, N. et al., "A fully distributed 10G-EPON-based converged fixed-mobile networking transport infrastructure for next generation broadband access," IEEE J. of Optical Com. and Networking, vol.4, no.5, May 2012
[37] Ahmed A., Shami A., "RPR-EPON-WiMAX hybrid network: A solution for access and metro networks," Optical Communications and Networking, IEEE/OSA Journal of , vol.4, no.3, pp.173-188, March 2012
[38] Ranaweera C., Wong E., Lim C.. Nirmalathas A., "Next generation optical-wireless converged network architectures " Network, IEEE , vol.26, no.2, pp.22-27, March-April 2012.
[39] Hajduczenia M., Toy M., Mallette E., Knittle C., "DOCSIS provisioning of EPON (DPoE): architecture and services" Communications Magazine, IEEE , vol.50, no.9, pp.58-65, September 2012
[40] Zin A.M., Idrus S.M., Zulkifli N., "Performance of IEEE 802.11 over fiber at MAC layer employing GPON architecture" Photonics (ICP), 2011 IEEE 2nd International Conference on , vol., no., pp.1-3, 17-19 Oct. 2011
[41] Ghazisaidi N., Scheutzow M., Maier M., "Survivability Analysis of Next-Generation Passive Optical Networks and Fiber-Wireless Access Networks", IEEE Transactions on Reliability, vol.60, no.2, pp.479-492, June 2011

[42] Ghazisaidi N., Maier. M.. Reisslein M., "VMP: A MAC Protocol for EPON-Based Video-Dominated FiWi Access Networks," Broadcasting, IEEE Transactions on , vol.58, no.3, pp.440-453, Sept. 2012.

[43] A. Chowdhury, C. Hung-Chang; F. Shu-Hao; Y. Jianjun, N. Jayant, G.K. Chang, "Radio over fiber technology for next-generation e-health in converged optical and wireless access network," Optical Fiber Communication Conference and Exposition (OFC/NFOEC), 2011.

[44] J. Beas, G. Castanon, I. Aldaya, A. Aragon-Zavala, and G. Campuzano, 'Millimeter-wave frequency radio over fiber systems: A survey,' Communications Surveys Tutorials, IEEE, vol. PP, no. 99, pp. 1–27, 2013.

[45] J. Capmany, J. Mora, I. Gasulla, J. Sancho, J. Lloret, and S. Sales, 'Microwave photonic signal processing,' Journal of Lightwave Technology, vol. 31, no. 4, pp. 571–586, 2013.

[46] H. Kosek, Y. He, X. Gu, and X.N. Fernando, 'All-optical demultiplexing of WLAN and cellular CDMA radio signals,' Journal of Lightwave Technology, vol. 25, no. 6, pp. 1401–1409, 2007.

[47] B. Lannoo, D.Colle, M. Pickavet, P.Demeester, "Radio-over-fiber-based solution to provide broadband internet access to train passengers," IEEE Comm. Mag., vol. 45, no.2, pp.56-62, Feb. 2007.

[48] N. Pleros, K. Tsagkaris and N. D. Tselikas, "A Moving Extended Cell concept for seamless communication in 60 GHz Radio-over-Fiber networks", IEEE Comm. Lett., Vol. 12, No. 11, pp. 852-854, Nov. 2008.

[49] H. B. Kim and A. Wolisz, "Performance evaluation of a MAC protocol for radio over fiber wireless LAN operating in the 60-GHz band," Global Telecommunications Conference, 2003. GLOBECOM '03. IEEE, 2003, pp. 2659-2663 vol.5.

[50] C.-T. Lin et al., "Hybrid Optical Access Network Integrating Fiber-to-the- Home and Radio-Over-Fiber Systems," IEEE Photonics Tech. Letters, vol. 19, no. 8, Apr. 2007, pp. 610–12.

[51] J. Hu, D. Qian, and T. Wang, "Wireless Intermediate Frequency Signal over Passive Optical Networks: Architecture and Experimental Performance Evaluation," Proc. OFC/NFOEC, San Diego, CA, Feb. 2008, pp.1–6.

[52] M. Mjeku, and N.J. Gomes,, "Analysis of the Request to Send/Clear to Send Exchange in WLAN Over Fiber Networks", J. of Lightwave Technol., Vol. 26, No. 15, pp. 2531-2539, Aug. 2008.

[53] B. Kalantari-Sabet, M. Mjeku, N.J. Gomes and J.E. Mitchell, "Performance Impairments in Single-Mode Radio-over-Fiber Systems due to MAC Constraints", J. of Lightwave Technol., Vol. 26, No. 15, pp. 2540-2548, Aug. 2008.

[54] Das, M. Mjeku, A. Nkansah and N.J. Gomes, "Effects on IEEE 802.11 MAC Throughput in Wireless LAN over Fiber Systems", J. of Lightwave Technol., Vol. 25, No. 11, pp. 3321-3328, Nov. 2007.

[55] M. Hossen, B.-J. Jang, K.-D. Kim, and Y. Park, "Extension of wireless sensor network by employing rof-based 4g network," in ICACT 2009. 11th International Conference on, vol. 01, pp. 275 –278, feb. 2009.

[56] T. P. C. de Andrade; N. L. S. da Fonseca; L. A. Villas; O. C. Branquinho, "Protocols for Wireless Sensors Networks Connected by Radio-Over-Fiber Links," in IEEE Systems Journal , vol.PP, no.99, pp.1-11, 2016.

[57] T. P. C. de Andrade, N. L. S. da Fonseca, L. B. Oliveira and O. C. Branquinho, "MAC protocols for wireless sensor networks over radio-over-fiber links," 2012 IEEE International Conference on Communications (ICC), Ottawa, ON, 2012, pp. 254-259.

[58] T. P. C. de Andrade, L. B. Oliveira, N. L. S. da Fonseca and O. C. Branquinho, "HMARS: A MAC Protocol for Integration of Radio-over-Fiber and Wireless Sensor Networks," in IEEE Latin America Transactions, vol. 10, no. 4, pp. 1981-1986, June 2012.

[59] T. P. C. de Andrade, L. B. Oliveira, N. L. S. da Fonseca and O. C. Branquinho, "HMARS: A MAC protocol for integration of Radio-over-Fiber and Wireless Sensor Networks," 2011 IEEE Third Latin-American Conference on Communications, Belem do Para, 2011.

[60] T. P. C. de Andrade, L. A. Villas and N. L. S. da Fonseca, "Medium access control protocol for Hybrid Radio-over-Fiber Wireless Sensors Networks," 2014 IFIP Wireless Days (WD), Rio de Janeiro, 2014.

[61] Lona, D. G., Assumpção, R. M., Branquinho, O. C., Abbade, M. L.F., Hernández-Figueroa, H. E. and Sodré, A. C. (2012), Implementation and performance investigation of radio-over-fiber systems in wireless sensor networks. Microw. Opt. Technol. Lett., 54: 2669–2675.

[62] B. L. Dang, R. Prasad and I. Niemegeers, "On the MAC protocols for. Radio over Fiber indoor networks," First International Conference on Communications and Electronics, ICCE '06, 10-11 October 2006.

[63] D. Wake, D. Johansson, and D.G. Moodie, 'Passive picocell: A new concept in wireless network infrastructure,' Electronics Letters, vol. 33, no. 5, pp. 404–406, February 1997.

[64] X.-H. Yu, G. Chen, M. Chen, and X. Gao, 'Toward beyond 3G: The FUTURE project in China,' IEEE Communications Magazine, vol. 43, no. 1, pp. 70–75, 2005.

[65] C. Kwang, B. Roberto de Marca, "WiBro A 2.3 GHz Mobile WiMAX: System Design, Network Deployment, and Services", Mobile WiMAX 1, Wiley-IEEE Press, 2008, pp.257-290.

[66] D.Wake, A. Nkansah, and N.J. Gomes, 'Radio over fiber link design for next generation wireless systems,' Journal of Lightwave Technology, vol. 28, no. 16, pp. 2456–2464, 2010.

[67] S. Pan and Z. Tang, 'A radio over fiber link for the wireless distribution of 3-Gb/s uncompressed HD video' (invited paper) in Proceedings of 7th International ICST Conference on Communications and Networking in China, Kun Ming, China, 2012, pp. 54–57.

[68] W.J. Fang, X. Huang, and G. Li, 'A full duplex radio-over-fiber transmission of OFDM signals at 60 GHz employing frequency quintupling optical up-conversion,' Optics Communications, vol. 294, pp. 118–122, 2013.

[69] L. Tao, Z. Dong, J. Yu, N. Chi, J. Zhang, X. Li, Y. Shao, and G.-K. Chang, 'Experimental demonstration of 48-Gb/s PDM-QPSK radio-over-fiber system over 40-GHz mm-wave MIMO wireless transmission,' IEEE Photonics Technology Letters, vol. 24, no. 24, pp. 2276–2279, 2012.

[70] H. S. Chung, S. H. Chang, J. D. Park, M.-J. Chu, and K. Kim, "Transmission of Multiple HD-TV Signals Over a Wired/Wireless Line Millimeter-Wave Link With 60 GHz", J. of Lightwave Technol., vol. 25, no. 11, pp. 3413-3418, Nov. 2007.

[71] Z. Jia, J. Yu, G. Ellinas and G.-K. Chang, "Key Enabling Technologies for Optical–Wireless Networks: Optical Millimeter-Wave Generation, Wavelength Reuse, and Architecture", J. of Lightwave Technol., vol. 25, no. 11, pp. 3452-3471, Nov. 2007.

[72] M. Bakaul, A. Nirmalathas, C. Lim, D. Novak, and R. B. Waterhouse, "Simultaneous multiplexing and demultiplexing of wavelength-interleaved channels in DWDM millimeter-wave fiber-radio networks," J. Lightw. Techol., vol. 24, no. 9, pp. 3341–3352, Sep. 2006.

[73] C.-S. Choi, Y. Shoji, and H. Ogawa, "Millimeter-Wave Fiber-Fed Wireless Access Systems Based on Dense Wavelength-Division-Multiplexing Networks", IEEE Trans. on Microwave Theory and Techniques, Vol. 56, No. 1, pp. 232-241, Jan. 2008.

[74] M. García Larrodé and A.M.J. Koonen, "All-Fiber Full-Duplex Multimode Wavelength-Division-Multiplexing Network for Radio-Over-Multimode-Fiber Distribution of Broadband Wireless Services", IEEE Trans. on Microwave Theory and Techniques, Vol. 56, No. 1, pp. 248-255, Jan. 2008.

[75] A. Maziotis, C. Stamatiadis, Ch. Kouloumentas, K. Vyrsokinos and N. Pleros, "Dual-User Wireless Heterogeneous Services over a Single Optical Carrier using Optical Frequency Multiplication", IEEE/LEOS Annual Meeting 2009, ThK1, Belek-Antalya, Turkey, 4 - 8 October 2009 Turkey.

[76] Z. Jia, J. Yu, A. Chowdhury, G. Ellinas, and G.-K. Chang, "Simultaneous Generation of Independent Wired and Wireless Services Using a Single Modulator in Millimeter-Wave-Band Radio-Over-Fiber Systems", IEEE Photon. Technol. Lett., Vol. 19, No. 20, pp.1691-1693, Oct. 2007.

[77] J. J. Vegas Olmos, T. Kuri, and K. Kitayama, “Dynamic Reconfigurable WDM 60-GHz Millimeter-Waveband Radio-Over-Fiber Access Network: Architectural Considerations and Experiment”, J. of Lightwave Technol., vol. 25, no. 11, pp. 3374-3380, Nov. 2007.
[78] L. Chen et al, “A Novel Scheme for Seamless Integration of ROF With Centralized Lightwave OFDM-WDM-PON System”, J. of Lightwave Technol., vol. 27, no. 14, pp. 2786-2791, July 2009.
[79] C. Cordeiro, "Evaluation of Medium Access Technologies for Next Generation Millimeter-Wave WLAN and WPAN," in ICC 2009.
[80] http://www.micronoptics.com/tunable_filters.php
[81] M Becchi, “From Poisson processes to self-similarity: a survey of network traffic models”, Washington University in St. Louis, Tech. Rep, 2008.
[82] Benny Bing, “3D and HD Broadband Video Networking, Artech House Telecommunications Library, Published July 2012.
[83] Wireless Gigabit Alliance, http://wirelessgigabitalliance.org/
[84] Z. Xu, H. Wang and Y. Ji, "Multichannel Resource Allocation Mechanism for 60 GHz Radio-Over-Fiber Local Access Networks", IEEE J. of Optical Communications and Networking, vol. 5, no. 3, pp. 254-260, 2013.
[85] van Hoesel, L.F.W. and Havinga, P.J.M. (2009) “Analysis of a Self-organizing Algorithm for Time Slot Selection in Schedule-based Medium Access.” [Internal Report]
[86] S. T. Choi, K. S. Yang, S. Nishi, S. Shimizu, K. Tokuda and Y. H. Kim, “A 60-GHz Point-to-Multipoint Millimeter-Wave Fiber-Radio Communication System”, IEEE Trans. on Microwave Theory and Techniques, vol. 54, no. 5, May 2006
[87] B. Lannoo et al., "Analytical model for the IPACT dynamic bandwidth allocation algorithm for EPONs," J. Opt. Netw. 6, 677-688 (2007)
[88] Kani, J.; Nakamura, H., "Recent progress and continuing challenges in optical access network technologies," Photonics (ICP), 2012 IEEE 3rd International Conference on , vol., no., pp.66,70, 1-3 Oct. 2012.
[89] Milosavljevic, M., Kourtessis, P., Lim, W. & Senior, J. M., “Next generation PONs with wireless backhauling“, 2011 IEEE International Conference on Transparent Optical Networks, Stockholm.
[90] Pamvotis IEEE 802.11 WLAN simulator. Available on-line: http://pamvotis.org/
[91] Diane Teare, “CCDA Self-Study: Designing for Cisco Internetwork Solutions”, 2003, Cisco Press, ISBN-10: 1-58705-141-9
[92] ITU-T, G987.1, “10-Gigabit-capable passive optical networks (XG-PON): General requirements”, 2010.
[93] ITU-T G.989.1 "SERIES G: TRANSMISSION SYSTEMS AND MEDIA, DIGITAL SYSTEMS AND NETWORKS, Digital sections and digital line system – Optical line systems for local and access networks, 40-Gigabit-capable passive optical networks (NG-PON2): General requirements", 03/2013.